Università degli Studi di Pisa

FACOLTÀ DI INGEGNERIA

DIPARTIMENTO DI INGEGNERIA DELL'ENERGIA E DEI SISTEMI

CORSO DI DOTTORATO IN
AUTOMATICA, ROBOTICA E BIOINGEGNERIA

SSD: ING-INF/04

PH.D. DISSERTATION ON

FROM OPTIMAL SYNTHESIS TO OPTIMAL VISUAL SERVOING FOR AUTONOMOUS VEHICLES

Candidate Student: **Paolo Salaris**

Supervisors: **Prof. Antonio Bicchi**

Dott.ssa Lucia Pallottino

Course Cycle XXIII — Year of Enrolling 2008

Abstract

This thesis focuses on the characterization of optimal (shortest) paths to a desired position for a robot with unicycle kinematics and an on-board camera with limited Field-Of-View (FOV), which must keep a given feature in sight. In particular, I provide a complete optimal synthesis for the problem, i.e., a language of optimal control words, and a global partition of the motion plane induced by shortest paths, such that a word in the optimal language is univocally associated to a region and completely describes the shortest path from any starting point in that region to the goal point. Moreover, I provide a generalization to the case of arbitrary FOVs, including the case that the direction of motion is not an axis of symmetry for the FOV, and even that it is not contained in the FOV.

Finally, based on the shortest path synthesis available, feedback control laws are defined for any point on the motion plane exploiting geometric properties of the synthesis itself. Moreover, by using a slightly generalized stability analysis setting, which is that of stability on a manifold, a proof of stability is given for the controlled system. At the end, simulation results are reported to demonstrate the effectiveness of the proposed technique.

Acknowledgement

First and foremost I offer my sincerest gratitude to my supervisor, Professor Antonio Bicchi, who has supported me throughout these last years with his patience and wide knowledge. I attribute the level of my PhD thesis to his encouragement, effort and precious suggestions. One simply I could not wish for a better and friendlier supervisor.

I also would like to express my deep and sincere gratitude to my supervisor Dott.ssa Lucia Pallottino. Her knowledge and her logical way of thinking have been of great value for me. Her understanding, encouraging and personal guidance have provided an essential improvement for the present thesis. It is a pleasure to thank also Daniele Fontanelli, Luca Greco and Felipe A. W. Belo for their willingness to talk with me about various concerns regarding my research during these last years.

I owe my most sincere gratitude to Professor Seth Hutchinson who gave me the opportunity, during my PhD, to work with him at University of Illinois in the Department of Electrical and Computer Engineering at Beckman Institute for Advanced Science and Technology (Urbana-Champaign, USA) for eight months.

I wish to thank my best friends, colleagues and administrative staff of the Interdepartmental Center of Research "E. Piaggio" for providing a stimulating, efficient and fun environment in which to learn, work and grow.

Lastly, and most importantly, I wish to thank my family, in particular my mother, my grandparents, my brother, my sister, her husband and especially their little daughter.

Contents

Introduction

This thesis deals with the study of optimal paths and controls for a vehicle equipped with a limited Field-Of-View (FOV) camera and subjected to nonholonomic constraints. The vehicle, moving on a plane, have to reach a target position while making so that some points fixed in the environment are kept always in view. The contribution of this thesis is important because, no much is the work that had been devoted to optimal control of visually-servoed robotic vehicles where both nonholonomic and FOV constraints are taking into account minimizing at the same time a cost functional (e.g., the time necessary for the robot to reach desired configuration, the length of path, and so on).

Regarding optimal (shortest) paths in absence of sensor constraints, the seminal work on unicycle vehicles, [11], provides a characterization of shortest curves for a car with a bounded turning radius. In [12], authors determine a complete finite partition of the motion plane in regions characterizing the shortest path from all points in the same region, i.e., a synthesis. A similar problem with the car moving both forward and backward has been solved in [13] and refined in [14]. The global synthesis for the Reeds and Shepp vehicle has been obtained combining necessary conditions given by Pontryagin's Maximum Principle (PMP) with Lie algebraic tools in [15]. More recently, [16], [17] determined time optimal trajectories for differential–drive robots and

nonholonomic bidirectional robots, respectively, while [18] solved the minimum wheel rotation problem for differential-drive robots.

Visual servoing techniques use visual information directly, by the computation of an image error signal, or indirectly, by the evaluation of the state of the system [19, 20]. These two approaches, often referred to as *Image–Based* (IBVS) and *Position–Based* (PBVS) [21], can be regarded as the end-points of a range of different possibilities, whereby the raw sensorial information is gradually abstracted away to a more structured representation using some knowledge of the robot-environment model.

PBVS and in general higher-level control schemes have important, attractive features. Using the PBVS approach, for instance, the control law can be synthesized in the usual working coordinates for the robot, usually making the synthesis simpler, as in [22]. On the other hand, IBVS and other sensor-level control schemes have also several advantages, such as robustness (or even insensitivity) to modeling errors [23] and hence suitability to unstructured scenes and environments. There exist also hybrid solutions where the advantages of position-based visual servoing and image-based visual servoing are merged [24].

Thanks to well-established advances in point-feature extraction and tracking algorithms, such as the *Scale Invariant Feature Transform* proposed in [25], visual control is getting widespread in robotics. However, few practical problems still affect visual servoing approaches and depend on the particular available robotic set-up. One such issue arising with limited FOV cameras is that of keeping the features in view during the robot maneuvers, with the aim of localize the robot in the environment and compute a feedback control law. This problem has been addressed at times using omni-directional cameras [26], or image path planning [27]. In mobile robotic, especially for nonholonomic vehicle, a solution to this problem becomes very difficult and challenging. In [28] and in [29] authors present a visual control approach for mobile robots consisting in a switching control scheme based on the epipolar geometry. Anyway, whereas [28] does not con-

sider the problem of keeping the features in the FOV, in [29] it is assumed that difference in depth from the initial position to the goal is greater than the side distance from the initial position to the goal, avoiding the need of high rotations. On the other hand, in [30] authors propose a visual control where the advantages of position-based visual servoing and image-based visual servoing are merged, and a hybrid error vector is defined. In this case the camera FOV constraints are alleviated — but not taking into account explicitly — because the algorithm works well with few feature points.

The FOV problem has been successfully solved for a unicycle-like vehicle in [31–33] but, the resultant path is inefficient and absolutely not optimal. The optimal control of visually guided robotic manipulators has also received considerable attention (see e.g., [34]). Optimal trajectory planning for robot manipulators controlled via a limited FOV camera has been first presented in [35], where two algorithms based on homography and on epipolar geometry, respectively, have been proposed to generate the optimal trajectory of the robot to its goal configuration. Minimal trajectories have been also presented in [36] in case of large displacements, again for a six degrees of freedom robot manipulator. Until now, much less is the work that had been devoted to optimal control for nonholonomic vehicles taking into account FOV constraints and minimizing at the same time a cost functional, i.e., the time necessary to reach the goal position or the length of the path covered by the vehicle.

Motivations. This thesis is motivated by several applications in mobile robotics. Indeed, in addition to the Visual-Based control field where the vehicle usually has an on-board monocular camera with limited FOV, the problem addressed in this thesis, in particular the generalization to the case of arbitrary FOVs, is particularly relevant in the field of underwater surveying and navigation. In this field, a common task for Autonomous Underwater Vehicles (AUV) equipped with side sonar scanners is to detect and recognize objects (mines, wrecks or archeological find, etc.) on the sea bed (see e.g. [37, 38]).

Side-scan sonar is a category of sonar systems that is used to efficiently create an image of large areas of the sea. Therefore, in order to recognize objects AUVs must move keeping them inside the limited range of the sensor.

An inspiring motivation for the study, however, comes also from the naturalistic observation of paths followed by raptors during hunting activities. Indeed, falcons, hawks and eagles have two regions of the retina in each eye that are specialized for acute vision: the deep fovea and the shallow fovea. The line of sight of the deep fovea points forwards and approximately 45º to the right or left of the head axis, while that of the shallow fovea also points forwards but approximately 15º to the right or left of the head axis. The most acute vision information for raptors comes from their deep foveae (see figure 1). The deep fovea system has a limited FOV, so that raptors possess no accurate front sight. This causes a conflict for these predators, which dive a prey from great distances at high speeds: at a speed of 70 m/s, turning their head sideways to view the prey with high visual acuity may increase aerodynamic drag by a

Figure 1: A frontal section through an ideal falcon's head at the foveal plane.

factor of 2 or more, and slow the raptor down. In [39] and [40], it has been shown that raptors resolve this conflict by diving along a logarithmic spiral path with their head straight and one eye looking sideways at the prey, rather than following the straight path to the prey with their head turned sideways (see figure 2).

**Thesis Contributions.** This thesis focus on the problem of visual servo control for a unicycle-like vehicle equipped with a monocular fixed vision system. The system, subject to nonholonomic constraints imposed by the vehicle kinematics and to FOV constraints imposed by
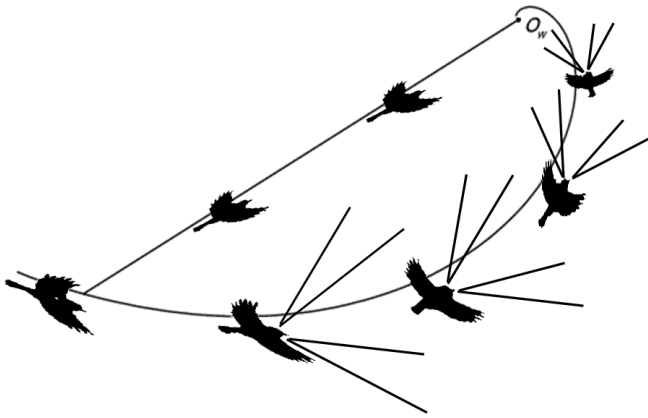
Figure 2: In order to keep the prey in view, a raptor follows a logarithmic spiral rather than a straight line.

camera, must reach a desired position on the motion plane following the optimal (shortest) path. In order to localize itself and to compute a visual servo control, the robot must keep at least three features in view. Indeed given three or more features both in the current image and in the desired one, by using the estimation technique proposed in [30], state variables of the vehicle are available up to a scale factor. A first step toward the solution of this problem has been done in [41] and in this thesis, considering a single feature to be kept in sight. Indeed, the work in [41] represents the first attempts to find minimum length paths for nonholonomic vehicles equipped with limited FOV monocular cameras. The optimal control synthesis presented in [41] consists of 10 regions, for each point of which the shortest path is of the same type and described by a word using up to 3 symbols. In this work, starting from the observation made in [41] that extremal arcs for the considered problem are of three types (rotations on the spot, straight lines and logarithmic spirals, as raptors during their hunting activities), we study the same problem, and show that the synthesis of [41] is valid locally, i.e., for starting positions of the robot

close enough to the goal. However, a correct and complete synthesis for the whole plane of motion requires a finer partition in 18 regions, and the use of words of up to 5 symbols. For this reason, this thesis provides a complete optimal synthesis for the problem, i.e. a language of optimal control words, and a global partition of the motion plane induced by shortest paths, such that a word in the optimal language is univocally associated to a region and completely describes the shortest path from any starting point in that region to the goal point (these results can be found in the published papers [A1] and [A2]). Moreover, a generalization to the case of arbitrary FOVs, including the case that the direction of motion is not an axis of symmetry for the FOV, and even that it is not contained in the FOV is given and can be found also in [A3]. The impracticability of paths that point straight to the feature lead to a more complex analysis of the reduction to a finite and sufficient family of optimal paths by excluding particular types of path.

Towards the practical application of the optimal path synthesis proposed in this work, a crucial step is to translate the optimal trajectories (which are evaluated from any initial condition as plans to be executed in open-loop) into feedback control laws, i.e., to write laws which determine the control inputs (the vehicle velocities) as a function of the current state of the system only. Only when such a feedback control law is derived, it will be possible to make the system reach the desired posture with robustness against disturbances and uncertainties, i.e., it will be possible to show *stability* of the system at the desired configuration.

A first result in this direction has been reported in [42]. Based on the locally optimal synthesis in [41], rewritten in terms of the parameters of the homography matrix, the authors of [42] provide a visual control law based on an iterative steering scheme, which is a generalized form of feedback control (cf. e.g. [43]). The authors discuss the stability of the method. However, as we will discuss later on in chapter 4 (see the example in remark 4.2 in section 4.2), the application of any feedback control scheme congruent with the optimal synthesis

in [41] and in this thesis is not — strictly speaking — stabilizing the final posture in the sense of Lyapunov.

In this work, based on the geometric properties of the globally optimal synthesis obtained in chapter 2 and also in [A2], optimal feedback control laws are defined for any point on the motion plane. These laws are provided in explicit form as simple algebraic functions of the current state only, which can be easily computed to give in real time the velocity input to be used - thus requiring no replanning procedure, and being intrinsically more robust. Also, the method does not require the use of homography, thus being computationally cheaper and not causing ambiguities. Stability properties for the proposed control scheme are proven in a properly generalized analysis setting, which is that of stability on a manifold [44], and the LaSalle's invariance principle [45]. Finally, based on a visual control scheme where a combination of position-based visual servoing and image-based visual servoing are merged, simulations results are reported to show the effectiveness of the proposed technique (these results can be found in [A4]).

This thesis is organized as follow: in the first part, and in particular in chapter 1 the optimal problem for a unicycle equipped with a limited FOV sensor is defined and extremal curves, i.e., curves that satisfy necessary conditions for optimality are given. In the following chapter 2, the optimal synthesis in case of a sensor modelled as a symmetric (w.r.t. robot forward direction) planar cone moving with the robot is given. Moreover, in chapter 3 a generalized optimal synthesis in case of arbitrarily FOVs is obtained. In the second part, chapter 4 presents feedback control laws for any point on the motion plane exploiting geometric properties of the synthesis itself. Moreover, by using a slightly generalized stability analysis setting, which is that of stability on a manifold, a proof of stability is given. Finally, chapter 5 reports simulations demonstrate the effectiveness of the proposed technique.

Part I

Optimal Paths Synthesis with Limited Field-Of-View Sensors

THIS PART presents a complete characterization of shortest paths to a goal position for a robot with nonholonomic constraints and an on-board sensor with limited Field-Of-View (FOV) (e.g., cameras or sonar scanners), which must keep a given landmark in sight. More precisely, Chapter 1 introduces the shortest paths problem for an unicycle-like robot equipped with a limited FOV sensor modelled as a four-sided right rectangular pyramid. Extremal curves or else the alphabet of the elementary paths by which build optimal ones, i.e., the shortest paths from any initial robot position to desired one, will be obtained. Chapter 2 presents the shortest paths synthesis in case of a frontal, symmetrically limited FOV sensor modeled as a planar cone moving with the robot, i.e., a degenerate case of a four-sided right rectangular pyramid model with horizontal limits. Finally, the following Chapter 3 presents a generalization to the case of arbitrary planar sensor, including the case that the direction of motion is not an axis of symmetry for the sensor cone, and even that it is not included.

Extremal Paths for a Robot with Nonholonomic and Field-Of-View Constraints

THIS CHAPTER introduces the optimal control problem for a unicycle-like vehicle subject to nonholonomic constraints and equipped with limited Field-Of-View (FOV) sensors. Extremal curves, i.e., curves that satisfy necessary conditions for optimality, are then obtained. A finite alphabet of the extremal arcs by which build the optimal ones, i.e., the shortest paths from any initial robot position to desired one, will be obtained.

1.1 Introduction

In several mobile robot applications, a unicycle-like vehicle with non-holonomic kinematics is equipped with a limited Field-Of-View sensor systems. For example, in the field of underwater surveying and navigation, a common task for Autonomous Underwater Vehicles (AUV) equipped with side sonar scanners is to detect and recognize objects (mines, wrecks or archeological find, etc.) on the sea bed, keeping any-

time them inside the limited scanning angle of the sensor. Side-scan sonar is a category of sonar systems that is used to efficiently create an image of large areas of the sea. Therefore, in order to recognize objects AUVs must move keeping them inside the limited FOV of the sensor. On the other hand, in the Visual-Based control field, the robot usually has an on-board monocular camera with limited FOV and, subject to nonholonomic constraints on its motion, must move toward a desired configuration, usually maintaining in sight some specified landmarks of the environment with respect to which it have to locate. Indeed, in order to localize itself, the robot must keep at least three features in view. For example, in [30] authors present an estimation technique such that given three or more features both in the current image and in the desired one, state variables of the vehicle are available up to a scale factor.

Motivated by those applications in which a nonholonomic vehicle have to move maintaining a reference object of the environment, or some of its features, inside a limited sensor with the aim of localize itself and compute the feedback control laws, the final objective of this work is to solve the optimal paths problem for a nonholonomic vehicle moving in a plane to reach a desired position while making so that some given landmarks fixed in the world are kept inside the limited FOV sensor. In order to move a first step toward this final objective, this thesis presents the shortest paths synthesis for a nonholonomic vehicle in a simplified scenario in which *only* one landmark belongs to an object fixed in the world is kept inside the FOV sensor during robot's maneuvers from initial to desired configuration.

1.2   Problem Statement

Consider a vehicle moving on a plane where a right-handed reference frame $\langle W \rangle$ is defined with origin in O_w and axes X_w, Z_w. The kind of vehicle considered here is referred to as *unicycle*. Its configuration can be described by a vector q of three generalized coordinates
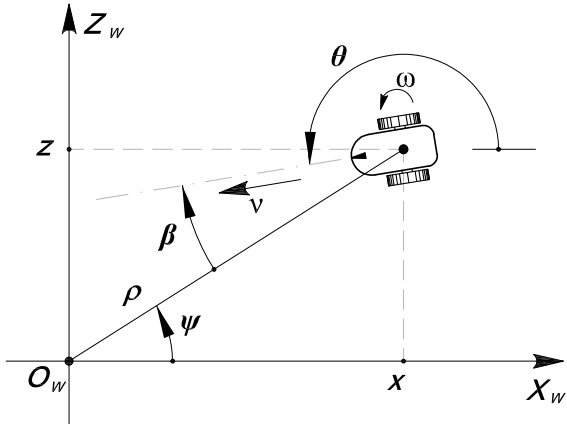
Figure 1.1: Mobile robot and system coordinates $\langle W \rangle$.

$q(t) = (x(t), z(t), \theta(t))$, where $(x(t), z(t))$ is the position in $\langle W \rangle$ of the midpoint of the wheel axle, and $\theta(t)$ is the vehicle heading with respect to the X_w axis (see figure 1.1). The system generalized velocities $\dot{q}(t)$ can not assume independent values; in particular, they must satisfy the constraint

$$
\begin{bmatrix} \sin\theta & -\cos\theta & 0 \end{bmatrix}
\begin{bmatrix} \dot{x} \\ \dot{z} \\ \dot{\theta} \end{bmatrix} = 0\,,
\tag{1.1}
$$

entailing that the lateral velocity of the vehicle is zero or, in other words, the rolling without slipping condition between the wheels and the ground must be anytime guaranteed. Equation (1.1) is a typical example of *Pfaffian* constraints $C(q)\dot{q} = 0$, i.e., linear in the generalized velocities. Notice that, the kinematic constraints in equation (1.1) can not be integrated. For this reason, the kinematic constraint is said to be nonholonomic (or non-integrable) and a mechanical system that is subject to at least one such constraint is called nonholonomic ([46]).

Extremal Paths for a Robot with Nonholonomic and Field-Of-View Constraints
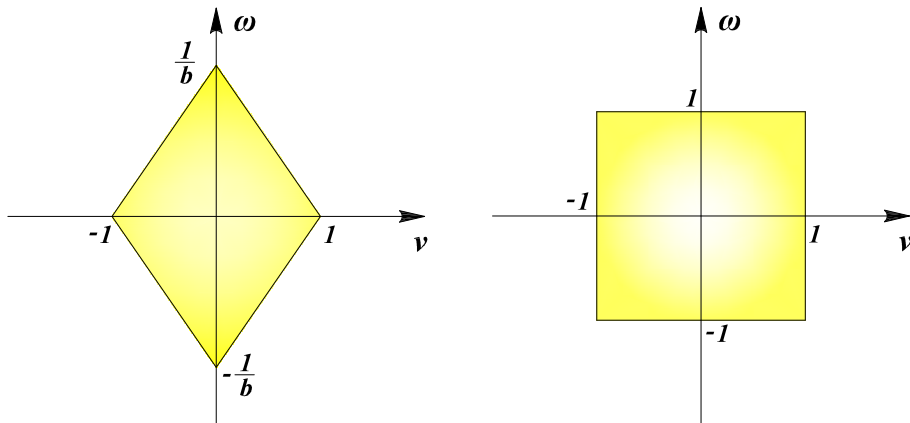
(a) Differential Drive Robot (DDR)   (b) Convexified Reeds–Shepp (CRS)

Figure 1.2: Admissible velocities for DDR and CRS: both vehicle can rotate on the spot.

For the unicycle vehicle, all admissible generalized velocities are contained in the null space of the constraint matrix $C(q)$, obtaining the kinematic model

$$
\dot{q} = \begin{bmatrix} \cos\theta \\ \sin\theta \\ 0 \end{bmatrix} \nu + \begin{bmatrix} 0 \\ 0 \\ 1 \end{bmatrix} \omega,
\tag{1.2}
$$

where $\nu(t)$ and $\omega(t)$ are the forward and angular velocities, respectively. We assume here that the dynamics of the vehicle are negligible, and that $\nu(t)$ and $\omega(t)$ are the control inputs to the kinematic model of the vehicle, given by equation (1.2).

Let us consider vehicles with bounded velocities which can turn on the spot. In other words,

$$
(\nu, \omega) \in U,
\tag{1.3}
$$

with U a compact and convex subset of $\mathbb{R}^2$, containing the origin in its interior. Two examples of this typology of vehicles are the

Differential Drive Robot (DDR) and the Convexified Reeds–Shepp model (CRS), whose admissible velocities are represented in figure 1.2. For a DDR robot, let ω_1 and ω_2 be the wheel angular velocities, than input controls are

$$\nu = \frac{\omega_1 + \omega_2}{2},$$

$$\omega = \frac{\omega_2 - \omega_1}{2b},$$

where $2b$ is the wheels axle length.

In the following, in order to simplify the synthesis of shortest paths, vehicle configuration will be described with polar coordinates instead of cartesian ones (see figure 1.1). Hence, setting

$$\eta = \begin{bmatrix} \rho \\ \psi \\ \beta \end{bmatrix} = \begin{bmatrix} \sqrt{x^2 + z^2} \\ \arctan\left(\frac{z}{x}\right) \\ \arctan\left(\frac{z}{x}\right) - \theta + \pi \end{bmatrix}, \tag{1.4}$$

the kinematic model of the unicycle-like robot becomes

$$\begin{bmatrix} \dot{\rho} \\ \dot{\psi} \\ \dot{\beta} \end{bmatrix} = \begin{bmatrix} -\cos\beta & 0 \\ \frac{\sin\beta}{\rho} & 0 \\ \frac{\sin\beta}{\rho} & -1 \end{bmatrix} \begin{bmatrix} \nu \\ \omega \end{bmatrix}. \tag{1.5}$$

Because I will frequently be interested only in the projection of η onto the robot's workspace, i.e., in the polar coordinates of the midpoint of the wheel axle, I introduce the notation $Q = (\rho, \psi)$ as a shorthand notation.

The vehicle is equipped with a rigidly fixed limited sensor, for example a monocular camera. The most limited FOV sensors, as cameras, can be generically modelled as a four-sided right rectangular pyramid, as shown in figure 1.3. Its characteristic solid angle is given by

$$\Omega = 4\arcsin\left(\sin\frac{\varepsilon}{2}\sin\frac{\delta}{2}\right),$$

Extremal Paths for a Robot with Nonholonomic and Field-Of-View Constraints
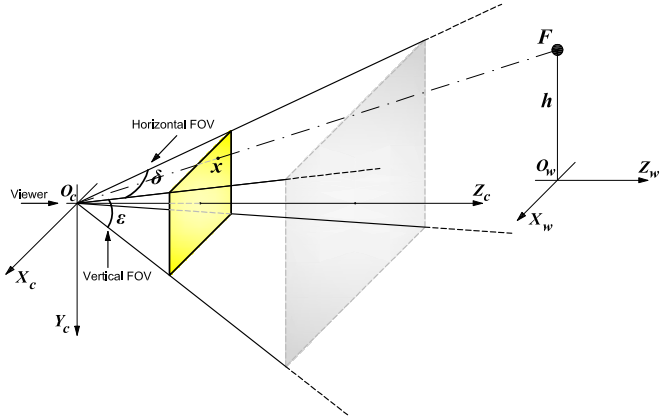
Figure 1.3: Sensor model: four-sided right rectangular pyramid.

where $\varepsilon = 2\hat{\phi}$ and $\delta = 2\phi$ are the apex angles, i.e., dihedral angles measured to the opposite side faces of the pyramid. We will refer to those angles as the vertical and horizontal angular aperture of the sensor, respectively. Moreover, $\hat{\phi}$ is half of the Vertical-FOV (V-FOV) angular aperture, whereas ϕ is half of the Horizontal-FOV (H-FOV) angular aperture. In the following, I consider the most interesting problem in which ε and δ are less than $\pi/2$. Moreover, let us introduce a sensor's reference frame $\langle C \rangle = \{O_c, X_c, Y_c, Z_c\}$ such that the center O_c, i.e., the apex of the pyramid, corresponds to the robot's center $[x(t), z(t)]^T$, $X_c \times Z_c$ plane is parallel to the motion plane and the axis Z_c, coincident with the axis of symmetry of the sensor, forms an angle Γ with respect to the robot's forward direction. Without loss of generality, I will consider $0 \leq \Gamma \leq \frac{\pi}{2}$, so that, when $\Gamma = 0$ the Z_c axis is aligned with the robot's forward direction, whereas, when $\Gamma = \frac{\pi}{2}$, is aligned with the axle direction. Consider $\phi_1 = \Gamma - \frac{\delta}{2}$ and $\phi_2 = \Gamma + \frac{\delta}{2}$ the angles between the robot's forward direction and the right or left sensor's border with respect to Z_c axis, respectively. The restriction on $0 \leq \Gamma = \frac{\phi_1 + \phi_2}{2} \leq \frac{\pi}{2}$ will be removed in the following, and an easy procedure to obtain the optimal paths for any value of Γ will be given exploiting symmetries of the problem.

We assume that the feature to be kept within the on-board limited FOV sensor is placed on the axis through the origin O_w, perpendicular to the plane of motion and with height h from it, so that its projection on the motion plane coincides with the center O_w (see figure 1.3). Moreover, let us consider the position of the robot target point P to lay on the X_w axis, with coordinates $(\rho, \psi) = (\rho_P, 0)$.

In order to maintain the feature within the limited FOV sensor, following inequality constraints must be anytime satisfied during robot's maneuvers:

$$\beta - \phi_1 \;\geq\; 0 \,, \tag{1.6}$$

$$\beta - \phi_2 \;\leq\; 0 \,, \tag{1.7}$$

$$\rho \cos{(\beta - \Gamma)} \;\geq\; \left| \frac{h}{\tan \hat{\phi}} \right| = R_b \,, \tag{1.8}$$

where inequalities (1.6) and (1.7) concern H-FOV limits, whereas inequality (1.8) concerns V-FOV limits.

The goal of this work is to determine, for any point $Q \in \mathbb{R}^2$ in the robot space, the shortest path from Q to P, such that the feature F is maintained in the FOV of the sensor. In other words, the objective is to minimize the length of the path covered by the center of the vehicle, i.e., to minimize the cost functional

$$L = \int_0^\tau |\nu| \, dt \,, \tag{1.9}$$

under the *feasibility constraints* (1.3), (1.5), (1.6), (1.7) and (1.8), respectively. Here τ is the time needed to reach P, that is $\rho(\tau) = \rho_P$ and $\psi(\tau) = 0$. Notice that, cost functional (1.9) does not weigh β, i.e., rotations on the spot have zero length. As a consequence, in the following these maneuvers will be used only to properly connect other maneuvers.
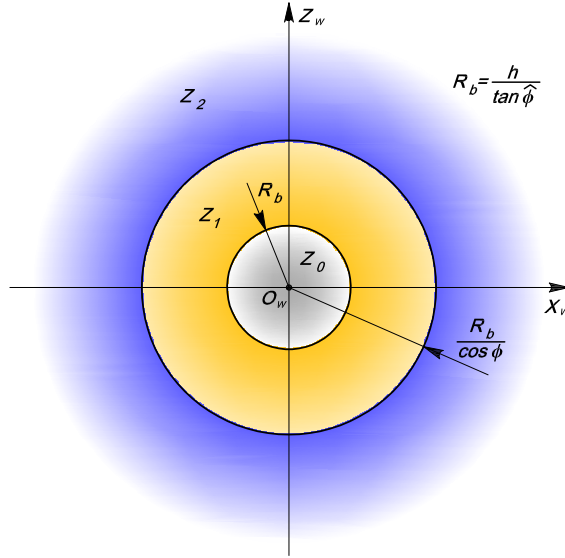
Figure 1.4: Subdivision of the motion plane in region according to Proposition 1.1.

1.3 Analysis of FOV Constraints

In this section inequalities (1.6), (1.7) and (1.8) are taken under investigation in order to determine a preliminary partition of the motion plane in regions, for each point of which the optimal paths synthesis can be studied considering separately H-FOV or V-FOV constraints according to the following result.

Proposition 1.1 *Given a point $Q = (\rho, \psi) \in \mathbb{R}^2$, the plane $X_w \times Z_w$ can be subdivided as follows (see figure 1.4).*

$\boldsymbol{Z_0}$: *in this region V-FOV constraint is never satisfied, i.e., $\rho \cos(\beta - \Gamma) < R_b$, for all β and ρ. Let $Z_0 = \big\{ (\rho, \psi) | \rho < R_b \big\}$ be such region of points Q, with R_b the minimal distance from O_w reachable with $\beta = \Gamma$;*

$\boldsymbol{Z_1}$: *in this region, recalling that $\phi_1 = \Gamma - \phi$ and $\phi_2 = \Gamma - \phi_2$, the*

following inequalities

$$|\beta - \phi_1| \ge |\rho \cos(\beta - \Gamma) - R_b| \ge 0 \,,$$
$$|\beta - \phi_2| \ge |\rho \cos(\beta - \Gamma) - R_b| \ge 0 \,,$$

hold for all β and ρ. In other words, V-FOV constraint is more restrictive than H-FOV ones. Let $Z_1 = \left\{ (\rho, \psi) | R_b \le \rho \le \frac{R_b}{\cos \phi} \right\}$ be such region of points Q;

Z_2: *in this region, recalling that $\phi_1 = \Gamma - \phi$ and $\phi_2 = \Gamma - \phi_2$, the following inequalities*

$$|\rho \cos(\beta - \Gamma) - R_b| > |\beta - \phi_1| \ge 0 \,,$$
$$|\rho \cos(\beta - \Gamma) - R_b| > |\beta - \phi_2| \ge 0 \,,$$

hold for all β and ρ. In other words, H-FOV constraint are more restrictive than V-FOV one. Let $Z_2 = \left\{ (\rho, \psi) | \rho > \frac{R_b}{\cos \phi} \right\}$ be such region of points Q.

The proof follows straightforwardly by trigonometric and geometric properties. Notice that, for $\rho = \frac{R_b}{\cos \phi}$ and $\beta = \phi_1$ (or $\beta = \phi_2$) both H-FOV and V-FOV constraints are active and vehicle is on the boundary between region Z_1 and region Z_2. As a consequence of Proposition 1.1, the shortest paths study can be simplified solving preliminarily two particular subproblem:

Problem 1: no restrictions on the *vertical* dimension of the FOV are placed, that is $\hat{\phi} = \pi/2$ and hence $\varepsilon = \pi$. As a consequence, $R_b = 0$ and all points Q of the motion plane belong to region Z_2 as shown in figure 1.5a. Notice that region Z_0 and region Z_1 degenerate in O_w.

Problem 2: no restrictions on the *horizontal* dimension of the FOV are placed, that is $\phi = \pi/2$ and hence $\delta = \pi$. As a consequence, all points Q with $\rho_Q \ge R_b$ belong to region Z_1 as shown in figure 1.5b. Notice that region Z_1 extends to the whole motion plane outside of region Z_0.

(a) Problem 1. (b) Problem 2.
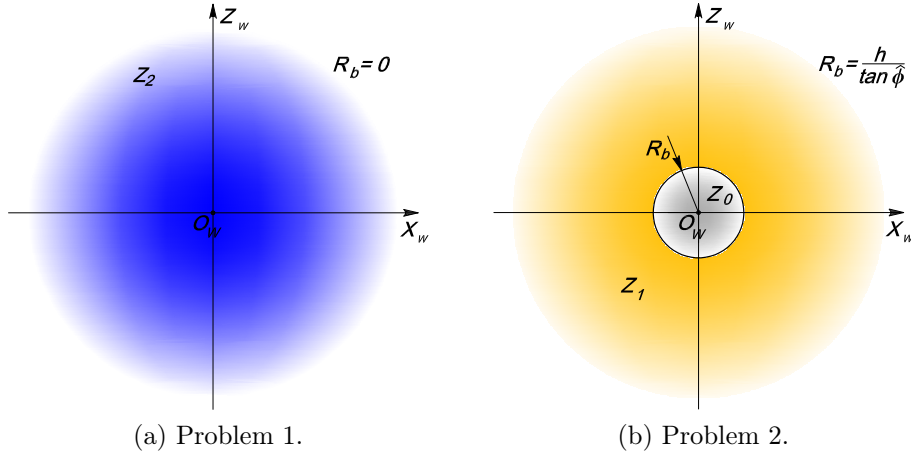
Figure 1.5: Subdivision of the motion plane according to particular cases in which no restriction on vertical or horizontal FOV is placed.

1.4 Problem 1: H-FOV Constraints

Let us consider a unicycle equipped with sensors which have no restrictions on the vertical dimensions. This kind of sensors can be modelled as a planar cone moving with the robot (see figure 1.6). For this reason, height h of the landmark on the motion plane, which corresponds to its Y_c coordinate in the sensor frame $\langle C \rangle$, is irrelevant to this particular problem. Therefore, it is necessary to know only the projection of the landmark on the motion plane, i.e., O_w. Notice that the planar cone model can be obtained by using the more complex four-sided right rectangular pyramid (see figure 1.3) assuming the vertical angle aperture $\varepsilon = \pi$.

The planar sensor system is fixed on the robotics platform so that axis Z_c forms an angle Γ with respect to the robot's forward direction, as generically shown in figure 1.6.

Referring to figure 1.6, the planar sensor, whose characteristic angle is $\delta = |\phi_2 - \phi_1|$, generates only constraints (1.6) and (1.7), i.e., for
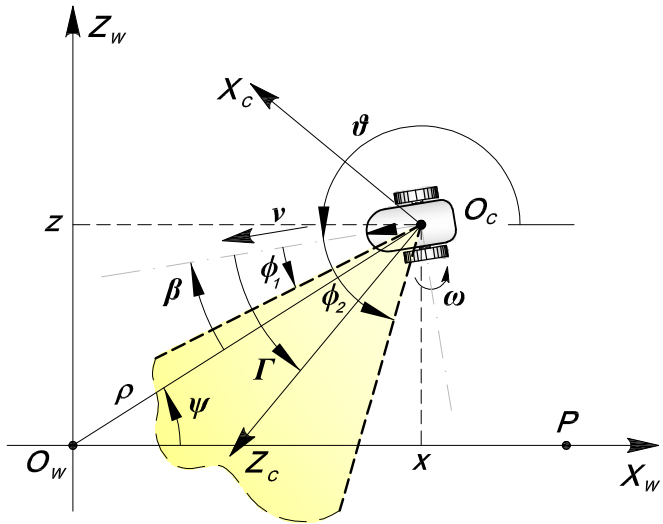
Figure 1.6: Nonholonomic vehicle equipped with a sensor modelled as a planar cone (shadowed in figure) which may not include robot's forward direction. Z_c axis, i.e., axis of symmetry for the sensor, forms an angle Γ with vehicle heading.

reader convenience,

$$\beta - \phi_1 \geq 0\,,$$
$$\beta - \phi_2 \leq 0\,,$$

for right and left sensor border, respectively. The time derivative of constraints (1.6) and (1.7) computed along the trajectories of system (1.5) brings to

$$\dot{\beta} = \frac{\sin\beta}{\rho}\,\nu - \omega\,, \tag{1.10}$$

for both constraints. From the theory of optimal control, with state

and control constraints [47], the associated Hamiltonian is

$$H(\eta, \nu, \omega) = |\nu| - \lambda_1 \cos \beta \nu + \lambda_2 \frac{\sin \beta}{\rho} \nu +$$
$$+ (\lambda_3 + \mu_1 + \mu_2) \left(\frac{\sin \beta}{\rho} \nu - \omega \right),$$

with $\lambda = (\lambda_1, \lambda_2, \lambda_3) \neq 0$ and $\mu = (\mu_1, \mu_2) \geq 0$. When constraints (1.6) and (1.7) are not active (i.e., $\mu = 0$), extremal curves, i.e., curves that satisfy necessary conditions for optimality, include straight lines (corresponding to $\omega = 0$ and denoted by the symbol S) and rotations on the spot (corresponding to $\nu = 0$ and denoted by the symbol $*$). Indeed, as rotations on the spot have zero length, the shortest path between two point is straightforward a straight line.

On the other hand, when $\mu > 0$ we have

$$\beta - \phi_1 \equiv 0 \qquad \Rightarrow \qquad \tan \beta = \tan \phi_1$$
$$\beta - \phi_2 \equiv 0 \qquad \Rightarrow \qquad \tan \beta = \tan \phi_2 \,,$$

and, by (1.5),

$$\dot{\psi} \;\; = \;\; \tan \phi \frac{\dot{\rho}}{\rho} = - \tan \phi_1 \frac{d}{dt} (\ln \rho) \,, \;\; \text{when } \beta = \phi_1 \qquad (1.11)$$

$$\dot{\psi} \;\; = \;\; \tan \phi_2 \frac{\dot{\rho}}{\rho} = - \tan \phi_2 \frac{d}{dt} (\ln \rho) \,, \;\; \text{when } \beta = \phi_2 \,. \qquad (1.12)$$

Integrating, we obtain

$$\psi \;\; = \;\; \tan \phi_1 \ln \left(\frac{\rho}{\rho_o} \right) , \;\; \text{when } \beta = \phi_1 \,, \qquad (1.13)$$

$$\psi \;\; = \;\; \tan \phi_2 \ln \left(\frac{\rho}{\rho_o} \right) , \;\; \text{when } \beta = \phi_2 \,, \qquad (1.14)$$

where ρ_o is a constant that depends on initial conditions. Equations (1.13) and (1.14) represent two logarithmic spirals with

(a) Symmetric Frontal: $\Gamma = 0$ (b) Frontal: $0 < \Gamma < \frac{\delta}{2}$
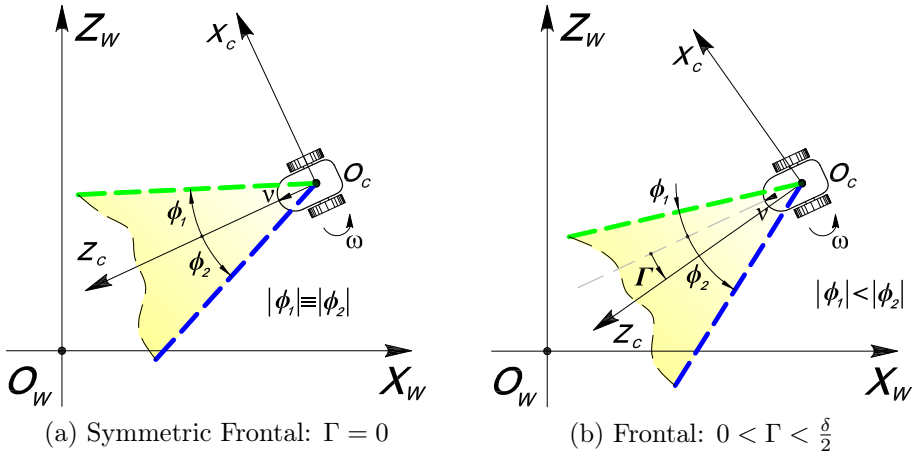
Figure 1.7: Robot's forward direction is included inside cone (shadowed in figures): $0 \leq \Gamma < \frac{\delta}{2}$.

characteristic angle ϕ_1 and ϕ_2, respectively, rotating around the landmark located in O_w. Logarithmic spirals with characteristic angle $\phi_i < 0$ rotate counterclockwise around O_w, whereas with $\phi_i > 0$ they rotate clockwise around O_w. We refer to these two kind of spirals as *Left* and *Right* and by symbols T_i^L and T_j^R with $i, j \in \{1, 2\}$. The adjectives "Left" and "Right" indicate the half-plane where the spiral starts for an on-board observer aiming at the landmark.

Notice that, with a characteristic angle $\phi = \pi/2$ spirals become circumferences centered in O_w, whereas for $\phi = 0$ spirals become half lines through O_w. We will denote these circumferences by symbol C and these half lines through O_w by symbol H. Moreover, as extremal arcs can be executed by the vehicle in either forward or backward direction, I will use superscripts $+$ and $-$ to make this explicit (e.g., S^- stands for a straight line executed backward).

In order to define the finite alphabet by which optimal paths can be built, it is worthwhile to consider separately the following cases, according to values of angles Γ and δ:

Extremal Paths for a Robot with Nonholonomic and Field-Of-View Constraints

Symmetric Frontal. Axis Z_c is aligned with robot's forward direction, i.e., $\Gamma = 0$ and $|\phi_1| = |\phi_2| = \phi$ as shown in figure 1.7a. As logarithmic spirals have the same characteristic angle ϕ, I omit subscript on symbols, that is $T^L \equiv T_1^L$ and $T^R \equiv T_2^R$. Hence, the alphabet of the Symmetric Frontal case is $\mathcal{A}_{\Gamma=0} = \{*, S^+, S^-, T^{L+}, T^{L-}, T^{R+}, T^{R-}\}$.

Frontal. In this case $0 < \Gamma < \frac{\delta}{2}$, and axis Z_c in not an axis of symmetry of the sensor. As a consequence, logarithmic spirals have two different characteristic angles, i.e., ϕ_1 and ϕ_2 with $|\phi_1| > |\phi_2|$, as shown in figure 1.7b. Hence, the alphabet of the Frontal case is $\mathcal{A}_{0<\Gamma<\frac{\delta}{2}} = \{*, S^+, S^-, T_1^{L+}, T_1^{L-}, T_2^{R+}, T_2^{R-}\}$.

Borderline Frontal. Axis Z_c forms an angle $\Gamma = \frac{\delta}{2}$ with respect to robot's forward direction (see figure 1.8a). Hence, right sensor border is aligned with vehicle heading and $\phi_1 = 0$, whereas $\phi_2 = \delta$. As a consequence, spiral T_1^L degenerates in a straight line through O_w, denoted by H. Hence, the alphabet of the Borderline Frontal case is $\mathcal{A}_{\Gamma=\frac{\delta}{2}} = \{*, S^+, S^-, H^+, H^-, T_2^{R+}, T_2^{R-}\}$.

Side. In this case, $\frac{\delta}{2} < \Gamma < \frac{\pi-\delta}{2}$, i.e., the planar cone is entirely contained inside a sector delimited by robot's forward direction and wheel axle direction, as shown in figure 1.8b. Hence, the alphabet of the Side case is $\mathcal{A}_{\frac{\delta}{2}<\Gamma<\frac{\pi-\delta}{2}} = \{*, S^+, S^-, T_1^{R+}, T_1^{R-}, T_2^{R+}, T_2^{R-}\}$, where both spirals rotate counterclockwise around O_w.

Borderline Side. Axis Z_c forms an angle $\Gamma = \frac{\pi-\delta}{2}$ with respect to robot's forward direction. Hence, left sensor border is aligned with wheels axle direction, with $\phi_1 = \frac{\pi}{2} - \delta$ and $\phi_2 = \frac{\pi}{2}$, as shown in figure 1.8c. For this reason, spiral T_2^R degenerates in a circumference centered in O_w, denoted by C, and the alphabet of the Borderline Side case is $\mathcal{A}_{\Gamma=\frac{\pi-\delta}{2}} = \{*, S^+, S^-, T_1^{R+}, T_1^{R-}, C^+, C^-\}$.

(a) Borderline Frontal: $\Gamma = \frac{\delta}{2}$

(b) Side: $\frac{\delta}{2} < \Gamma < \frac{\pi-\delta}{2}$

(c) Borderline Side: $\Gamma = \frac{\pi-\delta}{2}$
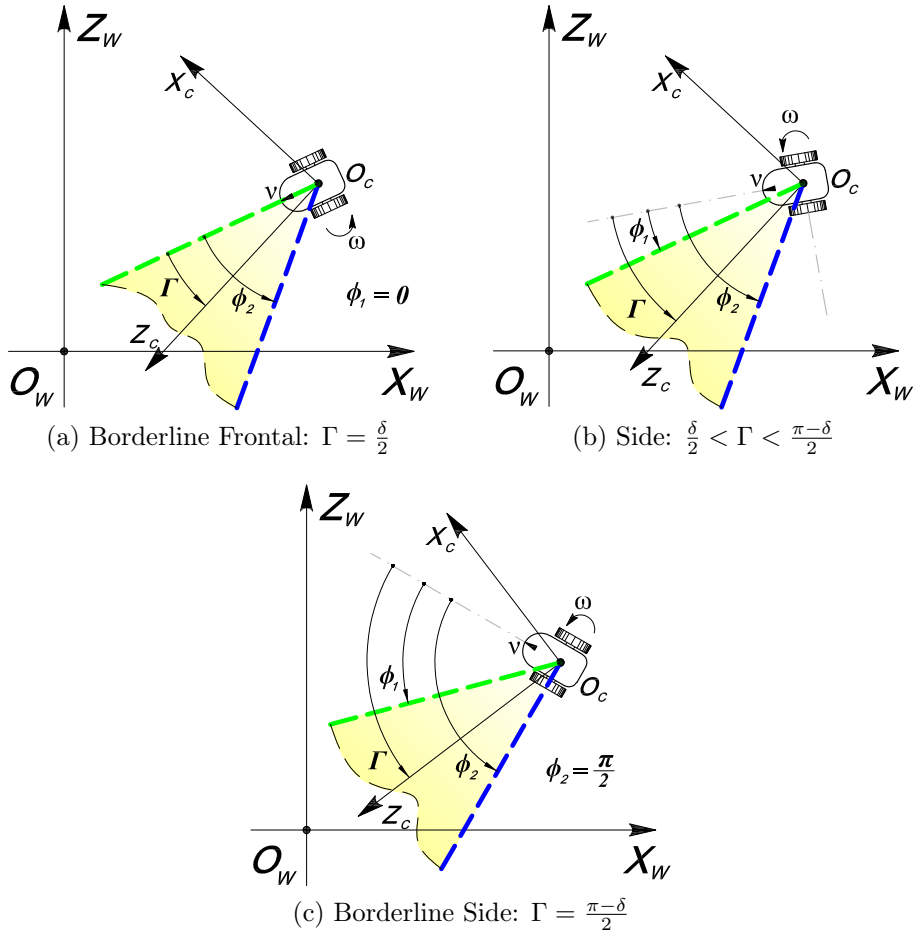
Figure 1.8: Robot's forward direction is not included inside cone (shadowed in figures): $\frac{\delta}{2} \leq \Gamma \leq \frac{\pi-\delta}{2}$.

Lateral. In this case $\frac{\pi-\delta}{2} < \Gamma < \frac{\pi}{2}$ and wheels axle direction is included inside planar cone, as shown in figure 1.9a. Logarithmic spirals have two different characteristic angle, with $\phi_1 < \frac{\pi}{2} < \phi_2$. As a consequence, the alphabet of the Lateral case is $\mathcal{A}_{\frac{\pi-\delta}{2} < \Gamma < \frac{\pi}{2}} = \left\{ *, S^+, S^-, T_1^{R+}, T_1^{R-}, T_2^{L+}, T_2^{L-} \right\}$. Notice that,

spiral with characteristic angle ϕ_2 becomes a left spiral and the vehicle must move on T_2^L backward to move towards O_w rather than forward as in the Frontal case.

Symmetric Lateral. In this case $\Gamma = \frac{\pi}{2}$ and hence, axis Z_c is aligned with wheels axle direction (see figure 1.9b). Logarithmic spirals have characteristic angles $\phi_1 = \frac{\pi - \delta}{2}$ and $\phi_2 = \frac{\pi + \delta}{2}$, and equations are

$$\rho_1 = \rho_{1o}\, e^{\psi\, t_1}$$
$$\rho_2 = \rho_{2o}\, e^{\psi\, t_2},$$

where $t_1 = 1/\tan\left(\frac{\pi - \delta}{2}\right)$, whereas $t_2 = 1/\tan\left(\frac{\pi + \delta}{2}\right) = -t_1$, i.e., two logarithmic spirals, right and left respectively, with the same characteristic angle $\phi = \frac{\pi - \delta}{2}$. For this reason, I omit subscript on symbols, i.e., $T^L \equiv T_1^L$ and $T^R \equiv T_2^R$. The alphabet of the Symmetric Lateral case is $\mathcal{A}_{\Gamma = \frac{\pi}{2}} = \left\{*,\, S^+,\, S^-,\, T^{R+},\, T^{R-},\, T^{L+},\, T^{L-}\right\}$. Notice that, even in this case, the vehicle must move on T^L backward to move towards O_w.

In conclusion, extremal paths consist of sequences of symbols, or *words*, in the finite alphabet $\mathcal{A}_\Gamma = \left\{*,\, S^+,\, S^-,\, E_1^+,\, E_1^-,\, E_2^+,\, E_2^-\right\}$, where the actual meaning of symbols depends on angles Γ and δ as discuss previously. Rotations on the spot ($*$) have zero length, but may be used to properly connect other maneuvers. The set of possible words generated by the symbols in $\mathcal{A}_\Gamma$ is a language $\mathcal{L}_\Gamma$.

Following Chapters 2 and 3 are dedicated to showing that, due to the physical and geometrical constraints of the considered problem, a sufficient optimal finite language $\mathcal{L}_\Gamma^O \subset \mathcal{L}_\Gamma$ can be built such that, for any initial condition, it contains a word describing a path to the goal which is no longer than any other feasible path. Correspondingly, a partition of the plane in a finite number of regions is described, for which the shortest path is one of the words in $\mathcal{L}_\Gamma^O$. In particular, in Chapter 2, the shortest path synthesis in case of $\Gamma = 0$ (i.e., the Symmetric Frontal) is obtained, exploiting the symmetric properties of the problem. Then, by using most of the results obtained for the

(a) Lateral: $\frac{\pi - \delta}{2} < \Gamma < \frac{\pi}{2}$ (b) Symmetric Lateral: $\Gamma = \frac{\pi}{2}$
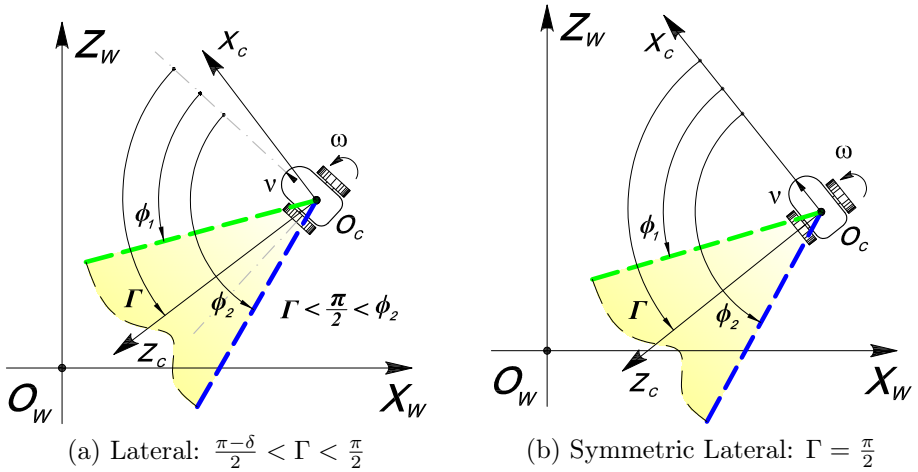
Figure 1.9: The wheel axle direction is included inside cone (shadowed in figures): $\frac{\pi - \delta}{2} < \Gamma \leq \frac{\pi}{2}$.

Symmetric Frontal case, in Chapter 3 the shortest path synthesis for all values of Γ will be given showing that the Symmetric Frontal is a particular case of the Frontal one.

Remark 1.1 *In previous section, we have considered the most interesting case in which $\delta < \frac{\pi}{2}$. Of course, extremal curves for $\delta \geq \frac{\pi}{2}$ and $0 \leq \Gamma \leq \frac{\pi}{2}$ can be obtained appropriately exploiting previous results. For example, let us consider the particular case in which $\delta = \frac{\pi}{2}$ and $\Gamma = \frac{\delta}{2}$. In this case, the right sensor border is aligned with the robot motion direction whereas the left sensor border is aligned with the axle direction. As a consequence, the extremal curves are straight line (S), rotation on the spot (∗), straight line through O_w (H) and circumference centered in O_w (C), that is the finite alphabet $\{*, S^+, S^-, H^+, H^-, C^+, C^-\}$.*

For $\phi \geq \frac{\pi}{2}$, a straight line followed forward and/or backward so as to keep the feature in view is always feasible and, hence, trivially optimal. In the rest of this chapter, we will only be concerned with the non-trivial case $\phi \in [0, \frac{\pi}{2}]$.

Remark 1.2 *For other values of* Γ*, the extremal curves and consequently, the shortest path synthesis can be obtained straightforwardly. In case of* $\frac{\pi}{2} < \Gamma \leq \pi$ *can be easy obtained by using that one for* $0 \leq \Gamma \leq \frac{\pi}{2}$ *considering extremal arcs and hence optimal paths followed in reverse order, i.e., forward arcs in backward arcs and viceversa. Finally, a symmetry w.r.t.* X_w *axis of each optimal synthesis of the motion plane for each* $\Gamma \in [0, \pi]$ *allows to obtain the corresponding synthesis for* $\Gamma \in [-\pi, 0]$*.*

1.5 Problem 2: V-FOV Constraints

In this section, I will analyze *Problem 2* for which sensors have no restrictions on the horizontal limits. This particular sensor model can be obtained by the four sided right rectangular pyramid model assuming angles $\delta = \pi$ and $\varepsilon = 2\hat{\phi}$, where $\hat{\phi}$ is the vertical characteristic angle of the sensor. In other words, sensor here is modeled as a portion of plane delimited by two straight line which are sensor's vertical borders (see figure 1.10). In this thesis, I will consider only the particular case with $\Gamma = 0$. The study of the other cases, i.e., with $0 < \Gamma \leq \frac{\pi}{2}$ and then for all values of Γ, is still an open issue and left to future works. Height h of the landmark on the motion plane, which corresponds to its Y_c coordinate in the sensor frame $\langle C \rangle$, is important for this particular problem. For $\Gamma = 0$ Sensor limits generate constraint

$$\rho \cos \beta \geq \frac{h}{\tan \hat{\phi}} = R_b \qquad \beta \in \left] -\frac{\pi}{2}, \frac{\pi}{2} \right[, \qquad (1.15)$$

for upper or lower sensor border, depending on $h > 0$ or $h < 0$, respectively. Notice that, with $\beta = 0$ landmark position w.r.t. $\langle C \rangle$ is $^cF = [0 \ h \ R_b]$ and vehicle reaches the minimum distance, i.e., R_b, from landmark without violating sensor constraint (1.15). As a consequence, vehicle is not able to reach any point with $\rho < R_b$; for this reason, point P is assumed to be on axis X_w, but with $\rho_P \geq R_b$.
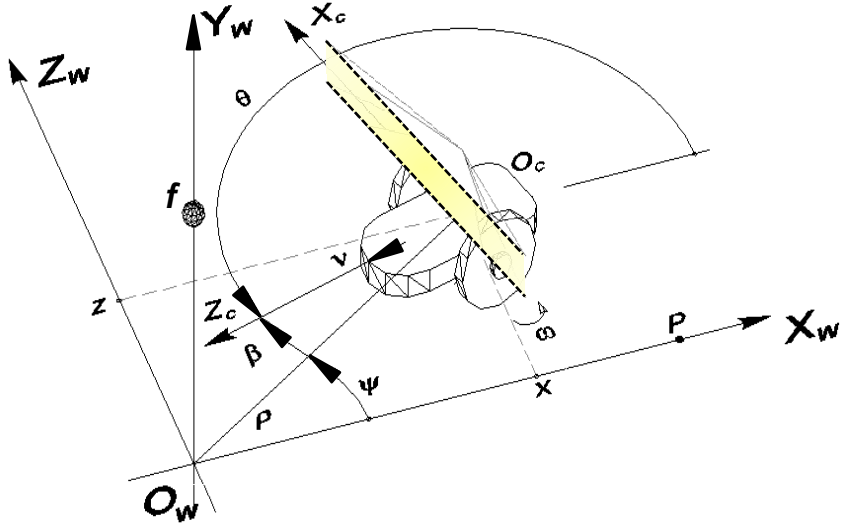
Figure 1.10: Sensor's horizontal borders with $\Gamma = 0$.

The goal here is again to determine, for any point $Q \in \mathbb{R}^2 \setminus R_0$ (see figure 1.5b) in the robot space, the shortest path from Q to P such that the landmark is maintained within sensor limits, i.e., to minimize the cost functional

$$L = \int_0^\tau |\nu| \, dt \, ,$$

under the *feasibility constraints* (1.5), (1.3), and (1.15), where τ is the time needed to reach P that is $\rho(\tau) = \rho_P, \psi(\tau) = 0$.

The time derivative of constraint (1.15) computed along the trajectories of system (1.5) brings to

$$u + \omega \rho \sin \beta = 0 \, . \tag{1.16}$$

From the theory of optimal control with state and control constraints

(see [47]), the associated Hamiltonian is

$$H(\eta, \nu, \omega) = |\nu| - \lambda_1 \cos\beta\nu + \lambda_2 \frac{\sin\beta}{\rho}\nu +$$
$$+ (\lambda_3 + \mu)(u + \omega\rho\sin\beta),$$

with $\lambda = (\lambda_1, \lambda_2, \lambda_3) \neq 0$ and $\mu \geq 0$. As for *Problem 1*, when constraint (1.15) is not active (i.e., $\mu = 0$), extremal curves, i.e., curves that satisfy necessary conditions for optimality, include straight lines (corresponding to $\omega = 0$ and denoted by the symbol S) and rotations on the spot (corresponding to $\nu = 0$ and denoted by the symbol $*$).

On the other hand, when $\mu > 0$ we have

$$u + \omega\rho\sin\beta = 0,$$

and the robot must follow a curve which equation is

$$\rho\cos\beta = R_b \qquad\qquad (1.17)$$

to maintain active the constraint.

Equation (1.17) is known as an *involute of a circle* expressed by polar coordinates and with $\psi = \psi_b + \tan\beta - \beta$, where ψ_b is the angular coordinate of a point on the involute such that $\beta = 0$, and hence $\rho = R_b$. The involute of a circle is the path traced out by a point on a straight line that rolls around a circle without slipping (see figure 1.11). Moreover, for any point on circumference C_{R_b} with radius R_b and centered in O_w there are two involutes of circle, rotating counterclockwise ($\beta > 0$) and clockwise ($\beta < 0$) around the landmark located in O_w. We refer to these two involutes as *Right* and *Left*, and by symbols I^R and I^L, respectively. The adjectives "Right" and "Left" indicate the half-plane where the spiral starts for an on-board observer aiming at the landmark. In conclusion, if $\Gamma = 0$, four extremal maneuvers are obtained and represented by symbols $\{*, S, I^R, I^L\}$. Moreover, as extremal arcs can be executed by the vehicle in either forward or backward direction, superscripts $+$ and $-$ will be used in
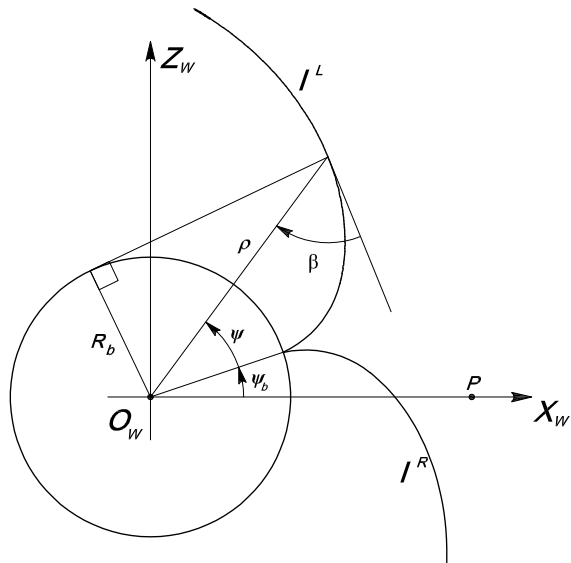
Figure 1.11: Extremal arc in case of $\Gamma = 0$: the involute of a circle.

the following in order to make this explicit. As a consequence, extremal paths consist of sequences, or *words*, comprised of symbols in the finite alphabet $\mathcal{B}_{\Gamma=0} = \big\{ *, \ S^+, \ S^-, \ I^{R+}, \ I^{R-}, \ I^{L+}, \ I^{L-} \big\}$. Rotations on the spot $(*)$ have zero length, but may be used to properly connect other maneuvers. The set of possible words generated by the symbols in $\mathcal{B}_{\Gamma=0}$ is a language $\mathcal{L}_{\Gamma=0}$.

Next section is dedicated to present only some preliminary results and for the particular case in which $\Gamma = 0$. The complete optimal synthesis and partition of the motion plane is still an open issue.

1.5.1 Some preliminary results

In this section, as a preliminary result, regions whose points Q are reachable by a forward or a backward straight line without violating the V-FOV constraints, will be characterized for $\Gamma = 0$. In this regard,
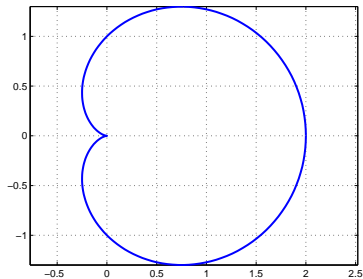
(a) Limaçon of Pascal with $a = b$.
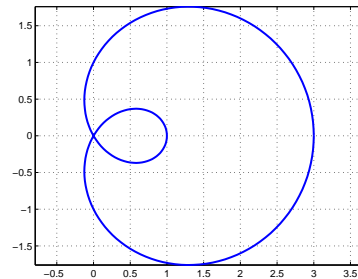
(b) Limaçon of Pascal with $a < b$.
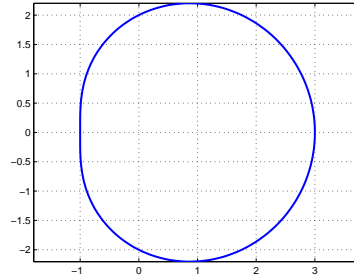
(c) Limaçon of Pascal with $a > b$.

Figure 1.12: Limaçon of Pascal $\rho = a + b \cos \beta$ for different values of parameters a and b.

let us preliminarily introduce a particular polar curve of the form

$$\rho = a + b \cos \beta \,,$$

also called the *Limaçon of Pascal* (see figure 1.12). It was discovered by Ètienne Pascal, father of Blase Pascal, and the word "Limaçon" comes from the latin "limax", meaning "snail". It is defined as a roulette formed when a circle C_1 with radius b rolls around the outside of a circle C_2 of equal radius and the point generating the roulette is at distance a from the center of circle C_1. Thus, they belong to the family of curves called centered trochoids, more specifically, epitro-
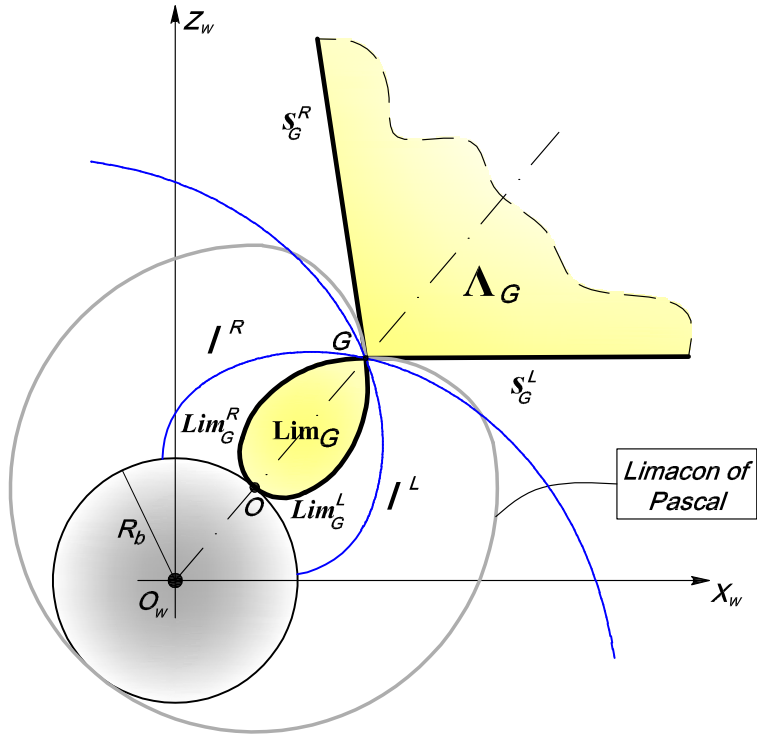
Figure 1.13: Region Lim_G with its border $\partial Lim_G = Lim_G^R \cup Lim_G^L$ and cone Λ_G delimited by half-lines s_G^R and s_G^L.

choids. The cardioid is the special case in which the point generating the roulette lies on the rolling circle and the resulting curve has a cusp.

Definition 1.1 *For a point* $G \in \mathbb{R}^2$, *let* Lim_G^R (Lim_G^L) *denote the arc of the Limaçon from* G *to* O *such that,* $\forall V \in Lim_G^R$ (Lim_G^L), $\widehat{GVO_w} = \pi - \bar{\beta}$, *with* $\bar{\beta} = \arctan\left(\frac{\rho_G}{h} \tan\hat{\phi} \sin\beta\right)$, *in the half-plane on the right (left) of* $\overline{GO_w}$ *(cf. figure 1.13). Also, let* Lim_G *denote the region delimited by* Lim_G^R *and* Lim_G^L *from* G *to* O.

We will refer to Lim_G^R (Lim_G^L) as the right (left) $\hat{\phi}$-arc in G.

Definition 1.2 *For a point $G \in \mathbb{R}^2$, let s_G^R (s_G^L) denote the half-line from G forming an angle $\psi_G + \tilde{\beta}$ ($\psi_G - \tilde{\beta}$), where $\tilde{\beta} = \arccos\left(\frac{h}{\rho_G \tan \hat{\phi}}\right)$, with the X_w axis (cf. figure 1.13). Also, let Λ_G denote the cone delimited by s_G^R and s_G^L.*

We will refer to s_G^R (s_G^L) as the right (left) $\hat{\phi}$-radius in G.

Proposition 1.2 *For any starting point Q, all points of Lim_Q (Λ_G) are reachable by a forward (backward) straight path without violating the FOV constraint.*

Proof: Thanks to projective geometry properties (see [48]), for any elementary maneuvers of the vehicle, i.e., rotations on the spot and straight line motion, it is possible to know as feature moves within the sensor limits and in particular, values of state variables ρ, ψ and β whenever V-FOV is active. Indeed, for any starting point $Q = (\rho_Q, \psi_Q)$, V-FOV constraints is active after a rotation on the spot of angle $\beta_{MAX} = \arccos\left(\frac{h}{\rho_G \tan \hat{\phi}}\right)$ and hence, region of points reachable with a backward straight line is Δ_G. In order to determine the region reachable with a forward straight line, let us suppose $\eta_Q = (\rho_Q, \psi_Q, \beta_Q)$ with $\beta_Q \in] - \beta_{MAX}, \beta_{MAX}[$. Of course, V-FOV is not active yet but it will be after a forward straight line such that $\beta^* = \arctan\left(\frac{\rho_G}{h} \tan \hat{\phi} \sin \beta_Q\right)$ and $\rho_Q = \frac{R_b}{\cos \beta^*}$. By using the Carnot theorem, also called cosine rule, distance d covered by the vehicle is $d = a + b \cos \beta$ with $a = R_b$ and $b = \frac{\tan \hat{\phi}}{h} \rho_G R_b > a$, i.e., a Limaçon of Pascal as show in figure 1.12b. As a consequence, points of Lim_Q are reachable by a forward straight line. ■

1.6 Extremal Curves with the Pyramid Sensor Model

In previous sections, extremal curves corresponding to two simplified cases have been obtained. In particular, in section 1.4 extremal curves

for a nonholonomic vehicle equipped with a planar cone whose axis of symmetry forms a generic angle Γ with respect to vehicle heading have been found, showing that extremal paths consist of sequences of symbols in the finite alphabet $\mathcal{A}_\Gamma = \left\{ *,\ S^+,\ S^-,\ E_1^+,\ E_1^-,\ E_2^+,\ E_2^- \right\}$. Extremal curves E_1 and E_2 could be spirals (denoted with T_i^R and T_j^L, with $i,\ j \in \left\{ 1, 2 \right\}$), circumference centered in O_w (denoted with C) or straight line through O_w (denoted with H), depending on values of angles Γ and δ. On the other hand, in section 1.5, considering only the case with $\Gamma = 0$, extremal curves for a vehicle equipped with a sensor modelled as a portion of plane delimited by two straight line, i.e., sensor's vertical borders, and perpendicular to the motion plane have been found, showing that extremal paths consist of sequences of symbols in the finite alphabet $\mathcal{B}_{\Gamma=0} = \left\{ *,\ S^+,\ S^-,\ I^{R+},\ I^{R-},\ I^{L+},\ I^{L-} \right\}$.

Let us consider now a sensor with both vertical and horizontal limits and, based on results obtained in previous sections, let us consider axis Z_c aligned with the robot's forward direction, i.e., $\Gamma = 0$. The model adopted in this thesis is a four-sided right rectangular pyramid and extremal curves can be obtained from results reported in sections 1.4 and 1.5. Therefore, based on sensor constraints analysis done in section 1.3, the motion plane is subdivided into three regions, as shown in figure 1.5. The first region, named Z_0, is the set of points that vehicle is not able to reach without violate the sensor constraints. In the second region, named Z_1, the V-FOV constraint is the first to be violated whatever maneuver the vehicle performs. Hence, for any Q in Z_1, it is straightforward to consider only the alphabet $\mathcal{B}_\Gamma$ in order to find optimal path from Q to P, if P belongs to this region, or from Q to the boundary between Z_1 and Z_2, if P belongs to Z_2. The third region, named Z_2, H-FOV constraints are the first to be violated whatever maneuver the vehicle performs. As a consequence, it is sufficient to consider only the alphabet $\mathcal{A}_\Gamma$ in order to find optimal path from Q to P, if P belongs to Z_2, or from Q to the boundary between Z_1 and Z_2, if P belongs to Z_1.

Anyway, as optimal synthesis of shortest paths for the problem 2 is not available yet, the optimal synthesis in case of both V-FOV

and H-FOV constraints is an open issue and left to future works. For this reason, next chapters are dedicated to solve completely the shortest path synthesis for Problem 1, i.e., considering only H-FOV, and to define a feedback control laws capable of maintaining the vehicle aligned with these shortest path from any initial robot position to the desired one.

1.7 Conclusion

In this chapter I have provided a complete characterization of extremal curves for a vehicle with nonholonomic kinematics to reach a desired configuration along the shortest paths while keeping a fixed point within a four-sided right rectangular pyramid region relative to itself. Based on the analysis of FOV constraints, the study has been simplified considering separately two particular subproblem. The first problem, named *Problem 1*, concerns only the Horizontal-FOV constraints and extremal curves are straight line (denoted by S), rotation on the spot (denoted by $*$) and, depending on the horizontal angle aperture of the sensor and on the angle between robot's motion direction and the symmetric axis of the sensor, spirals (denoted with T_i^R and T_j^L, with $i, j \in \{1, 2\}$), circumference centered in O_w (denoted with C) or straight line through O_w (denoted with H). Following Chapters 2 and 3 are dedicated to showing that, due to the physical and geometrical constraints of the considered problem, a sufficient optimal finite language can be built such that, for any initial condition, it contains a word describing a path to the goal which is no longer than any other feasible path. Correspondingly, a partition of the plane in a finite number of regions is described, for which the shortest path is one of the words in the optimal finite language.

The second problem, named *Problem 2*, concerns only the Vertical-FOV constraint and, having considered $\Gamma = 0$, extremal curves are straight line, rotation on the spot and involute of circle (denoted by I^R and I^L). In previous section 1.5.1, only some preliminary have

been presented for $\Gamma = 0$. The generalization to any values of Γ, the complete optimal synthesis and the partition of the motion plane is still an open issue and hence, left to future works. As a consequence, also the complete optimal solution in case of a sensor modelled as a four sided right rectangular pyramid is not possible yet and left to future work.

Chapter 2

Shortest Paths Synthesis With Symmetrically Limited Planar Sensors

THIS CHAPTER presents a complete characterization of shortest paths to a goal position for a robot with unicycle kinematics and an on-board sensor with symmetric and planar (i.e., without V-FOV constraints) limited Field-Of-View, which must keep a given landmark in sight. In particular, I provide a complete optimal synthesis for the problem, i.e., a global partition of the motion plane induced by shortest paths, such that a word in the optimal finite language is univocally associated to a region and completely describes the shortest path from any starting point in that region to the goal point. Results reported in this chapter can be found in papers [A1, A2].

2.1   Introduction

In chapter 1, it has been proved that for a nonholonomic vehicle equipped with a frontal, symmetric and planar sensor with limited FOV (i.e., with $\Gamma = 0$), as shown in figure 2.1, extremal maneu-

vers are represented by the symbols $\{*,\, S,\, T^R,\, T^L\}$, i.e., rotations on the spot, straight lines and right, left logarithmic spirals. Moreover, as extremal arcs can be executed by the vehicle in either forward or backward direction, I will build extremal paths consisting of sequences, or *words*, comprised of symbols in the finite alphabet $\mathcal{A}_{\Gamma=0} = \{*,\, S^+,\, S^-,\, T^{R+},\, T^{R-},\, T^{L+},\, T^{L-}\}$. The set of possible words generated by the above symbols is a language $\mathcal{L}_{\Gamma=0}$.

Following sections are dedicated to show that, due to the physical and geometrical constraints of the considered problem, a sufficient optimal finite language $\mathcal{L}^O_{\Gamma=0} \subset \mathcal{L}_{\Gamma=0}$ can be built such that, for any initial condition, it contains a word describing a path to the goal which is no longer than any other feasible path. Correspondingly, a partition of the plane in a finite number of regions is described, for which the shortest path is one of the words in $\mathcal{L}^O_{\Gamma=0}$.

2.2 Shortest paths synthesis: symmetries and invariants

In this section, I introduce the basic tools that will allow me to study the optimal synthesis on the whole state space of the robot.

Let $\eta(\tau)$ denote a trajectory of the vehicle corresponding to a solution of (1.5) with (1.3). Because I am interested in finding shortest paths for the vehicle's center point, let us define a *path* γ as the canonical projection of the graph $(\eta(\tau),\, \tau)$ on the first two coordinates. In other terms, a path γ parameterized by t, is a continuous map from the interval $I = [0, 1]$ to the plane of motion $\gamma(t) = (\rho(t),\, \psi(t))$, $t \in I$. We denote with $\mathcal{P}_Q$ the set of all feasible extremal paths from $\gamma(0) = Q$ to $\gamma(1) = P$.

Definition 2.1 *Given the goal point P, with $P = (\rho_P, 0)$ in polar coordinates, and $Q \in \mathbb{R}^2 \setminus O_w$, $Q = (\rho_Q, \psi_Q)$ with $\rho_Q \neq 0$, let $f_Q :$*
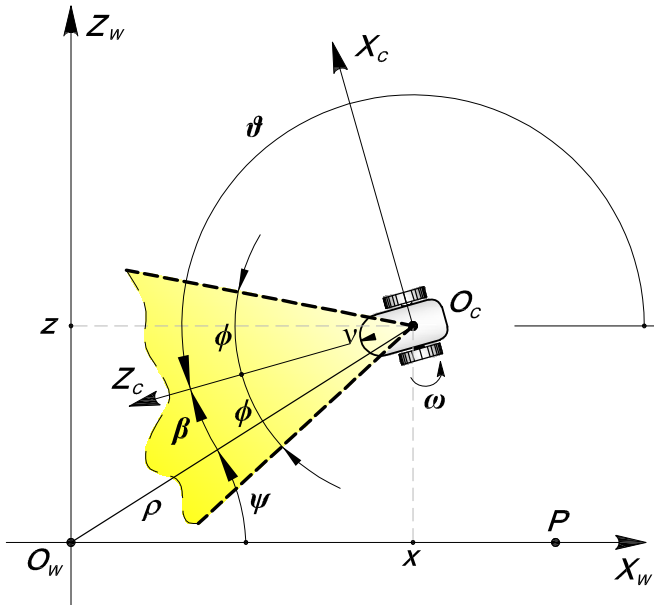
Figure 2.1: Mobile robot and systems coordinates. The robot's task is to reach P while keeping O_w within a limited FOV (shadowed in figure).

$\mathbb{R}^2 \to \mathbb{R}^2$ *denote the map*

$$f_Q \left(\rho_G, \psi_G\right) = \begin{cases} \left(\dfrac{\rho_G \rho_P}{\rho_Q}, \psi_Q - \psi_G\right) & \text{for } \rho_G \neq 0 \\ (0,0) & \text{otherwise.} \end{cases} \tag{2.1}$$

Remark 2.1 *The map f_Q can be regarded as the combination of a clockwise rotation R_Q by an angle ψ_Q, a scaling S_Q by a factor ρ_P/ρ_Q, and an axial symmetry w.r.t. X_w. Indeed, if $R_Q : (\rho, \psi) \mapsto (\rho, \psi - \psi_Q)$ and $S_Q : (\rho, \psi) \mapsto (\rho(\rho_P/\rho_Q), \psi)$, we have $R_Q \circ S_Q : (\rho, \psi) \mapsto (\rho\rho_P/\rho_Q, \psi - \psi_Q)$.*

Definition 2.2 *Given the goal point $P = (\rho_P, 0)$ and $Q = (\rho_Q, \psi_Q)$*

with $\rho_Q \neq 0$, let the path transform *function* F_Q *be defined as*

$$F_Q : \mathcal{P}_Q \rightarrow \mathcal{P}_{f_Q(P)}$$
$$\gamma(t) \mapsto f_Q(\gamma(1-t)), \ \forall t \in I. \tag{2.2}$$

Remark 2.2 *Notice that* $\tilde{\gamma}(t) = F_Q(\gamma(1-t))$ *corresponds to* $\gamma(t)$ *transformed by* f_Q *and followed in opposite direction. Indeed,* $\tilde{\gamma}$ *is a path from* $\tilde{\gamma}(0) = f_Q(P)$ *to* $\tilde{\gamma}(1) = f_Q(Q) \equiv P$.

Turning our attention back to the map $f_Q(\cdot)$, it can be noticed that point Q is transformed in $f_Q(Q) = P$, while P goes into $f_Q(P) = \left(\frac{\rho_P^2}{\rho_Q}, \psi_Q \right)$.

Consider now the locus of points Q such that it further holds $f_Q(P) = Q$. This is clearly the circumference with center in O_w and radius ρ_P. We will denote this circumference, which will have an important role in the following developments, by $C(P)$. Properties of F_Q will allow me to solve the synthesis problem from points on $C(P)$, hence to extend the synthesis to any point inside the circle, and finally to the whole motion plane.

Remark 2.3 *As a first consequence of the fact that* $\forall Q \in C(P)$, $f_Q(P) = Q$ *and* $f_Q(Q) = P$, *we have that* $\mathcal{P}_Q$ *is* F_Q*-invariant, i.e.* $Q \in C(P) \Rightarrow \forall \gamma \in \mathcal{P}_Q, F_Q(\gamma) \in \mathcal{P}_{f_Q(P)} \equiv \mathcal{P}_Q$.

Notice that Remark 2.1 is valid also for F_Q. As a consequence $F_{f_Q(P)}(F_Q(\gamma)) \equiv \gamma$. Furthermore, F_Q transforms forward straight lines in backward straight lines and viceversa. Moreover, F_Q maps left spiral arcs (T^{L+} and T^{L-}) in right spiral arcs (T^{R-} and T^{R+} respectively) and viceversa. Hence, F_Q maps extremal paths in $\mathcal{L}_{\Gamma=0}$ in extremal paths in $\mathcal{L}_{\Gamma=0}$. For example, let $w = S^- * T^{R-} * S^+ * T^{L+}$ be the word that characterize a path from Q to P, the transformed extremal path is of type $z = T^{R-} * S^- * T^{L+} * S^+$. With a slight abuse of notation, I will write $z = F_Q(w)$.

From previous remarks we also obtain that an extremal path $\gamma \in \mathcal{P}_Q$ with $Q \in C(P)$ is mapped in an extremal path $\tilde{\gamma} \in \mathcal{P}_Q$ symmetric to γ w.r.t. the bisectrix r of the angle $\widehat{QO_wP}$.
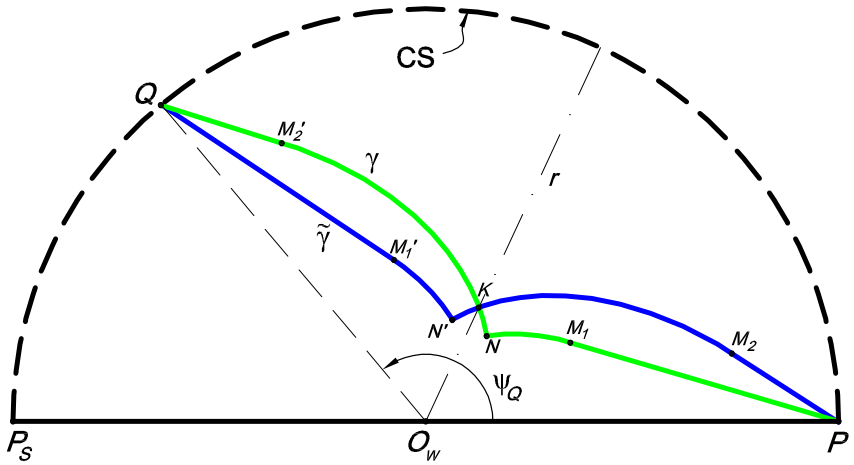
Figure 2.2: Construction of a palindrome symmetric path: γ is a generic path from Q to P and $\tilde{\gamma}$ the symmetric to γ w.r.t. the bisectrix r.

In the following, we will denote by $D(P)$ the closed disc within $C(P)$. Due to the symmetry of the problem, however, the analysis of optimal paths in $\mathcal{P}_Q$ can be done considering only the upper half plane w.r.t. the X_w axis. We denote therefore by DS the closure of the semidisk in the positive Z_w half-plane, by CS the upper semicircumference, and by $\overline{P_sP}$ the diameter such that $\partial DS = CS \cup \overline{P_sP}$ (see fig. 2.2).

Proposition 2.1 *Given $Q \in \mathbb{R}^2$ and a path $\gamma \in \mathcal{P}_Q$ of length l, the length of the transformed path $\tilde{\gamma} = F_Q(\gamma)$ is $\tilde{l} = \frac{\rho_P}{\rho_Q}l$.*

Proof: Given $Q \in (X_w, Z_w)$, from Remark 2.1, straight lines are scaled by ρ_P/ρ_Q. The distance of two points $P_1 = (\rho_1, \psi_1)$ and $P_2 = (\rho_2, \psi_2)$ on a logarithmic spiral with characteristic angle ϕ is $d = (\rho_1 - \rho_2)/\cos\phi$. Hence, the distance between transformed points is scaled by ρ_P/ρ_Q. The total path length is thus scaled by ρ_P/ρ_Q, i.e. increased if $Q \in DS$ and decreased if $Q \notin DS$. ∎

Definition 2.3 *An extremal path starting from Q and described by a word $w \in \mathcal{L}_{\Gamma=0}$ is a* palindrome path *if the transformed path through F_Q is also described by w.*

Definition 2.4 *An extremal path in $\mathcal{P}_Q$ which is a palindrome path and is symmetric w.r.t. the bisectrix r of $\widehat{QO_wP}$, is called a* palindrome symmetric path*.*

Proposition 2.2 *For any path in $\mathcal{P}_Q$ with $Q \in CS$ there always exists a palindrome symmetric path in $\mathcal{P}_Q$ whose length is shorter or equal.*

Proof: Consider $\gamma \in \mathcal{P}_Q$ with $Q \in CS$, and $\tilde{\gamma} = F_Q(\gamma)$ the transformed path, which is symmetric to γ w.r.t. the bisectrix r of $\widehat{QO_wP}$ (see fig. 2.2). Indeed, in this case, F_Q consists only in a rotation and axial symmetry, hence it corresponds to the bisectrix symmetry. Hence, from Proposition 2.1, γ and $\tilde{\gamma}$ have the same length l. Let $K \in r$ be the intersection point of the two paths, I denote with γ_1 and γ_2 ($\tilde{\gamma}_1$ and $\tilde{\gamma}_2$) the sub–paths of γ ($\tilde{\gamma}$) from Q to K and from K to P respectively. From the definition of $\tilde{\gamma}$, the length l_1 of γ_1 is equal to the length $\tilde{l}_2$ of $\tilde{\gamma}_2$, and the length l_2 of γ_2 is equal to the length $\tilde{l}_1$ of $\tilde{\gamma}_1$. Furthermore, $l_1 + l_2 = \tilde{l}_1 + \tilde{l}_2 = l$.

Suppose that $l_1 \geq l_2 = \tilde{l}_1$, then the path from Q to P obtained from a concatenation of $\tilde{\gamma}_1$ and γ_2 has length $\tilde{l}_1 + l_2 = 2l_2$ smaller than, or equal to, the length l of γ, and it is feasible and symmetric w.r.t. the bisectrix r, i.e., a palindrome symmetric path. If $l_1 < l_2$ the construction of a palindrome symmetric path can be done equivalently using γ_1 and $\tilde{\gamma}_2$. ∎

An important consequence of the properties of the path transform F_Q is the following

Theorem 2.1 *For any path in $\mathcal{P}_Q$ with $Q \in \partial DS$ there always exists a path in $\mathcal{P}_Q$ which evolves completely within DS whose length is shorter or equal.*
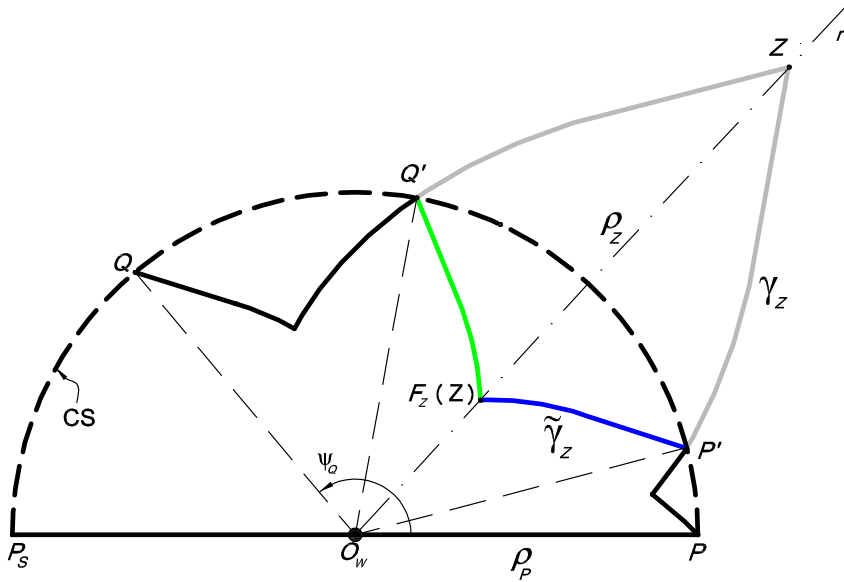
Figure 2.3: Construction of a path which evolves completely within DS: the path from Q to P throught points Q', Z and P' is shortened by the path from Q to P throught points Q', $F_z(Z)$ and P'.

Proof: We first prove that for any path κ between two points in $C(P)$, there exists a path completely inside $D(P)$ whose length is shorter or equal. Let Q' and P' be the extremal points of a sub-path of κ completely outside $D(P)$, and let l be length of such sub-path. From Proposition 2.2, there exists a palindrome path γ from Q' to P' of length l or shorter that evolves completely outside $D(P)$. The intersection of γ with the bisectrix r of the angle $\widehat{P'O_wQ'}$ is a point Z, with $\rho_Z > \rho_P$ (see figure 2.3). By symmetry, the length of the sub-path γ_Z from Z to P' is $l/2$. On the other hand, γ_Z is transformed by F_Z in $\tilde{\gamma}_Z$, going from $F_Z(Z)$ to P', with length $\frac{\rho_P}{\rho_Z}\frac{l}{2}$. Joining $\tilde{\gamma}_Z$ with its symmetric with respect to r, a path from Q' to P' of length $\frac{\rho_P}{\rho_Z}l < l$ is found.

As a consequence, any path from $Q \in C(P)$ to P can be shortened by an extremal feasible path completely inside $D(P)$. Moreover,

for Q on ∂DS, γ evolves in DS: indeed, if there existed a point of intersection $\bar{Z}$ with the X_w axis, the sub-path $\gamma_{\bar{Z}}$ from $\bar{Z}$ to P would be shortened by the segment $\overline{\bar{Z}P}$ lying on the axis itself, i.e., on $\overline{P_s P}$. ∎

2.3   Optimal paths for points on CS

The study of the optimal synthesis begins in this section addressing optimal paths from points on CS. An existence result will be preliminarily established.

Proposition 2.3 *For any $Q \in CS$ there exists a feasible shortest path to P.*

Proof: Because of state constraints (1.6), and (1.7), and the restriction of optimal paths in DS (Theorem 2.1) the state set is compact. Furthermore, for any point at distance ρ from O_w the optimal path is shorter or equal to $\rho + \rho_P$ (which corresponds to the path $S^+ * S^-$ through O_w). The system is also controllable (cf. [41]). Hence, Filippov existence theorem for Lagrange problems can be invoked [49]. ∎

A first simple result can be obtained for starting points on the diameter $\overline{P_s P}$ of $C(P)$.

Proposition 2.4 *For $Q \in \overline{P_s O_w}$ the optimal path is $S^+ * S^-$ with switching point in O_w. For $Q \in \overline{O_w P}$ the optimal path is S^-.*

Proof: The FOV constraint is not active from Q to O_w and from O_w to P, hence a straight line is the shortest path. ∎

Definition 2.5 *For a point $G \in \mathbb{R}^2$, let C_G^R (C_G^L) denote the circular arc from G to O_w such that, $\forall V \in C_G^R$ (C_G^L), $\widehat{GVO_w} = \pi - \phi$ in the half-plane on the right (left) of $\overline{GO_w}$ (cf. figure 2.4). Also, let C_G denote the region delimited by C_G^R and C_G^L from G to O_w.*
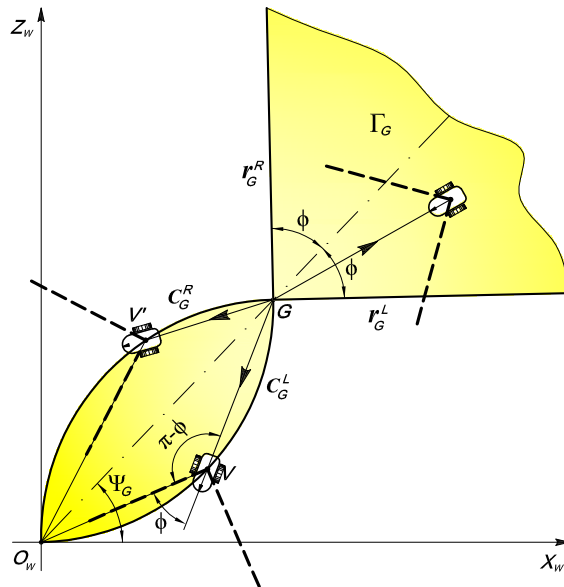
Figure 2.4: Region C_G with its border $\partial C_G = C_G^R \cup C_G^L$ and cone Γ_G delimited by half-lines r_G^R and r_G^L.

We will refer to C_G^R (C_G^L) as the right (left) ϕ-arc in G.

Definition 2.6 *For a point $G \in \mathbb{R}^2$, let r_G^R (r_G^L) denote the half-line from G forming an angle $\psi_G + \phi$ $(\psi_G - \phi)$ with the X_w axis (cf. figure 2.4). Also, let Γ_G denote the cone delimited by r_G^R and r_G^L.*

We will refer to r_G^R (r_G^L) as the right (left) ϕ-radius in G. The following result is obtained by elementary geometric arguments:

Proposition 2.5 *For any starting point Q, all points of C_Q are reachable by a straight path without violating the FOV constraint.*

Next part of this section is dedicated to show that shortest path from $Q \in CS$ to P, is contained in a sufficient family of (palindrome symmetric) optimal path.

Proposition 2.6 *If an optimal path $\gamma \in \mathcal{P}_Q$ includes a segment of type S^+ with extremes in A, B, then either $B = P \in C_A$ or $B \in C_A^R \cup C_A^L$.*

Proof: If $B \notin C_A$ the straight line violates either one of the FOV constraints. Furthermore, if $B \in C_A$ but $B \notin \partial C_A$ and $P \notin C_A$, the sub-path from B to P intersects ∂C_A in B'. Hence, γ could be shortened by replacing the sub-path from A to B' through B with the segment $\overline{AB'}$. If $P \in C_A$, then by the optimality principle $B = P$. ∎

Remark 2.4 *The argument of Proposition 2.6 can be repeated for any point A' on the S^+ segment ending in B. Hence, for any forward segment $\overline{AB}$ of an optimal path $\gamma \in \mathcal{P}_Q$, it holds either $B \in \bigcap_{A' \in \overline{AB}} \partial C_{A'}^R$ or $B \in \bigcap_{A' \in \overline{AB}} \partial C_{A'}^L$. Notice that this holds also for the particular cases $B = P$ and $B = O_w$.*

Proposition 2.7 *If an optimal path $\gamma \in \mathcal{P}_Q$ includes a segment of type S^- with extremes in B, A, then either $A = P \in \Gamma_B$ or $A \in r_B^R \cup r_B^L$.*

Proof: If $A \notin \Gamma_B$ the straight line violates either one of the FOV constraints. Furthermore, if $A \in \Gamma_B$ but $A \notin \partial \Gamma_B$ and $P \notin \Gamma_B$, the sub-path from A to P intersects $\partial \Gamma_B$ in A'. Hence, γ could be shortened by replacing the sub-path from B to A' through A with the segment $\overline{BA'}$. If $P \in \Gamma_B$, then by the optimality principle $A = P$. ∎

Proposition 2.8 *If a path $\gamma(t)$, $t \in [0, 1]$ is optimal, then its angle $\psi(t)$ is monotonic.*

Proof: Because γ is a continuous path, the angle of its points varies continuously. Should the angle be not monotonic (i.e. neither monotonically non-decreasing nor monotonically non-increasing), then there would exist two points on the path with the same angle, hence aligned with O_w. These two points could be connected with a feasible straight line, thus shortening γ, which on the contrary was supposed to be a shortest path. ∎

Remark 2.5 *By applying Proposition 2.8 to optimal paths from Q in the upper half-plane to P, and noticing that $\psi_Q \geq \psi_P = 0$, the angle is non increasing. Hence optimal paths in the upper half-plane, and in particular in DS, do not include counterclockwise extremals of type T^{R+} or T^{L-}.*

Proposition 2.9 *If a path $\gamma(t)$ is optimal, then its distance $\rho(t)$ has no local maximum for $t \in (0,1)$.*

Proof: Because γ is a continuous path, the distance $\rho(t)$ of its points from O_w is a continuous function of t. Assume that the distance has a maximum in an internal point $\bar{t} \in (0,1)$. Then, by classical analysis theorems, there exist two values t_G and t_H in $(0,1)$ such that $\rho(t_G) = \rho(t_H) < \rho(\bar{t})$, with the sub-path between t_G and t_H evolving outside the disk of radius $\rho(t_G)$. Applying the same arguments used in the proof of Theorem 2.1, replacing Q' with $\gamma(t_G)$ and P' with $\gamma(t_H)$, it is shown that a shorter sub-path between t_G and t_H exists evolving completely within the disk, i.e., a contradiction. ∎

Remark 2.6 *Observe that the distance from O_w is strictly increasing along backward extremal arcs (i.e., S^-, T^{R-}, T^{L-}) and strictly decreasing along forward extremal arcs (i.e., S^+, T^{R+}, T^{L+}). As a consequence of Proposition 2.9 in an optimal path a forward arc cannot follow a backward arc.*

Proposition 2.10 *Consider any two points G and H on a spiral arc T (either left or right). Let $\tilde{T}$ be the set of points between T and its symmetric w.r.t. $\overline{GH}$. A shortest path between G and H that evolves completely outside region $\tilde{T}$ is the arc of T between G and H.*

The proof of this proposition follows straightforwardly from the convexity property of $\tilde{E}$.

Proposition 2.11 *Any path of type $S^- * T^{R-}$ $(T^{L+} * S^+)$ can be shortened by a path of type $T^{R-}S^-$ (S^+T^{L+}).*
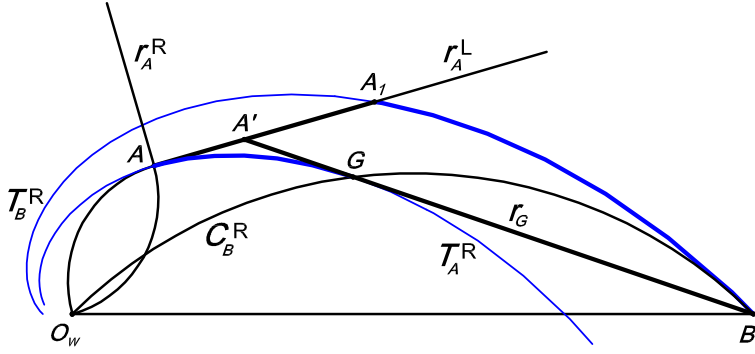
Figure 2.5: Construction used in the proof of Proposition 2.11.

Proof: Let A and B be the initial and final points of the $S^- * T^{R-}$, and let A_1 be the switching point between S^- and T^{R-} (see figure 2.5). Without loss of generality, I assume that A_1 belongs to r_A^L, the left ϕ-radius in A (if not, the path can be shortened by a path of the same type for which this is true). Let G be the intersection point between the spiral T_A^R through A and the ϕ-arc C_B^R through B. By Definitions 2.5, 2.6, and the properties of logarithmic spirals, the line r_G through B and G is tangent to T_A^R in G, while r_A^L is tangent to T_A^R in A. Let A' be the intersection of r_G with r_A^L. The segment $\overline{A'B}$ is shorter than the sub–path $S^- * T^{R-}$ from A' to B through A_1. By Proposition 2.10, however, the feasible spiral arc T_A^R from A to G shortens $\overline{AA'} \cup \overline{A'G}$, hence the thesis. The proof for $T^{L+}S^+$ is analogous. ∎

Thanks to all previuos results I am now able to prove the following important result:

Theorem 2.2 *For any $Q \in CS$ to P there exists a palindrome symmetric shortest path of type $S^+ T^{L+} * T^{R-} S^-$.*

Proof: According to Propositions 2.8-2.11 and Remarks 2.5-2.6, a sufficient optimal language $\mathcal{L}_O$ for $Q \in DS$ is described in figure 2.6. It is straightforward to observe that the number of switches between

extremals is finite and less or equal to 3, and a sufficient family of optimal paths is given by the word $S^+T^{L+}*T^{R-}S^-$ and its degenerate cases. Furthermore, by Proposition 2.2, for $Q \in CS$ optimal paths are palindrome symmetric. ∎
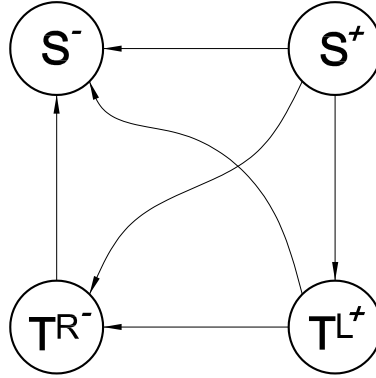
Figure 2.6: Feasible extremals and sequences of extremals from points in DS.

A palindrome symmetric path from Q on CS to P of the type $S^+T^{L+}*T^{R-}S^-$ is shown in figure 2.7. By symmetry, it follows that the sub-paths S^+ and S^- have the same length, and so do T^{L+} and T^{R-}. As a consequence, only two sub-words $T^{L+}*T^{R-}$ and S^+*S^- need be considered, which are obtained as degenerate cases with zero length arcs.

Referring to figure 2.7, let the switching points of the optimal path be denoted as M_2, N, and M_1, respectively. Notice that N is on the bisectrix r of $\widehat{QO_wP}$, while M_1 and M_2 are symmetric w.r.t. r. In figure 2.7 the region C_Q, locus of points reachable by a linear feasible path from Q, is also reported delimited by dashed curves.

We now study the length of extremal paths from CS to P in the sufficient family above. To do so, it is instrumental to parameterize the family by the angular position of the first switching point α_{M_1}.
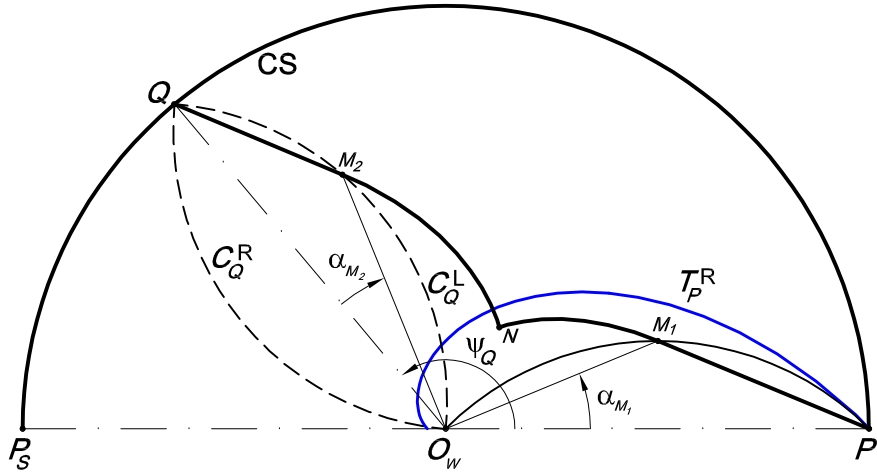
Figure 2.7: The palindrome symmetric path of type $S^+T^{L+} * T^{R-}S^-$ from $Q \in CS$ to P.

Theorem 2.3 *The length of a path $\gamma \in \mathcal{P}_Q$, $Q \in CS$, of type $S^+T^{L+} * T^{R-}S^-$ passing through $M_1 = (\rho_{M_1}, \alpha_{M_1})$ is*

$$L = 2\frac{\rho_P}{\cos\phi}\cos\alpha_{M_1} - \frac{2\rho_P\, e^{\left(\alpha_{M_1} - \frac{\psi_Q}{2}\right)t}}{\cos\phi \sin\phi}\sin(\phi - \alpha_{M_1}), \qquad (2.3)$$

when $\phi \in \left]0, \frac{\pi}{2}\right[$. In the extreme cases $\phi = 0$ and $\phi = \frac{\pi}{2}$, we have $L = 2\rho_P$ and $L = 2\rho_P \sin\frac{\psi_Q}{2}$, respectively.

Proof: Recalling that $P = (\rho_P, 0)$, $Q = (\rho_P, \psi_Q)$, when $\phi > 0$, $M_1 \in C_P^R$, by the sine rule we have

$$\rho_{M_1} = \rho_P \frac{\sin(\phi - \alpha_{M_1})}{\sin\phi}, \qquad (2.4)$$

On the other hand, for $M_2 = (\rho_{M_2}, \psi_Q - \alpha_{M_2})$ on C_Q^L it holds by symmetry $\rho_{M_2} = \rho_{M_1}$.

Also the lengths of segments S^+ and S^- are equal, and evaluate to

$$\overline{PM_1} = \overline{QM_2} = \rho_P \frac{\sin\alpha_{M_1}}{\sin\phi}. \qquad (2.5)$$

From (1.13), setting $t = \frac{\cos \phi}{\sin \phi}$, the right logarithmic spiral passing through M_1 (denoted with $T_{M_1}^R$) is given by

$$T_{M_1}^R : \left(\rho_{M_1} e^{(\alpha_{M_1} - \psi)t}, \psi \right) .$$

Similarly, the left spiral for M_2 (denoted with $T_{M_2}^L$) is given by

$$T_{M_2}^L : \left(\rho_{M_2} e^{-(\psi_Q - \alpha_{M_2} - \psi)t}, \psi \right) .$$

The intersection point between the spirals $T_{M_1}^R$ and $T_{M_2}^L$ is $N = (\rho_N, \psi_N)$, where

$$
\begin{aligned}
\rho_N &= \rho_P \frac{e^{\left(\frac{\alpha_{M_1} - \psi_Q + \alpha_{M_2}}{2} \right) t}}{\sin \phi} \sqrt{\sin(\phi - \alpha_{M_1}) \sin(\phi - \alpha_{M_2})} = \\
&= \rho_P \frac{e^{\left(\alpha_{M_1} - \frac{\psi_Q}{2} \right) t}}{\sin \phi} \sin(\phi - \alpha_{M_1})
\end{aligned}
\tag{2.6}
$$

$$\psi_N = \frac{(\alpha_{M_1} + \psi_Q - \alpha_{M_2})}{2} - \frac{\cos \phi}{2 \sin \phi} \ln \left(\frac{\sin(\phi - \alpha_{M_2})}{\sin(\phi - \alpha_{M_1})} \right) = \frac{\psi_Q}{2}. \tag{2.7}$$

Notice that, for $\phi = \frac{\pi}{2}$ we have $M_1 \equiv M_2 \equiv N$ and spiral arcs have zero length. Hence, from (3.12) and (2.7), $L = 2\rho_P \sin \frac{\psi_Q}{2}$.

For $\phi \in \left] 0, \frac{\pi}{2} \right[$, the length of the spiral arcs T^{L+} from M_1 to N and T^{L-} from M_2 to N are equal, and evaluate to

$$\overline{M_1 N} = \overline{M_2 N} = \frac{\rho_{M_1} - \rho_N}{\cos \phi} .$$

Adding up, after some simplifications, the total length L is therefore as reported in (2.3).

When $\phi = 0$, $M_1 \equiv M_2 \equiv O_w$ and spiral arcs have zero length, hence $L = 2\rho_P$. $\blacksquare$

Having an analytical expression for the length of the path as a function of a single parameter α_{M_1} (hence indirectly of $Q \in CS$), I am now in a position to minimize the length within the sufficient family. Notice that we need only to consider $\alpha_{M_1} \geq 0$ (because the problem is symmetric w.r.t. X_w), and $\alpha_{M_1} \leq \phi$ for the geometrical considerations above on C_Q^L (see figure 2.4).

Theorem 2.4 *Given* $Q = (\rho_P, \psi_Q) \in CS$,

- *for* $0 < \psi_Q \leq \psi_M \triangleq -4 \tan \phi \ln(\sin \phi)$, *the optimal path is of type* $T^{L+} * T^{R-}$;

- *for* $\psi_M < \psi_Q < \psi_V \triangleq 2\phi + \psi_M$, *the optimal path is of type* $S^+ T^{L+} * T^{R-} S^-$;

- *for* $\psi_V \leq \psi_Q < \pi$, *the optimal path is of type* $S^+ * S^-$

Proof: To find the value of $\alpha_{M_1} \in [0, \phi]$ which minimizes the length L, consider the first derivative

$$\frac{\partial L}{\partial \alpha_{M_1}} = 2\rho_P \frac{\sin \alpha_{M_1}}{\cos \phi} \left(\frac{e^{\left(\alpha_{M_1} - \frac{\psi_Q}{2}\right)t}}{\sin^2 \phi} - 1 \right). \tag{2.8}$$

The critical points of α_{M_1} are

$$^a\alpha_{M_1} = 0 \tag{2.9}$$

$$^b\alpha_{M_1} = \frac{\psi_Q}{2} + 2 \tan \phi \ln(\sin \phi). \tag{2.10}$$

To determine the local maximum or minimum nature of the critical values, consider the second derivative of L,

$$\frac{\partial^2 L}{\partial \alpha_{M_1}^2} = \frac{2\rho_P}{\cos \phi} \left[\cos \alpha_{M_1} \left(\frac{e^{\left(\alpha_{M_1} - \frac{\psi_Q}{2}\right)t}}{\sin^2 \phi} - 1 \right) + \right.$$
$$\left. + \sin \alpha_{M_1} \frac{e^{\left(\alpha_{M_1} - \frac{\psi_Q}{2}\right)t}}{\tan \phi} \right] \tag{2.11}$$

and

$$\left.\frac{\partial^2 L}{\partial \alpha_{M_1}^2}\right|_{^a\alpha_{M_1}} = \frac{2\rho_P}{\cos\phi}\left(\frac{e^{-\frac{\psi_Q}{2}t}}{\sin^2\phi} - 1\right) \tag{2.12}$$

$$\left.\frac{\partial^2 L}{\partial \alpha_{M_1}^2}\right|_{^b\alpha_{M_1}} = 2\rho_P \sin\phi \sin\left(\frac{\psi_Q}{2} + 2\tan\phi\ln(\sin\phi)\right). \tag{2.13}$$

Notice that, when the minimum of L is reached in $\alpha_{M_1} = 0$, the path is of type $T^{L+} * T^{R-}$. From equation (2.12), the critical point $\alpha_{M_1} = 0$ is a minimum of L if $\left.\frac{\partial^2 L}{\partial \alpha_{M_1}^2}\right|_{^a\alpha_{M_1}} \geq 0$, that is, if

$$\psi_Q \leq -4\tan\phi\ln(\sin\phi) \triangleq \psi_M$$

Hence, the shortest path from Q on CS to P is of type $T^{L+} * T^{R-}$ if the polar coordinate of Q are (ρ_P, ψ_Q) with $\psi_Q \in [0, \psi_M]$. The point on CS whose polar coordinates are (ρ_P, ψ_M) is point M.

On the other hand, from equation (2.13), if $\psi_M < \psi_Q \leq \pi$ the minimum of L is reached in $\alpha_{M_1} \in (0, \phi)$. This critical point depends on ψ_Q, as shown in (2.10), i.e., $\alpha_{M_1} = \frac{\psi_Q - \psi_M}{2}$. In this case, the shortest path is of type $S^+ T^{L+} * T^{R-} S^-$.

When the minimum of L is reached in $\alpha_{M_1} = \phi$, the optimal path is of type $S^+ * S^-$. The first value $\psi_Q \in (\psi_M, \pi]$ such that the optimal path is reached in $\alpha_{M_1} = \phi$ is, from equation (2.10),

$$2\phi - 4\tan\phi\ln(\sin\phi) = 2\phi + \psi_M \triangleq \psi_V.$$

The point on CS whose polar coordinates are (ρ_P, ψ_V) is point V. For all starting points Q between V and P_s, the shortest path is of type $S^+ * S^-$.

∎

I am now interested in determining the locus of switching points between extremals in optimal paths.

Proposition 2.12 *For $Q \in CS$ with $0 < \psi_Q \leq \psi_M$, the switching locus is the arc of T_P^R within the extreme points P and $m = (\rho_P \sin^2\phi, \psi_M/2)$ (included).*

Proof: From Theorem 2.4, the optimal path from $Q \in CS$ to P is of type $T^{L+} * T^{R-}$. Hence, the switching occurs in the intersection of T_Q^L and T_P^R. The point of intersection varies on T_P^R from P (when $\psi_Q = 0$) to $m = (\rho_P \sin^2 \phi, \psi_M/2) = T_M^L \cap T_P^R$ (when $\psi_Q = \psi_M$). ∎

Proposition 2.13 *For $Q \in CS$ with $\psi_M < \psi_Q < \psi_V$, the loci of switching points M_1, N, and M_2 are the right ϕ-arcs C_P^R, C_m^R, and C_M^R with $M = (\rho_P, \psi_M)$, respectively.*

Proof: From Proposition 2.6, the switching point M_1 between T^{R-} and S^- belongs to C_P^R.

In the proof of Theorem 2.4, for $Q \in CS$ with $\psi_M < \psi_Q < \psi_V$, the relation $\psi_Q = 2\alpha_{M_1} + \psi_M$ between angles in the optimal path has been obtained. Hence, from (3.11), (2.6), and (2.7), the coordinates of the switching points N are given by

$$\rho_N = \rho_{M_1} e^{\left(-\frac{\psi_M}{2}\right)t} = \rho_{M_1} \sin^2 \phi \qquad (2.14)$$

and

$$\psi_N = \alpha_{M_1} + \frac{\psi_M}{2}. \qquad (2.15)$$

Hence, N corresponds to M_1 after a rotation of $\frac{\psi_M}{2}$ and a scaling by $e^{\left(-\frac{\psi_M}{2}\right)t} = \sin^2 \phi$, which does not depend on ψ_Q. Notice that, applying the same rotation and scaling, $P = (\rho_P, 0)$ is transformed in m, and the right ϕ-arc C_P^R goes in C_m^R. Hence, the locus of switching points N is C_m^R.

Finally, for the palindromic symmetry of optimal paths, it holds that $\rho_{M_1} = \rho_{M_2}$, $\alpha_{M_1} = \alpha_{M_2}$ and $\psi_Q - \alpha_{M_2} = \alpha_{M_1} + \psi_M$. Hence, M_2 corresponds to M_1 after a rotation ψ_M, which does not depend on Q. With the same rotation, P is transformed in M and the locus of switching points M_1, C_P^R, in the locus of switching points M_2, C_M^R. ∎

Finally, for $Q \in CS$ with $\psi_V \leq \psi < \pi$, the switching locus reduces to the origin O_w. We provide an explicit procedure to compute the switching points for any given $Q \in CS$:
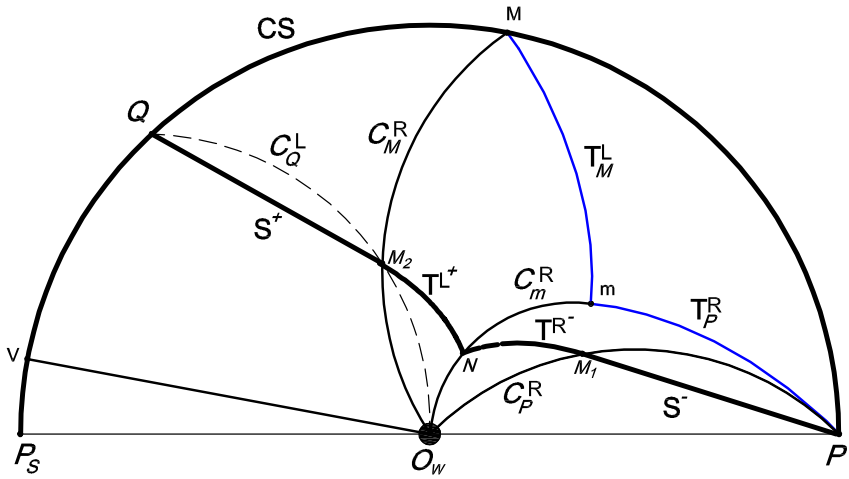
Figure 2.8: Optimal path from Q on CS to P. The locus of switching points between extremals S^+ and T^{L+} is the arc of circle C_M^R, whereas the locus of switching points between T^{L+} and T^{R-} is C_m^R.

Proposition 2.14 *Given $Q = (\rho_P, \psi_Q) \in CS$,*

- *for $0 < \psi_Q \leq \psi_M$, the switching point is $T_P^R \cap T_Q^L$;*

- *for $\psi_M < \psi_Q < \psi_V$, the switching points are $M_2 \in C_M^R \cap C_Q^L$, $N \in C_m^R \cap T_{M_2}^L$, and $M_1 \in C_P^R \cap T_N^R$.*

- *for $\psi_V \leq \psi_Q < \pi$, the switching point is O_w.*

Proof: From the proof of Proposition 2.12, for $Q \in CS$ with $0 < \psi_Q \leq \psi_M$, the switching point is $T_Q^L \cap T_P^R = (\rho_P\, e^{-\frac{\psi_Q}{2}t}, \frac{\psi_Q}{2})$.

From Propositions 2.13 and 2.6, for a given $Q \in CS$ with $\psi_M < \psi_Q < \psi_V$, the switching point M_2 of the optimal path from Q to P is the intersection point between C_M^R and C_Q^L that is univocally determined.

N belongs to C_m^R and lays on the arc T^L. Hence, it can be computed from M_2 as $C_m^R \cap T_{M_2}^L$.

M_1 belongs to C_P^R and lays on the arc T^R. Hence, it can be computed from N as $C_P^R \cap T_N^R$.

Finally, for $\psi_V \leq \psi_Q < \pi$, the optimal paths is characterized by $\alpha_{M_1} = \phi$ (proof of Theorem 2.4). From equations (3.11) and (2.6) it holds $\rho_N = \rho_{M_1} = \rho_{M_2} = 0$. Hence, in this case, the switching point is O_w. ∎

## 2.4 Optimal paths for points in the half-disc DS

Having solved the optimal synthesis for points on the boundary of DS, I now address optimal paths for internal points in DS by using the following simple idea: for any $Q \in DS \setminus \partial DS$, find a point $S \in \partial DS$ such that an optimal path γ from S to P goes through Q. By Bellmann's optimality principle [50], the sub-path from Q to P is also optimal.

Consider the partition of DS in six regions illustrated in figure 2.9. Regions of the partition are generalized polygonals whose vertices are the characteristic points in DS and whose boundaries belong either to the extremal curves, to the switching loci, or to ∂DS (cf. section 2.3). All regions have three vertices, except Region I which has two. The boundary arc T_P^R between Region II and Region VI is a degenerate case of measure zero in DS, and will be denoted as Region II$'$.

Theorem 2.5 *The optimal synthesis for $Q \in DS$ is described in figure 2.9 and table 2.1. For each region, the associated optimal path type entirely defines a feasible path of minimum length to the goal.*

Proof: We study each region separately:

Region I: From any point in this region it is possible to reach P with a straight path (in backward motion) without violating the FOV constraints (cf. Proposition 2.5). Such path is obviously optimal.
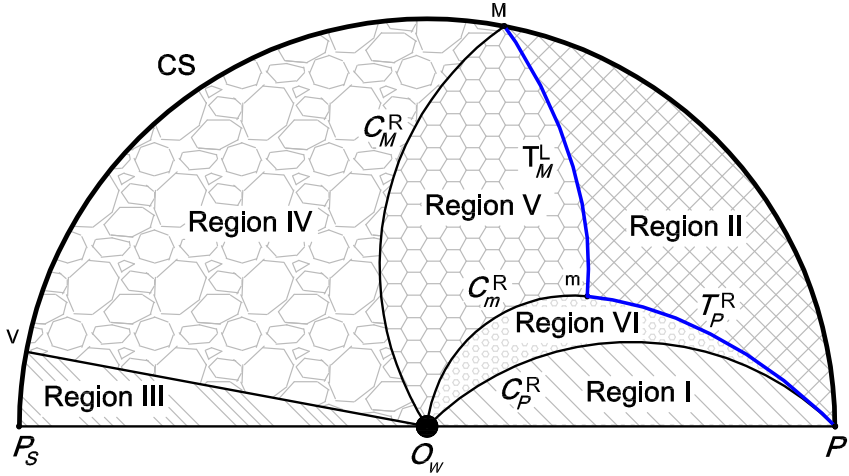
Figure 2.9: Partition of DS.

Region II: For any Q in this region consider the point s obtained by intersecting the spiral T_Q^L with CS. By the non-intersecting properties of left spirals, s lies between P and M on CS. By Theorem 2.4 the optimal path γ_s from s to P is of type $T_s^{L+} * T_P^{R-}$. The path $T_Q^{L+} * T_P^{R-}$ from Q is a sub-path of γ_s, hence it is also optimal.

Region II′: For any Q in the arc of T_P^R from m to P, the path T_P^{R-} from Q to P is a degenerate case of $T^{L+} * T_P^{R-}$ with a zero-length T^{L+} arc, hence it is also optimal.

Region III: For any Q in this region consider the line through O_w and Q, which intersects CS in a point s between point V and point P_s. By Theorem 2.4, the optimal path from point s to point P is of type $S^+ * S^-$ with the switch $*$ in O_w, hence (by the same argument) the thesis.

Region IV: For any Q in Region IV consider the left ϕ-arc C_Q^L, and the intersection point $r = C_Q^L \cap C_M^R \setminus O_w$. Consider now the straight line through Q and r, and let its intersection with CS

Region	Included Vertices	Included Boundaries	Optimal Path Type
I	O_w	$C_P^R, \overline{O_w P}$	S^-
II	M	CS, T_M^L	$T^{L+} * T_P^{R-}$
II′	m	T_P^R	T_P^{R-}
III	V	$\overline{P_S O_w}, \overline{O_w V}, CS$	$S^+ * S^-$
IV		CS	$S^+ T^{L+} * T^{R-} S^-$
V		C_M^R	$T^{L+} * T^{R-} S^-$
VI		C_m^R	$T^{R-} S^-$

Table 2.1: Optimal synthesis in the half-disc DS.

be denoted s. Such intersection lies between point V and point M. Indeed, the arc of circle through s, r and O_w is C_s^L and point V is such that C_V^L is tangent to C_M^R in O_w. Hence, by Theorem 2.4, the optimal path γ_s is of type $S^+ T^{L+} * T^{R-} S^-$. By Remark 2.4, γ_s contains Q in its first straight line segment, hence the thesis.

To finalize the synthesis, I recall that, as a straightforward consequence of Proposition 2.13, the optimal path for $Q \in C_m^R$ is of type $T_Q^{R-} S^-$, while for $Q \in C_M^R$, the optimal path type is $T_Q^{L+} * T^{R-} S^-$, where the two spiral extremals have the same length. As a consequence, we have:

Region V: For any Q in this region consider the intersection point s of the spiral T_Q^L with C_M^R. The optimal path γ_s from $s \in C_M^R$ to P is of type $T_s^{L+} * T^{R-} S^-$, and contains Q in its first arc, hence the thesis.

***Region* VI:** For any Q in this region consider the intersection point s of the spiral T_Q^R with C_m^R. The optimal path γ_s from $s \in C_m^R$ to P is of type $T_s^{R-}S^-$ and contains Q in its first arc, hence the thesis.

$\blacksquare$

Remark 2.7 *From the argument of the proof above and Proposition 2.3, the existence of optimal paths from points in DS follows directly.*

2.5 Optimal paths for points outside DS

In this section I exploit the properties of the path transform F_Q to extend the optimal synthesis outside the half-disk DS.

Indeed, recall from section 2.2 that F_Q transforms a path from Q to P in a path from $f_Q(P) = \left(\frac{\rho_P^2}{\rho_Q}, \psi_Q \right)$ to P. To highlight the dependence of the new initial point $f_Q(P)$ on Q, I will use alternatively the notation $F(Q) := f_Q(P)$. Notice that $F : \mathbb{R}^2 \backslash (0, 0) \rightarrow \mathbb{R}^2$ is continuous and is an involution, i.e., $F(F(Q)) \equiv Q$, hence $F^{-1} = F$. The locus of fixed points of F is CS. Notice also that, if Q is inside the half-disk DS, $F(Q)$ is outside, and viceversa.

To relate regions of the optimal synthesis inside and outside DS we need the following definition.

Definition 2.7 *Two regions A and B are* complementary $(A \leftrightsquigarrow B)$ *when $Q \in A \Leftrightarrow F(Q) \in B$.*

It is worthwhile to highlight the following result, which is an immediate consequence of Proposition 2.1:

Proposition 2.15 *If $A \leftrightsquigarrow B$, optimal paths from points $Q \in A$ of type w_A are mapped by F_Q in optimal paths from $F(Q) = f_Q(P) \in B$ of type $w_B = F_Q(w_A)$.*

Remark 2.8 *Existence of optimal paths from points in the upper half-plane outside DS follows from Remark 2.7 and the previous proposition. Indeed, for any point $Q \notin DS$, an optimal path from $F(Q) \in DS$ to P exists, which is mapped by F_Q in an optimal path from Q to P. Piecing together this with the results of Proposition 2.3 and Remark 2.7, and using the symmetry of optimal paths in the lower half-plane, I thus have established the global existence of optimal paths to our problem.*

To determine the borders of the regions outside DS, I now describe how F maps the borders of regions inside DS.

Proposition 2.16 *Map F transforms:*

1. *arcs of CS into themselves;*

2. *line segments from $Q \in DS$ to O_w in half-lines from $F(Q)$ to infinity with the same slope;*

3. *arcs of a right spiral T_Q^R in arcs of a left spiral $T_{F(Q)}^L$, and viceversa;*

4. *arcs of a circle C_Q^R with $Q \in DS$ in half-lines from $F(Q)$ with slope $\tan(\phi + \psi_Q)$*

Proof:

1. The first statement follows straightforwardly from the definition of points of CS.

2. Points on the segment from O_w to $Q \in DS$ have polar coordinates (ρ, ψ_Q) with $\rho \in (0, \rho_Q]$. Such points are mapped by F in $(\rho_P^2/\rho, \psi_Q)$ with $\rho_P^2/\rho \in [\rho_P^2/\rho_Q, +\infty]$, hence in the half-line from $F(Q) = (\rho_P^2/\rho_Q, \psi_Q)$ with slope ψ_Q.

3. Points on the arc of a right spiral T^R from $A = (\rho_A, \psi_A)$ to $B = (\rho_A e^{(\psi_A - \psi_B)t}, \psi_B)$ have coordinates $(\rho_A e^{(\psi_A - \psi)t}, \psi)$ with $\psi \in$

$[\psi_A, \psi_B]$. Map F transforms such points in $(\rho_P^2/\rho_A \, e^{-(\psi_A-\psi)t}, \psi)$. These are points on a left spiral T^L from $F(A) = (\rho_P^2/\rho_A, \psi_A)$ to $F(B) = (\rho_P^2/\rho_A \, e^{-(\psi_A-\psi_B)t}, \psi_B)$. The viceversa follows from the involutive property of F.

4. Points of C_Q^R have coordinates $(\rho_Q \sin(\phi-\psi+\psi_Q)/\sin\phi, \psi)$ with $\psi \in [\psi_Q, \psi_Q+\phi]$. Such points are mapped in $(\rho_P^2 \sin\phi/(\rho_Q \sin(\phi-\psi+\psi_Q)), \psi)$. On the other hand, the straight line from $F(Q)$ forming an angle $\phi + \psi_Q$ with the X_w axis is described by the equation

$$y = \tan(\phi + \psi_Q)x - \frac{\rho_P^2}{\rho_Q}\frac{\sin\phi}{\cos(\phi + \psi_Q)}.$$

Rewriting this equation in polar coordinates, it is straightforward to check that it is satisfied by the image of C_Q^R under F, hence the thesis.

∎

Let r_P be the right ϕ-radius in P of equation $y = \tan\phi(x - \rho_P)$; X_w^+ (X_w^-) the half-line from P (P_s) in the direction of the positive (negative) X_w axis; r_V the half-line from V parallel to $\overline{O_wV}$; r_M the right ϕ-radius in M, which is tangent to the spiral T_M^L, and r_{M_m} the right ϕ-radius in $M_m = F(m)$ which is tangent to the spiral T_P^L. Notice that r_{M_m} is described by the equation

$$y = \tan\left(\phi + \frac{\psi_M}{2}\right)\left(x - \frac{\rho_P}{\sin\phi\sin\left(\phi + \frac{\psi_M}{2}\right)}\right).$$

Theorem 2.6 *The optimal synthesis for Q outside DS is described in figure 2.10 and table 2.2.*

Proof: We only need to show that Region "R" and Region "R$_C$" are complementary, for R = I, II, ... VI. To do so, by continuity of F, it will be enough to prove that the borders of R are mapped in the borders of R$_C$. This is in turn a direct consequence of application of Proposition 2.16. ∎

Region	Included Vertices	Included Boundaries	Optimal Path Type
$I_\mathbf{c}$		$X_w^+,\ r_P$	S^+
$II_\mathbf{c}$		T_M^R	$T^{L+} * T_P^{R-}$
$II'_\mathbf{c}$	M_m	T_P^L	T_P^{L+}
$III_\mathbf{c}$		$r_V,\ X_w^-$	$S^+ * S^-$
$IV_\mathbf{c}$			$S^+ T^{L+} * T^{R-} S^-$
$V_\mathbf{c}$		r_M	$S^+ T^{L+} * T_P^{R-}$
$VI_\mathbf{c}$		r_{M_m}	$S^+ T_P^{L+}$

Table 2.2: Optimal synthesis outside the half-disc DS.

2.6 Global optimal synthesis

From results in section 2.4 and 2.5, it can be observed that optimal paths from Region II and $II_\mathbf{c}$ are of the same type, i.e., $w_{II} = w_{II_\mathbf{c}}$. The same holds for Region III and $III_\mathbf{c}$, and for Region IV and $IV_\mathbf{c}$. These three pairs of regions can be merged in a single region in the final partition of the plane.

The optimal path synthesis can be therefore summarized as reported in figure 2.10 and in table 2.3.

Examples of optimal paths from points of different regions are plotted in figure 2.11 and described in table 2.4. Despite that every optimal path may begin and end with a turn on the spot, in table 2.4, I omit explicit mention of initial and final rotation in place to simplify notation.

It should be noticed that, while the obtained synthesis is valid in general, the position of the characteristic points and the shape of the
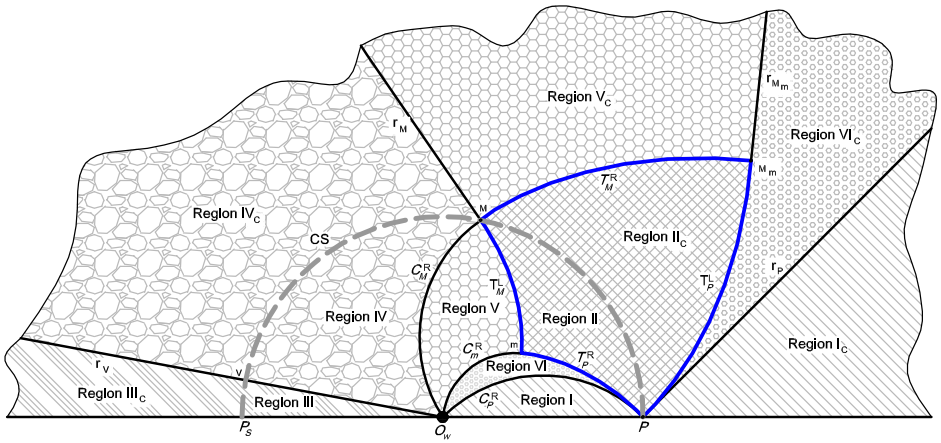
Figure 2.10: Partition of the upper half–plane with $\phi = \pi/4$.

regions varies with the FOV angle ϕ: compare e.g., the partition in figure 2.10, obtained for $\phi = \pi/4$, with the partition corresponding to $\phi = \pi/3$, which is reported in figure 2.12.

A particular case occurs for $\phi = \pi/2$ (see figure 2.13). Here, $M \equiv m \equiv M_m \equiv P$, $C_m^R \equiv C_R^M \equiv C_R^P$, and the spiral arcs T_P^R and T_P^L degenerate to zero length in a point on C_P^R. All optimal paths turn out to be of type $S^+ * S^-$, S^+, or S^-.

The partition of the whole plane of motion is obtained simply by symmetry with respect to the X_w axis, and is reported for completeness in figure 2.14. Regions in the lower half-plane are denoted with a subscript **s** (for symmetry), and are associated to optimal words obtained exchanging superscript R with L in the words reported in table 2.4 for the symmetric region. A comparison with the synthesis obtained in [41], reported in figure 2.15, is in order at this point. As it can be easily checked, the synthesis in [41] is correct for all initial points that are inside a circle centered in the goal point P and going through the characteristic point m. However, extrapolation of the synthesis in [41] outside this circle leads to quite different results from the synthesis obtained in this work, which is valid globally.
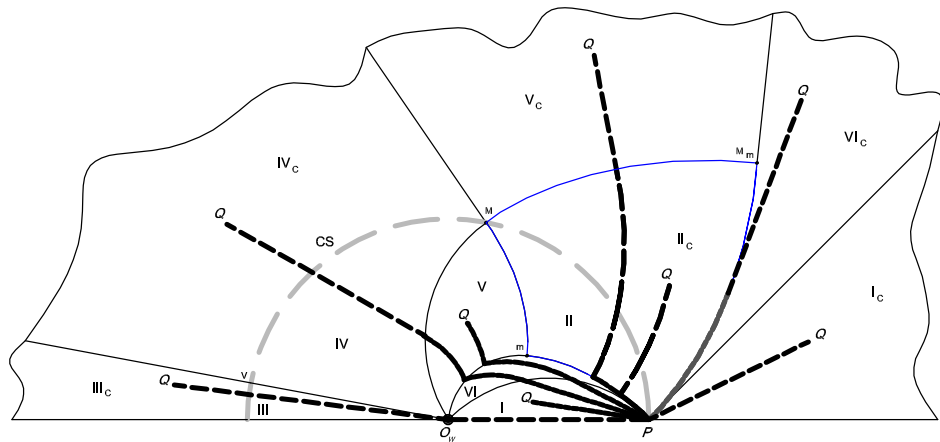
Figure 2.11: Examples of optimal paths from points Q in different regions to P.
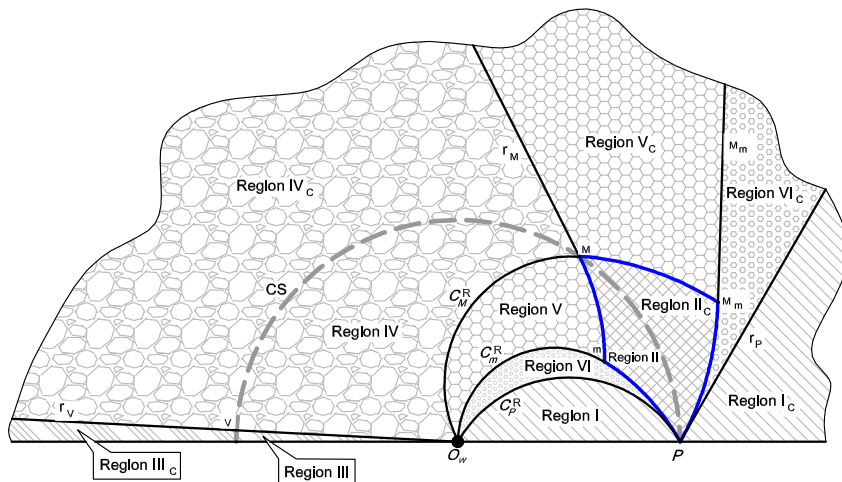

Figure 2.12: Partition of the upper half plane with $\phi = \pi/3$.

2.7 Conclusion

In this chapter, I have provided a complete characterization of shortest paths for a vehicle with nonholonomic kinematics to reach a desired

Region	Optimal Path Type
I	S^-
I$_\mathrm{c}$	S^+
II$\cup$II$_\mathrm{c}$	$T^{L+} * T_P^{R-}$
II$'$	T_P^{R-}
II$'_\mathrm{c}$	T_P^{L+}
III$\cup$III$_\mathrm{c}$	$S^+ * S^-$
IV$\cup$IV$_\mathrm{c}$	$S^+ T^{L+} * T^{R-} S^-$
V	$T^{L+} * T^{R-} S^-$
V$_\mathrm{c}$	$S^+ T^{L+} * T_P^{R-}$
VI	$T^{R-} S^-$
VI$_\mathrm{c}$	$S^+ T_P^{L+}$

Table 2.3: Optimal synthesis in the upper half-plane.
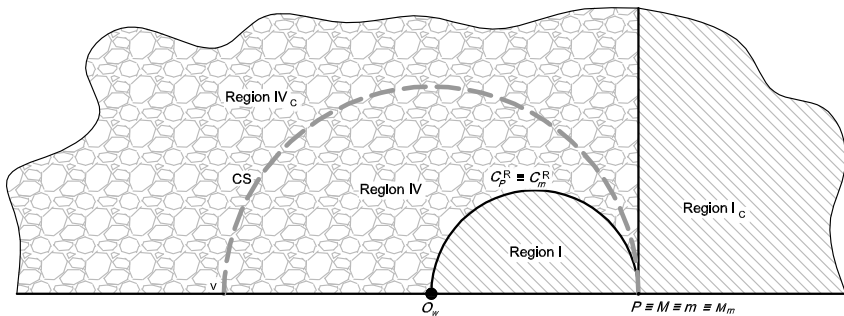
Figure 2.13: Partition of the upper half plane with $\phi = \pi/2$.
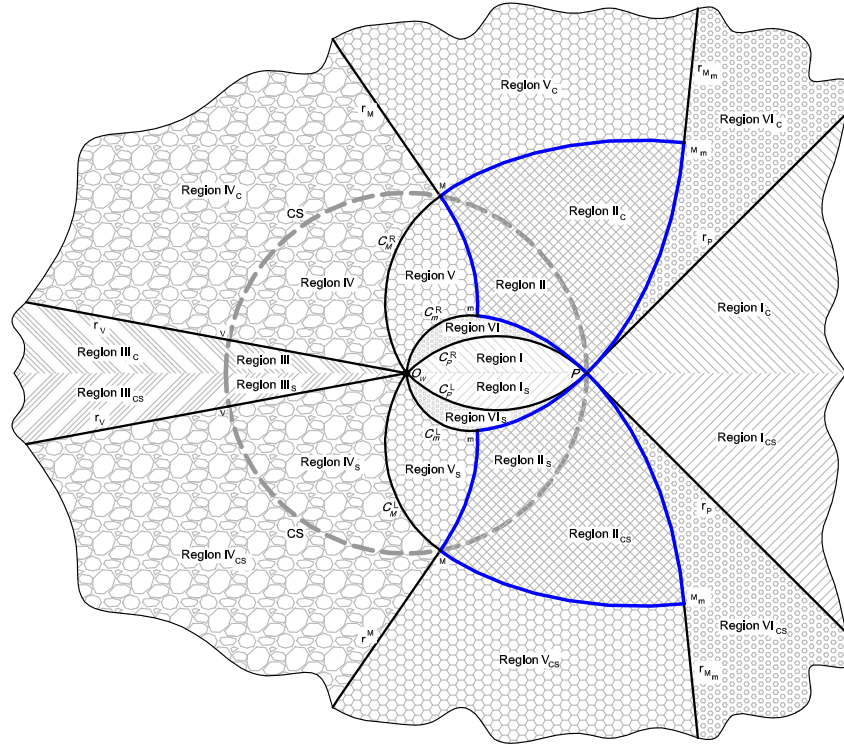
Figure 2.14: Partition of the (X_w, Z_w) plane with $\phi = \pi/4$.

position while keeping a fixed point within a conical region relative to itself. Symmetries and invariants of the problem have been exploited to determine optimal paths from any point of the motion plane to the goal, providing a substantial refinement and correction of existing results proposed in [41]. Next chapter is dedicated to extend these results to the case of arbitrarily FOVs, considering also the one in which the robot forward direction is not included inside FOV. The impracticability of paths that point straight to the feature lead to a more complex analysis of the reduction to a finite and sufficient family of optimal paths by excluding particular types of path.

Figure 2.15: Partition of the (X_w, Z_w) plane with $\phi = \pi/4$ according to [41].

Region	Optimal Path Type	Inclusion Conditions
I	S^-	$\rho \leq \rho_P \dfrac{\sin(\phi - \psi)}{\sin \phi}$, $\psi \leq \phi$
$\mathrm{I_c}$	S^+	$\rho > \rho_P \dfrac{\sin \phi}{\sin(\phi - \psi)}$, $\psi \leq \phi$
$\mathrm{II} \cup \mathrm{II_c}$	$T^{L+} * T_P^{R-}$	$\rho_P\, e^{(\psi - \psi_M)t} \leq \rho \leq \rho_P\, e^{-(\psi - \psi_M)t}$, $\rho_P\, e^{-\psi t} < \rho < \rho_P\, e^{\psi t}, \ \psi \leq \psi_M$
$\mathrm{II'}$	T_P^{R-}	$\rho = \rho_P\, e^{-\psi t}$, $\psi \leq \dfrac{\psi_M}{2}$
$\mathrm{II'_c}$	T_P^{L+}	$\rho = \rho_P\, e^{\psi t}$, $\psi \leq \dfrac{\psi_M}{2}$
$\mathrm{III} \cup \mathrm{III_c}$	$S^+ * S^-$	$2\phi + \psi_M \leq \psi \leq \pi$
$\mathrm{IV} \cup \mathrm{IV_c}$	$S^+ T^{L+} * T^{R-} S^-$	$\rho_P \dfrac{\sin \psi}{\sin \phi} \leq \rho \leq \rho_P \dfrac{\sin \phi}{\sin \bar{\psi}}$, $\psi_M \leq \psi \leq 2\phi + \psi_M$
V	$T^{L+} * T^{R-} S^-$	$\rho \leq \rho_P \dfrac{\sin \psi}{\sin \phi}$, $\rho_P\, e^{-(\psi_Q - \psi_M)t} \leq \rho \leq \rho_P\, e^{(\psi - \psi_M)t}$, $\dfrac{\psi_M}{2} \leq \psi \leq \psi_M + \phi$
$\mathrm{V_c}$	$S^+ T^{L+} * T_P^{R-}$	$\rho_P \dfrac{\sin \phi}{\sin \bar{\psi}} \leq \rho \leq \rho_P \dfrac{1}{\sin \phi \sin \hat{\psi}}$, $\rho \geq \rho_P\, e^{-(\psi - \psi_M)t}$, $\dfrac{\psi_M}{2} \leq \psi \leq \psi_M + \phi$
VI	$T^{R-} S^-$	$\rho_P \dfrac{\sin(\phi - \psi)}{\sin \phi} \leq \rho \leq \rho_P \sin \phi \sin \hat{\psi}$, $\rho \leq \rho_P\, e^{-\psi t}$, $\psi \leq \phi + \dfrac{\psi_M}{2}$
$\mathrm{VI_c}$	$S^+ T_P^{L+}$	$\rho_P \dfrac{1}{\sin \phi \sin(\phi - \psi)} \leq \rho \leq \rho_P \dfrac{\sin \phi}{\sin \hat{\psi}}$, $\rho \geq \rho_P\, e^{\psi t}$, $\psi \leq \phi + \dfrac{\psi_M}{2}$

Table 2.4: Optimal synthesis in the upper half-plane and Region inclusion conditions for initial position Q. Where $\bar{\psi} = \phi - \psi + \psi_M$ and $\hat{\psi} = \phi - \psi + \frac{\psi_M}{2}$.

Chapter 3

Shortest Paths Synthesis With Planar Side Sensors

THIS CHAPTER presents a complete characterization of shortest paths to a goal position for a robot with unicycle kinematics, generalizing results obtained in previous chapter to the case of arbitrary FOVs of the on-board sensor, including the case that the direction of motion is not an axis of symmetry for the FOV, and even that it is not included in the FOV itself. Sensors that do not necessarily include the forward direction of motion make paths pointing straight to the feature unfeasible, and lead to a more challenging synthesis problem. Results reported in this chapter can be found in paper [A3].

3.1 Introduction

In chapter 1, it has been proved that for a nonholonomic vehicle equipped with a limited sensor such that the forward sensor axis Z_c forms an angle Γ w.r.t the robot's forward direction (see figure 3.1), extremal maneuvers are generically represented by symbols in the finite alphabet $\{*, S, E_1, E_2\}$ where $*$ denotes a rotation on the spot and S denotes straight line. Moreover, depending on values of angles Γ
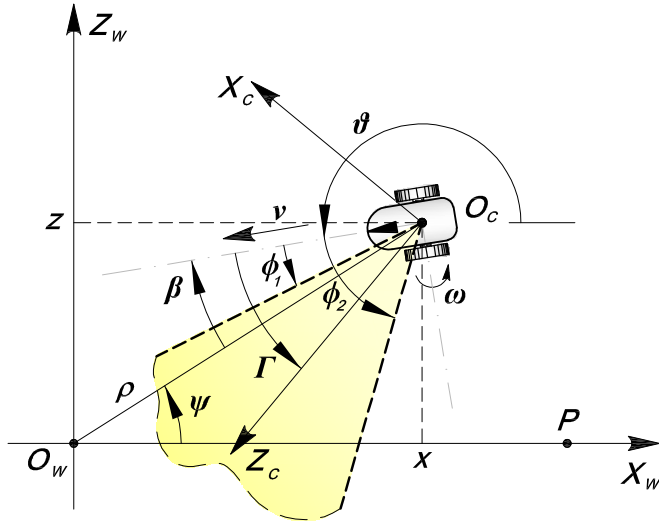
Figure 3.1: Mobile robot and systems coordinates. The robot's task is to reach P while keeping O_w within a limited FOV (shadowed in figure).

and $\delta = |\phi_2 - \phi_1|$, extremal curves E_1 and E_2 could be spirals (denoted with T_i^R and T_j^L, with $i, j \in \{1, 2\}$), circumference centered in O_w (denoted with C) or straight line through O_w (denoted with H) (see figures 3.2, 3.3).

Moreover, as extremal arcs can be executed by the vehicle in either forward or backward direction, I will build extremal paths consisting of sequences, or *words*, comprised of symbols in the finite alphabet $\mathcal{A}_\Gamma = \{*, \, S^+, \, S^-, \, E_1^+, \, E_1^-, \, E_2^+, \, E_2^-\}$. The set of possible words generated by the above symbols is a language $\mathcal{L}_\Gamma$.

Following sections are dedicated to showing that, due to the physical and geometrical constraints of the considered problem, a sufficient optimal finite language $\mathcal{L}_\Gamma^O \subset \mathcal{L}_\Gamma$ can be built such that, for any initial condition, it contains a word describing a path to the goal which is no longer than any other feasible path. Correspondingly, a partition of the plane in a finite number of regions is described, for which the

(a) Frontal: $0 < \Gamma < \frac{\delta}{2}$, $\mathcal{A} = \{*,$ $S^+,\ S^-,\ T_1^{L+},\ T_1^{L-},\ T_2^{R+},\ T_2^{R-}\}$.

(b) Borderline Frontal: $\Gamma = \frac{\delta}{2}$, $\mathcal{A} = \{*,\ S^+,\ S^-,\ H^+,\ H^-,\ T_2^{R+},\ T_2^{R-}\}$.
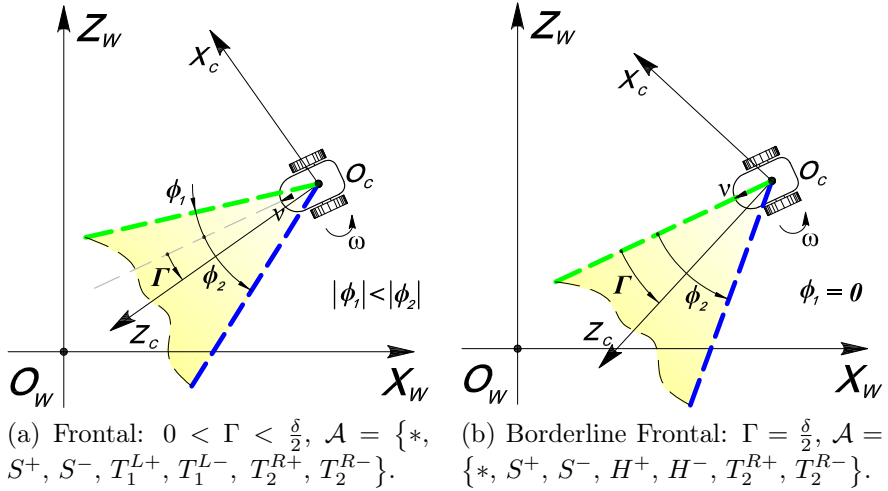
Figure 3.2: Robot's forward direction is included inside cone (shadowed in figures): $0 \leq \Gamma \leq \frac{\delta}{2}$.

shortest path is one of the words in $\mathcal{L}_\Gamma^Q$.

3.2   Shortest path synthesis

In this section, I introduce the basic tools that will allow me to study the optimal synthesis of the whole state space of the robot, beginning from points on a particular sub-set of $\mathbb{R}^2$ such that the optimal paths are in a sufficient optimal finite language. In chapter 2 similar basic tools have already been introduced. Nevertheless, as this problem looses the symmetry properties, they become inappropriate here and hence I need to introduce a generalized version of them.

Definition 3.1 *Given the goal point* $P = (\rho_P, 0)$ *in polar coordinates, and* $Q \in \mathbb{R}^2 \setminus O_w$, $Q = (\rho_Q, \psi_Q)$ *with* $\rho_Q \neq 0$, *let* $f_Q : \mathbb{R}^2 \to \mathbb{R}^2$

(d) Side: $\frac{\delta}{2} < \Gamma < \frac{\pi-\delta}{2}$, $\mathcal{A} = \{*,$ S^+, S^-, T_1^{R+}, T_1^{R-}, T_2^{R+}, $T_2^{R-}\}$.

(e) Borderline Side: $\Gamma = \frac{\pi-\delta}{2}$, $\mathcal{A} =$ $\{*$, S^+, S^-, T_1^{R+}, T_1^{R-}, C^+, $C^-\}$.

(f) Lateral: $\frac{\pi-\delta}{2} < \Gamma < \frac{\pi}{2}$, $\mathcal{A} = \{*,$ S^+, S^-, T_1^{R+}, T_1^{R-}, T_2^{L+}, $T_2^{L-}\}$.

(g) Symmetric Lateral: $\Gamma = \frac{\pi}{2}$, $\mathcal{A} = \{*$, S^+, S^-, T^{R+}, T^{R-}, T^{L+}, $T^{L-}\}$.
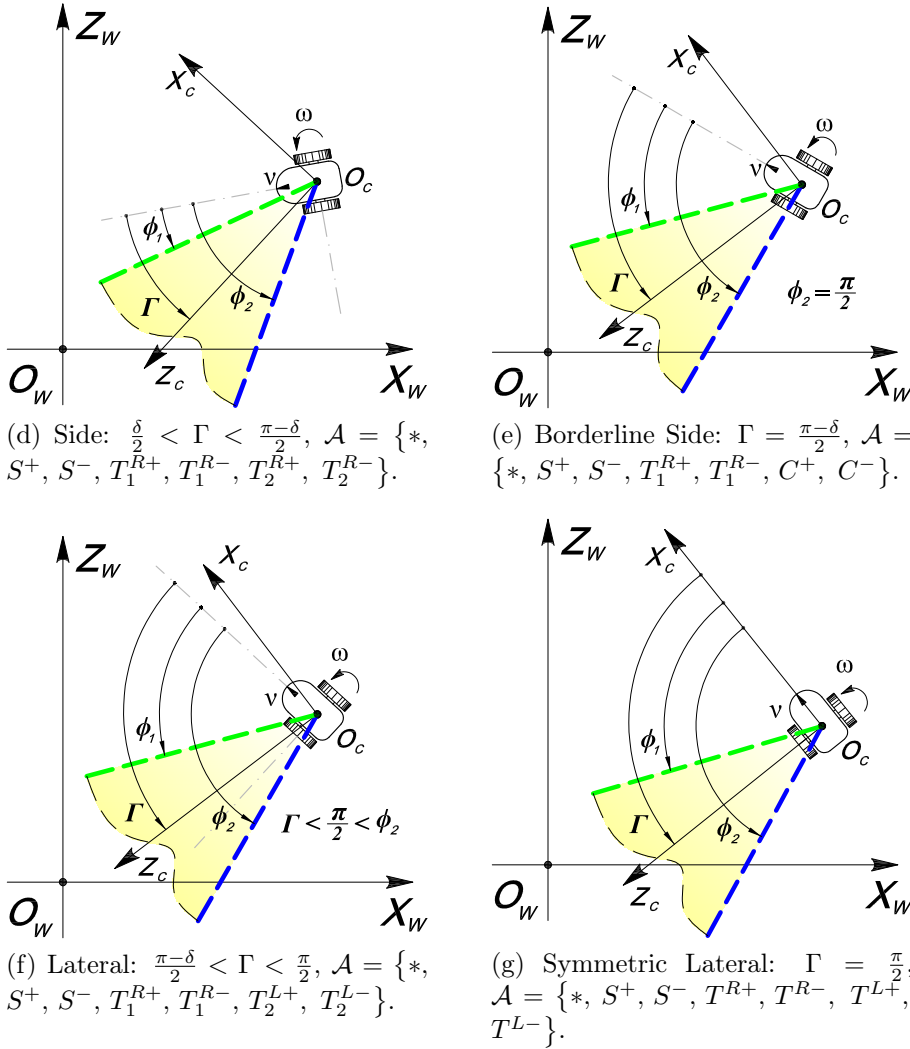
Figure 3.3: Robot's forward direction is not included inside cone (shadowed in figures): $\frac{\delta}{2} < \Gamma \leq \frac{\pi}{2}$.

denotes the map

$$
f_Q\left(\rho_K, \psi_K\right) = \begin{cases} \left(\dfrac{\rho_K \rho_P}{\rho_Q}, \psi_K - \psi_Q\right) & \text{for } \rho_K \neq 0 \\ (0,0) & \text{otherwise.} \end{cases} \tag{3.1}
$$

The map f_Q is the combination of a clockwise rotation by angle $\psi_K - \psi_Q$, and a scaling by a factor ρ_P/ρ_Q that maps Q in P.

Remark 3.1 *The alphabet $\mathcal{A}_\Gamma$ is invariant w.r.t. rotation and scaling. However, it is not invariant w.r.t. axial symmetry, as it happened in the particular case (i.e., the Frontal case with $\Gamma = 0$) considered in previous chapter 2, where the map f_Q was defined as a combination of rotation, scaling and axial symmetry. For example, logarithmic spirals are self-similar and self-congruent (under scaling and rotation they are mapped into themselves). On the other hand, left (right) spirals are mapped into right (left) spirals through an axial symmetry and alphabet invariancy can be lost. Indeed, for example, considering the Side case alphabet (see section 1.4 in chapter 1) $\mathcal{A}_{\frac{\delta}{2} < \Gamma < \frac{\pi - \delta}{2}} = \left\{ *, S^+, S^-, T_1^{R+}, T_1^{R-}, T_2^{R+}, T_2^{R-} \right\}$, and applying an axial symmetry we have $T_1^R \rightarrow T_1^L \notin \mathcal{A}_{\frac{\delta}{2} < \Gamma < \frac{\pi - \delta}{2}}$. The same occurs for the Frontal alphabet with $\Gamma > 0$.*

Let γ be a path parameterized by $t \in [0, 1]$ in the plane of motion $\gamma(t) = (\rho(t), \psi(t))$. Denote with $\mathcal{P}_Q$ the set of all feasible extremal paths from $\gamma(0) = Q$ to $\gamma(1) = P$.

Definition 3.2 *Given the target point $P = (\rho_P, 0)$ and $Q = (\rho_Q, \psi_Q)$ with $\rho_Q \neq 0$, let the* path transform *function F_Q be defined as*

$$
\begin{aligned}
F_Q : \mathcal{P}_Q &\rightarrow \mathcal{P}_{f_Q(P)} \\
\gamma(t) &\mapsto f_Q(\gamma(1 - t)), \ \forall t \in I.
\end{aligned}
\tag{3.2}
$$

Notice that $\tilde{\gamma}(t) = F_Q\left(\gamma(1 - t)\right)$ corresponds to $\gamma(t)$ transformed by f_Q and followed in opposite direction. Indeed, $\tilde{\gamma}$ is a path from $\tilde{\gamma}(0) = f_Q(P) = \left(\frac{\rho_P^2}{\rho_Q}, -\psi_Q \right)$ to $\tilde{\gamma}(1) = f_Q(Q) \equiv P$.

We will denote the circle with center in O_w and radius ρ_P by $C(P)$ and the closed disk within $C(P)$ by $D(P)$. As in previous chapter, $C(P)$ has an important role in the proposed approach since properties of F_Q will allow me to solve the synthesis problem from points on

$C(P)$, and hence to extend the synthesis to $D(P)$ and to the whole motion plane. Indeed, $\forall Q \in C(P)$ and $\forall \gamma \in \mathcal{P}_Q$, $F_Q(\gamma) \in \mathcal{P}_{f_Q(P)}$ with $f_Q(P) \in C(P)$, i.e., a path from a point $Q = (\rho_P, \psi_Q)$ on $C(P)$ to P is mapped in a path from point $f_Q(P) = (\rho_P, -\psi_Q)$ on $C(P)$ to P.

Furthermore, F_Q transforms an extremal in $\mathcal{A}$ in itself but followed in opposite direction. Hence, F_Q maps extremal paths in $\mathcal{L}_\Gamma$ in extremal paths in $\mathcal{L}_\Gamma$. For example, let $w = S^- * H^- * S^+ * T_2^{R+}$ be the word that characterize a path from Q to P, the transformed path is of type $z = T_2^{R-} * S^- * H^+ * S^+$. With a slight abuse of notation, I will write $z = F_Q(w)$.

Proposition 3.1 *Given $Q \in \mathbb{R}^2$ and a path $\gamma \in \mathcal{P}_Q$ of length l, the length of the transformed path $\tilde{\gamma} = F_Q(\gamma)$ is $\tilde{l} = \frac{\rho_P}{\rho_Q} l$.*

The proof is easily obtained by following the same procedure used in proposition 2.1.

Based on the properties of F_Q, optimal paths from points on $C(P)$ completely evolve inside $C(P)$. To prove this statement I first report the following result,

Theorem 3.1 *Given two points $A = (\rho_A, \psi_A)$ and $B = (\rho_B, \psi_B)$, with $\psi_A > \psi_B$ and $\rho = \rho_A = \rho_B$, and an extremal path γ from A to B such that for each point G of γ, $\rho_G > \rho$, there exists an extremal path $\tilde{\gamma}$ from A to B such that for each point $\tilde{G}$ of $\tilde{\gamma}$, $\rho_{\tilde{G}} < \rho$ and $\ell(\tilde{\gamma}) < \ell(\gamma)$ (see figure 3.4).*

Proof: Consider a point $Z = (\rho_Z, \psi_Z)$ such that $\rho_Z = \max_{G \in \gamma} \rho_G > \rho$. Let γ_1 and γ_2 the sub-paths of γ from Z to B and from Z to A.

The sub-path γ_1, is rotated and scaled (contracted of factor $\frac{\rho}{\rho_Z} < 1$) such that Z is transformed in A obtaining a path $\tilde{\gamma}_1$ from A to $\tilde{Z} = (\frac{\rho^2}{\rho_Z}, \psi_A + \psi_B - \psi_Z)$. Similarly, γ_2, can be rotated and scaled with the same scale factor but different rotation angle w.r.t. γ_1 such that Z is transformed in B, see figure 3.4. After geometrical considerations, it is easy to notice that the obtained path $\tilde{\gamma}_2$ starts in B and ends in $\tilde{Z}$.
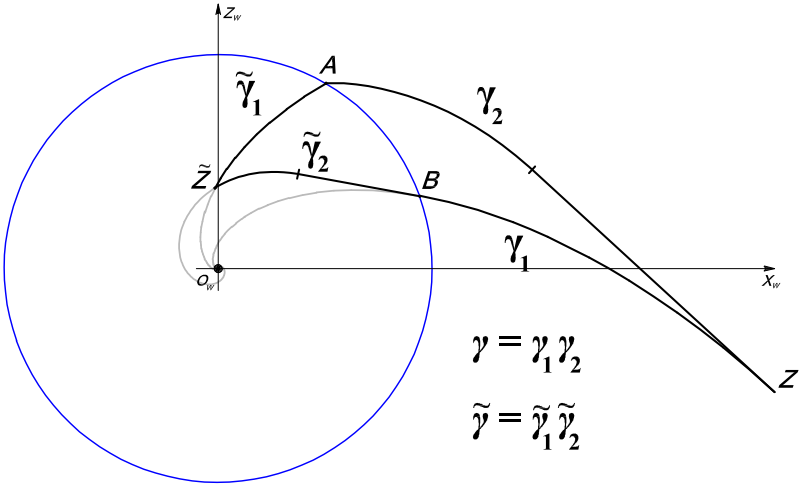
Figure 3.4: An example for theorem 3.1: path $\gamma = \gamma_2\gamma_1$ (γ_2 followed by γ_1) of type $T_2^{R-}S^- * T_1^{R+}$ from A to B is shortened by a path $\tilde{\gamma} = \tilde{\gamma}_1\tilde{\gamma}_2$ of type $T_1^{R+} * T_1^{R+}S^-$ by applying path transformation F_Z to path γ.

The obtained paths are a contraction of γ_1 and γ_2 respectively and hence shorter. Moreover, any point G of γ_1 or γ_2 has $\rho_G > \rho$ hence is scaled in $\tilde{G}$ of $\tilde{\gamma}_1$ or $\tilde{\gamma}_2$ with $\rho_{\tilde{G}} = \frac{\rho\rho_G}{\rho_Z} < \rho$.

Concluding, I have obtained a shorter path from A to B that evolves completely in the disk of radius ρ. ∎

An important but straightforward consequence of the theorem is the following

Corollary 3.1 *For any path in $\mathcal{P}_Q$ with $Q \in C(P)$ there exists a shorter or equal-length path in $\mathcal{P}_Q$ that completely evolves in $D(P)$.*

3.3 Optimal paths for points on $C(P)$

The study of the optimal synthesis begins in this section addressing optimal paths from points on $C(P)$. As in previous chapter, an existence result of optimal paths will be preliminarily established.

Proposition 3.2 *For any $Q \in C(P)$ there exists a feasible shortest path to P.*

Proof: Because of state constraints (1.6), and (1.7), and the restriction of optimal paths in $D(P)$ (Corollary 3.1) the state set is compact. Furthermore, it is possible to give an upper-bound on the optimal path length for all $\Gamma \in [0, \frac{\pi}{2}]$. Indeed, given a point Q at distance ρ from O_w the optimal path to P is shorter or equal to the following paths based on the value of Γ and δ:

- Frontal ($0 \leq \Gamma \leq \frac{\delta}{2}$): $S^+ * S^-$ or $H^+ * H^-$ of length $\rho + \rho_P$;

- Side ($\frac{\delta}{2} < \Gamma < \frac{\pi - \delta}{2}$): $T_{1Q}^{R+} * T_{2P}^{R-}$, of length $\left(\frac{\rho - \rho_N}{\cos \phi_1} + \frac{\rho_P - \rho_N}{\cos \phi_2} \right)$, where N is the intersection point between spirals T_{1Q}^R and T_{2P}^R through Q and P respectively;

- Borderline Side ($\Gamma = \frac{\pi - \delta}{2}$: $T_1^{R+} * C_P^-$) of length $\left(\frac{\rho - \rho_P}{\cos \phi_1} + (\psi_N - \psi_P)\rho_P \right)$, where N is the intersection point between spiral T_1^R and circumference C_P;

- Lateral ($\frac{\pi - \delta}{2} < \Gamma \leq \frac{\pi}{2}$): $T_{2Q}^{L-} * T_{1P}^{R-}$, of length $\left(\frac{\rho - \rho_N}{\cos \phi_2} + \frac{\rho_P - \rho_N}{\cos \phi_1} \right)$, where N is the intersection point between spirals T_{2Q}^L and T_{1P}^R.

The system is also controllable because there always exists an intersection point between two spirals (even if degenerated in half-lines or circumferences) with different characteristic angle even if both clockwise or counterclockwise around the feature. Hence, Filippov existence theorem for Lagrange problems can be invoked [49]. ■

In the following, I provide a set of propositions that completely describe a sufficient optimal finite language for all values of $\Gamma \in [0, \frac{\pi}{2}]$.

Definition 3.3 *For any starting point $G = (\rho_G, \psi_G)$, let $SF(G)$ $(SB(G))$ be the set of all points reachable from G with a forward (backward) straight line without violating FOV constraints.*
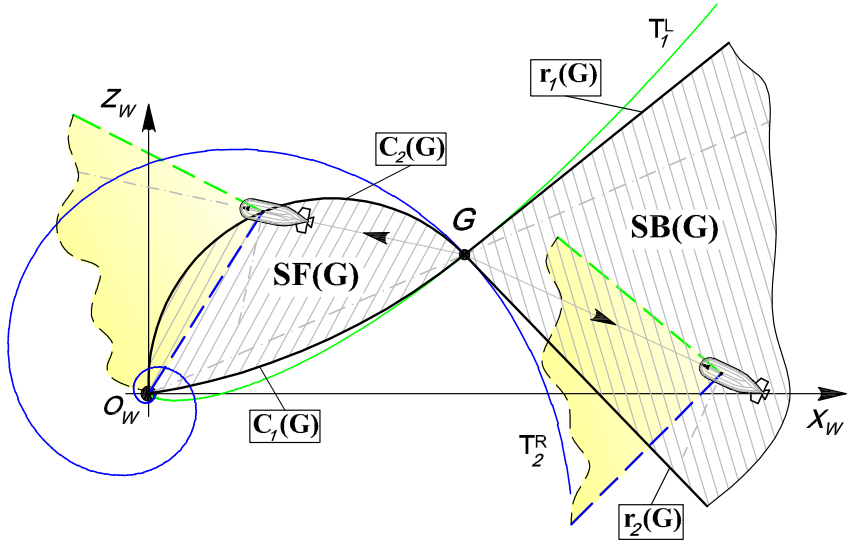
Figure 3.5: Forward and backward straight path Regions from G for $0 \leq \Gamma \leq \frac{\delta}{2}$.

Let $C_i(G)$ denote the circular arcs from G to O_w such that, $\forall V \in C_i(G)$ with $\psi_V \in [\psi_G - |\phi_1|, \psi_G]$ (or $\psi_V \in [\psi_G, \psi_G + |\phi_2|]$), $\widehat{GVO_w} = \pi - |\phi_i|$, $i \in \{1, 2\}$.

Remark 3.2 *Based on simple geometric considerations, for any starting point $G = (\rho_G, \psi_G)$, for $0 \leq \Gamma \leq \frac{\delta}{2}$ (Frontal Case), $SF(G)$ is the region between borders ∂SF_1 and ∂SF_2, where $\partial SF_1(G) = C_1(G)$ and $\partial SF_2(G) = C_2(G)$ (see figure 3.5). Notice that, $SF(G)$ lays completely in the circle with center in O_w and radius ρ_G. In the particular case in which $\Gamma = \frac{\delta}{2}$ (Borderline Frontal Case), $\partial SF_1(G)$ degenerates in the segment $(\overline{GO_w})$ between G and O_w.*

As a consequence of Remark 3.2, $SF(G)$ is tangent in G to T_1^L (or H) and T_2^R.

Remark 3.3 *For any starting point $G = (\rho_G, \psi_G)$, and for $\frac{\delta}{2} < \Gamma \leq \frac{\pi}{2}$ (Side and Lateral cases), let $G_F = (\rho_G \frac{\sin\phi_1}{\sin\phi_2}, \psi_G + (\phi_2 - \phi_1)) \in$*
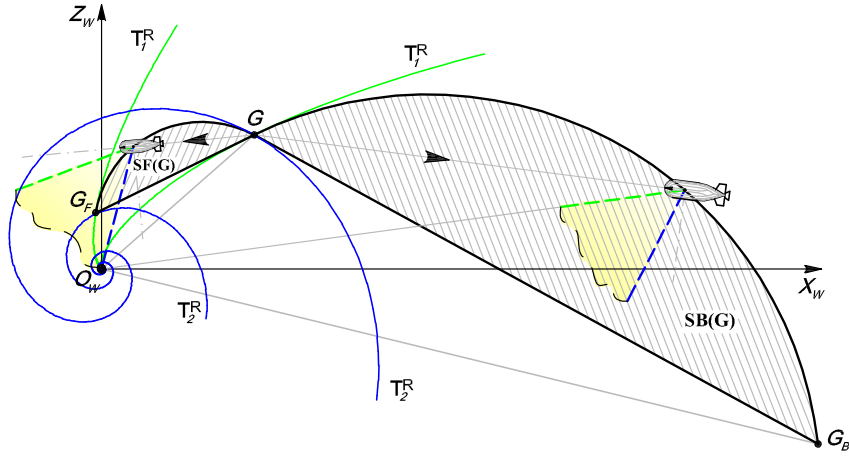
Figure 3.6: Forward and backward straight path regions from G for $\frac{\delta}{2} < \Gamma \leq \frac{\pi - \delta}{2}$.

$C_2(G)$, i.e., such that $\widehat{O_w G G_F} = \phi_1$ (cf. figure 3.6 and figure 3.7, respectively). Naming with $C_{G_F} \subset C_2(G)$ the arc between G and G_F, $SF(G)$ is the region between arc $\partial SF_2(G) = C_{G_F}$ and segment $\overline{GG_F}$. Notice that, for the Lateral case $SF(G)$ does not lay completely in the circle with center O_w and radius ρ_G. In the particular case in which $\Gamma = \frac{\pi - \delta}{2}$ (Borderline Side Case), $\partial SF_2(G)$ becomes the semicircle from G to $G_F \equiv O_w$ with diameter ρ_G.

As a consequence of Remark 3.3, $SF(G)$ is tangent in G to T_1^R and T_2^R (or C). Moreover, $SF(G)$ is tangent in G_F to T_1^R and T_2^R (or C), see figure 3.6.

A generalization of map f_Q (see definition 3.1) is a map that transforms the whole $\mathbb{R}^2$ rotating and scaling the point Q in a given point G, not necessarily in P as f_Q does. Let $F : \mathbb{R}^2 \backslash (0, 0) \to \mathbb{R}^2$ with $F(Q) = f_Q(G) = \left(\frac{\rho_G^2}{\rho_Q}, 2\psi_G - \psi_Q \right)$. The F map has some properties that make it very useful to the study of this problem in a way which is to some extent similar to what described (for a different F map) in previous chapter and in [A2]. Indeed, this map is continuous and
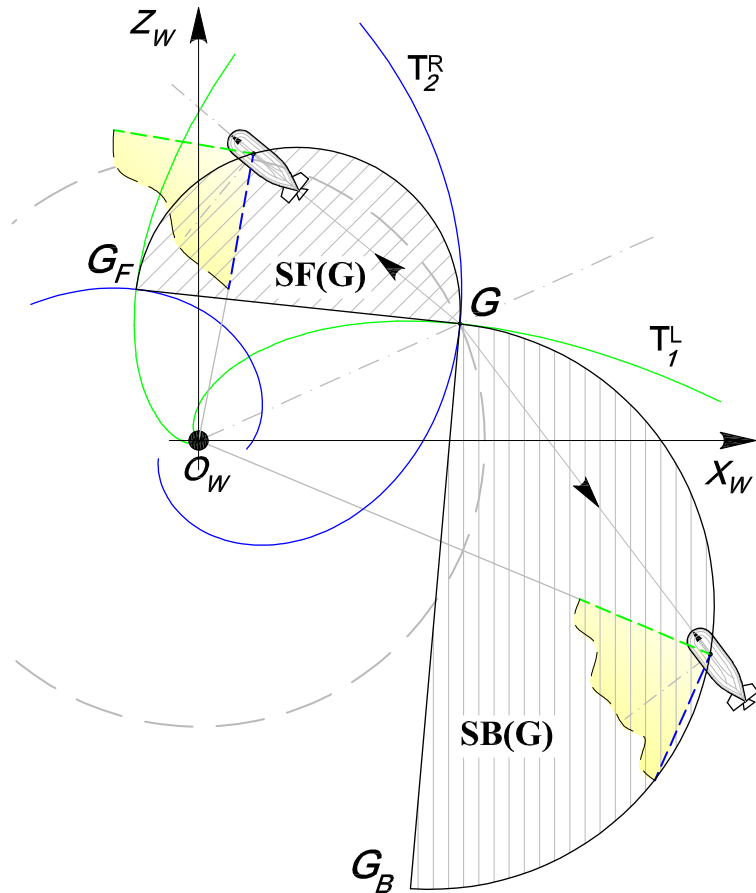
Figure 3.7: Forward and backward straight path Regions from G for $\frac{\pi-\delta}{2} \leq \Gamma \leq \frac{\pi}{2}$.

is an involution, i.e., $F(F(Q)) \equiv Q$, hence $F^{-1} = F$. The invariant set of F is the circle centered in O_w through G. Notice also that, if Q is inside this circle, $F(Q)$ is outside, and viceversa. Hence, with this map, borders defined in remarks 3.2 and 3.3 are mapped in borders of $SB(G)$ regions of definition 3.3 as described in the following proposition.

Proposition 3.3 *Map F transforms arcs of a circle $C_i(G)$ in half-lines from G and forming an angle $\psi_G - \phi_i$ with the X_w axis.*

Proof: Points of $C_i(G)$ have coordinates $(\rho_G \sin(\phi_i - \psi + \psi_G)/\sin\phi_i,\ \psi)$ with $\psi \in [\psi_G - |\phi_1|,\ \psi_G]$ (or $\psi \in [\psi_G,\ \psi_G + |\phi_2|]$). Such points are mapped in $(\rho_G \sin\phi_i/\sin(\phi_i - \psi + \psi_G),\ 2\psi_G - \psi)$. On the other hand, the straight line from G forming an angle $\psi_G + \phi_i$ with the X_w axis is described by the equation

$$y = \tan(\psi_G - \phi_i)x - \rho_G \frac{\sin\phi_i}{\cos(\psi_G - \phi_i)}\ .$$

Rewriting this equation in polar coordinates, it is straightforward to check that it is satisfied by the image of $C_i(G)$ under F, hence the thesis. ■

Remark 3.4 *For $0 \leq \Gamma \leq \frac{\delta}{2}$ (Frontal Case), let $r_i(G)$ denote the half-lines from G forming an angle $\psi_G - \phi_i$ with the X_w axis (cf. figure 3.5). $SB(G)$ is the cone delimited by $\partial SB_1(G) = r_1(G)$ and $\partial SB_2(G) = r_2(G)$, outside circle with center in O_w and radius ρ_G. Moreover, for $\frac{\delta}{2} < \Gamma \leq \frac{\pi}{2}$ (Side and Lateral cases), consider the rotation and scale that maps G_F in G and G in G_B we have $SB(G) \equiv SF(G_B)$, hence $\partial SB_1(G) = \partial SF_1(G_B)$ and $\partial SB_2(G) = \partial SF_2(G_B)$. Moreover, for all points V on the circular arc C_{G_B} from G_B to G, angle $\widehat{G_B V O_w} = \pi - |\phi_2|$, and angle $\widehat{O_w G_B G} = \phi_1$.*

This remark is a straightforward consequence of proposition 3.3.

Proposition 3.4 *If an optimal path from Q to P includes a segment of type S^+ (S^-) with extremes in G, K, then either $K = P \in SF(G)$ ($K = P \in SB(G)$) or $K \in \partial SF_1(G) \cup \partial SF_2(G)$ ($K \in \partial SB_1(G) \cup \partial SB_2(G)$).*

Proof: Consider the case of a segment of type S^+, if $K \notin SF(G)$ the straight line violates either one of FOV constraints. Furthermore,

if $K \in SF(G)$ but $K \notin \partial SF_1(G) \cup \partial SF_2(G)$ and $P \notin SF(G)$ the sub-path from K to P intersects $\partial SF_1(G) \cup \partial SF_2(G)$ in K'. Hence, γ could be shortened by replacing the sub-path from G to K' through K with the segment $\overline{GK'}$. If $P \in SF(G)$, then by the optimality principle $K = P$. For a segment of type S^- a similar proof can be followed. ∎

Based on all the above properties, I am now able to obtain a sufficient family of optimal paths by excluding particular sequences of extremals.

Theorem 3.2 *Any path consisting in a sequence of a backward extremal arc followed by a forward extremal arc is not optimal.*

Proof: Observe that the distance from O_w is strictly increasing along backward extremal arcs (i.e. S^-, E_1^-, E_2^- with $E_2 \neq C$) and strictly decreasing along forward extremal arcs (i.e. S^+, E_1^+, E_2^+ with $E_2 \neq C$). For continuity of paths, for any sequence of a backward extremal followed by a forward one, there exist points A and B that verify hypothesis of Theorem 3.1, hence it is not optimal.

Any sequence consisting in an extremal S (or E_1) of length ℓ and an extremal $E_2 = C$ (in any order and direction) is inscribed in two circumferences centered in O_w. Hence, the shortest sequence is the one with $E_2 = C$ along the circle of smaller radius necessarily preceded by a forward S (or E_1) of same length ℓ.

Concluding, in an optimal path a forward arc cannot follow a backward arc. ∎

Theorem 3.3 *Any path consisting in a sequence of an extremal arcs E_i and E_j followed in the same direction is not optimal for any $i, j \in \{1, 2\}$ with $i \neq j$.*

Proof: By proving the non-optimality of $E_i^+ * E_j^+$ the non-optimality of $E_j^- * E_i^-$ follows straightforwardly. Without loss of generality, I suppose $i = 1$ and $j = 2$. Let A and B be the initial and final points of the path γ of type $E_1^+ * E_2^+$ and N the intersection points between
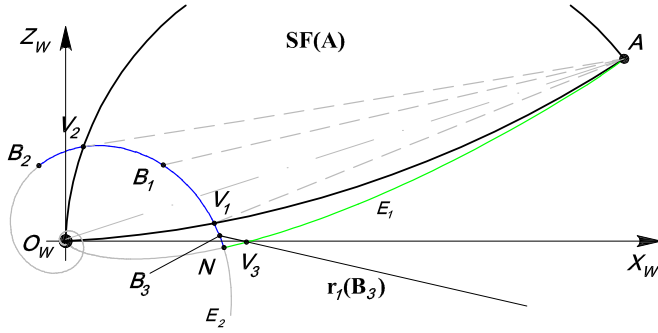
Figure 3.8: Construction of a path shorter than $E_1^+ * E_2^+$ for $0 \leq \Gamma \leq \frac{\delta}{2}$.

E_1^+ and E_2^+. We now show for any value of Γ and δ there exists a sub-path of γ that can be shortened with a straight arc.

For $0 \leq \Gamma \leq \frac{\delta}{2}$, referring to figure 3.8, $SF(A)$ intersects the extremal E_2 in two points $V_1 \in \partial SF_1(A)$ and $V_2 \in \partial SF_2(A)$ and three cases occur: if $B \in SF(A)$, i.e., $B = B_1$ between V_1 and V_2 along E_2, γ is obviously longer than $\overline{AB}$; if $B = B_2$ is between V_2 and O_w, γ can be shortened by $\overline{AV}_2$; finally, if $B = B_3$ is between V_1 and N, considering $SB(B)$ and the intersection point V_3 between $\partial SB_1(B) = r_1(B)$ and E_1, γ can be shortened by $\overline{V_3B}$.

For the Side case ($\frac{\delta}{2} < \Gamma < \frac{\pi-\delta}{2}$), there always exists a point G along E_1 between A and N such that $SF(G)$ intersects E_2 between N and B. Hence, γ can be shortened by $\overline{GG_F}$ (see figure 3.9). ∎

Notice that the feasible sequences consisting of two extremals that I still need to discuss, and eventually excluded, are those starting or ending with S followed in any direction ($E_i^+ E_i^-$ and $E_i^- E_i^+$, with $i \in \{1, 2\}$, are obviously not optimal). A useful technical result will be preliminarily established.

Proposition 3.5 *Consider any two points G and H on a spiral arc E_i ($i = 1, 2$). Let $\tilde{E}$ be the set of points between E_i and its symmetric w.r.t. $\overline{GH}$. A shortest path between G and H that evolves completely outside region $\tilde{E}$ is the arc of E_i between G and H.*
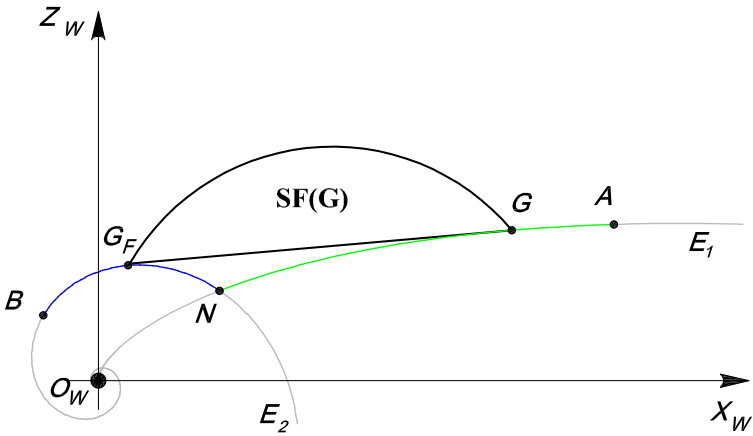
Figure 3.9: Construction of a path shorter than $E_1^+ * E_2^+$ for $\frac{\delta}{2} < \Gamma \leq \frac{\pi - \delta}{2}$.

The proof of this proposition follows straightforwardly from the convexity property of $\tilde{E}$.

Based on proposition 3.5, I am able to prove following results.

Proposition 3.6 *From any starting point A, any path γ of type $S^+ * E_2^+$ $(S^- * E_1^-)$ and $S^+ * E_1^-$ to B can be shortened by a path of type $S^+ E_2^+$ $(S^- E_1^-)$, S^+ (S^-) or $E_2^+ * E_1^-$.*

Proof: To be optimal, a path of type $S^+ * E_2^+$ $(S^- * E_1^-)$ can be shortened by a path of type $S^+ E_2^+$ $(S^- E_1^-)$ or S^+ (S^-). Indeed, if $B \in SF(A)$ $(B \in SB(A))$, γ is shortened by $S^+ = \overline{AB}$ $(S^- = \overline{AB})$. However, let N be the intersection point between extremal arcs S^+ and E_2^+, from proposition 3.4 necessarily $N \in \partial SF_1(A) \cup \partial SF_2(A)$. In this case, for geometrical properties, S^+ and E_2^+ are tangent in N. Hence, path $S^+ * E_2^+$ is shortened by S^+ or $S^+ E_2^+$. Equivalently, $S^- * E_1^-$ is shortened by S^- or $S^- E_1^-$.

Let now consider the path of type $S^+ * E_1^-$ and the non trivial case of $B \notin SF(A)$. From proposition 3.4, the intersection point N between S^+ and E_1^- must lay on $\partial SF_2(A)$.
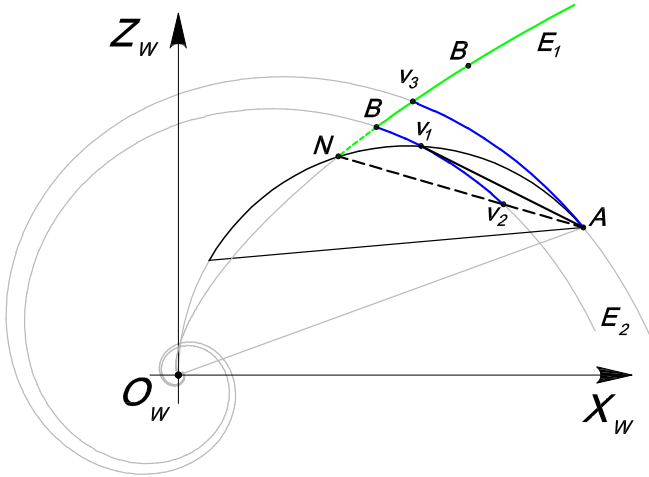
Figure 3.10: Construction used in the proof of proposition 3.6 to short path $S^+ * E_1^-$.

Considering now an arc $E_2(B)$ passing through B, two cases occur (see figure 3.10):

- if arc E_2 intersects $\partial SF_2(A)$ in V_1 and S^+ in V_2, by using proposition 3.5, arc E_2 shortens path $S^+ * E_1^-$ between V_2 and B. A path from A to B of type $S^+ * E_2^+$ has been obtained, that in turn can be shortened by $S^+ E_2^+$ through $V_1 \in \partial SF_2(A)$;

- otherwise, let us consider the arc E_2 through A. It intersects E_1 between B and O_w in V_3. By proposition 3.5, the sub-path of γ between A and V_3 can be shortened by E_2. Hence, a shorter path of type $E_2^+ * E_1^-$ is has been obtained.

■

Proposition 3.7 *For $\frac{\delta}{2} \leq \Gamma \leq \frac{\pi - \delta}{2}$ (Side and Lateral cases), from any starting point A, any path γ of type $S^+ * E_1^+$ ($S^- * E_2^-$) or $S^+ * E_2^-$ can be shortened by a path of type S^+ (S^-), $E_1^+ S^+$ ($E_2^- S^-$) or $E_1^+ * E_2^-$.*

Proof: If $B \in SF(A)$, γ is shortened by $S^+ = \overline{AB}$ ($S^- = \overline{AB}$). However, let us consider first a path γ of type $S^+ * E_1^+$ whose switching point $N \in \partial SF_1(A)$ for proposition 3.4. There always exists a straight line from B tangent to the extremal arc E_1 from A in V_1 between A and O_w. Let V_2 be the intersection point of this straight line and border $\partial SF_1(A)$ ($\partial SB_1(A)$). The unfeasible piecewise straight path from A to B through V_2 shortens path γ (see figure 3.11). In turn, the unfeasible polygonal path is longer than path $E_1^+ S^+$ through V_1. Equivalently $S^- * E_2^-$ can be shortened by $E_2^- S^-$.

For a path γ of type $S^+ * E_2^-$ whose switching point $N \in \partial SF_1(A)$ for proposition 3.4. Let us consider an extremal arc E_1 through B. Two cases can occur (see figure 3.12):

- if E_1 for A intersects arc E_2^- in V but B lays on E_2^- between V and O_w, by using the same construction of the unfeasible polygonal path above, γ can be shortened by $E_1^+ S^+$;

- otherwise the extremal V lays between B and O_w and for proposition 3.5, path of type $E_1^+ * E_2^-$ through V is shorter than $S^+ * E_2^-$.

∎

Notice that, as an extension of proposition 3.4 for the Side and Lateral cases only, if an optimal path from Q to P includes a segment of type S^+ (or S^-) from G, then it ends on $\partial SF_2(G)$.

Proposition 3.8 *For $0 \le \Gamma < \frac{\delta}{2}$ (Frontal case), from any starting point A, any path γ of type $S^+ * E_1^+$ or $S^+ * E_2^-$ can be shortened by a path of type S^+, $S^+ E_1^+$ or $E_1^+ * E_2^-$. Furthermore, for any path γ of type $S^- * E_2^-$ or $S^- * E_1^-$ can be shortened by a path of type S^-, $E_2^- S^-$ or $E_1^+ * E_2^-$.*

Proof: Any path γ of type $S^+ * E_1^+$ can be shortened by a path of type S^+ or $S^+ E_1^+$ for proposition 3.4. For paths $S^+ * E_2^-$ a similar procedure used for the path of type $S^+ * E_1^-$ in the second part of proof of proposition 3.6, can be followed. Proofs for paths $S^- * E_2^-$ or $S^- * E_1^-$ are equivalent to proof of proposition 3.7. ∎
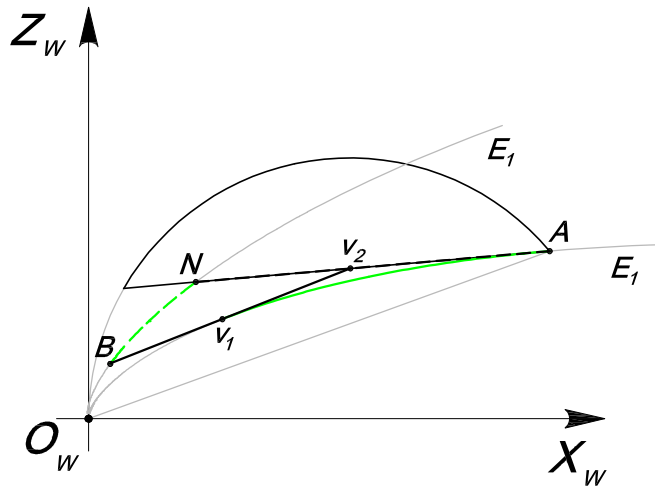
Figure 3.11: Construction used in the proof of proposition 3.7 to short path $S^+ * E_1^+$.
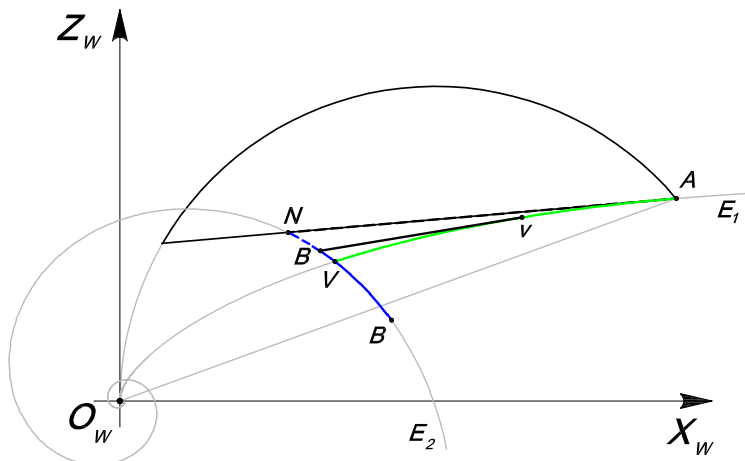

Figure 3.12: Construction used in the proof of proposition 3.7 to short path $S^+ * E_2^-$.

Remark 3.5 *Notice that if a sequence of extremals from A to B is not optimal, also the path from B to A following extremals in reverse*

order and opposite direction is not optimal. For example, $E_1^+ * S^-$ is not optimal since it is the inverse path of type $S^+ * E_1^-$ that is not optimal for proposition 3.6.

By using all previous results, a sufficient family of optimal paths is obtained in the following important theorem.

Theorem 3.4 *For $\frac{\delta}{2} < \Gamma \leq \frac{\pi}{2}$, i.e. Side and Lateral cases, and for any $Q \in D(P)$ to P there exists a shortest path of type $E_1^+ * E_2^- S^- E_1^-$ or of type $E_1^+ S^+ E_2^+ * E_1^-$. For $0 \leq \Gamma \leq \frac{\delta}{2}$, i.e. Frontal case, and for any $Q \in D(P)$ to P there exists a shortest path of type $S^+ E_1^+ * E_2^- S^-$ or of type $S^+ E_2^+ * E_1^- S^-$.*

Proof: According to all propositions above several concatenations of extremal have been proved to be non optimal. Considering extremals as node and, possibly optimal, concatenations of extremal as edges of a graph, the sufficient optimal languages $\mathcal{L}_\Gamma^O$ from Q in $D(P)$, for different values of Γ and δ, are described in figure 3.13. Indeed, it is straightforward to observe that the number of switches between extremals is finite and less or equal to 3, for any value of Γ and δ. Hence, the thesis. ∎

We now study the length of extremal paths from $C(P)$ to P in the sufficient family above.

3.4 Shortest paths from any point in the motion plane

In this section, starting from previous results, the subdivision of $C(P)$ will be obtained. Moreover, by using the Bellman's Principle [50], also the subdivision of $D(P)$ will be given. Finally, by using function F_Q defined in (3.2), paths starting from Q inside $C(P)$ will be transformed in paths starting from $f_Q(P) = \left(\frac{\rho_P^2}{\rho_Q}, -\psi_Q \right)$ outside $C(P)$. From other properties of F_Q, such as proposition 3.1, an optimal path is mapped into an optimal path. Hence, the optimal synthesis from
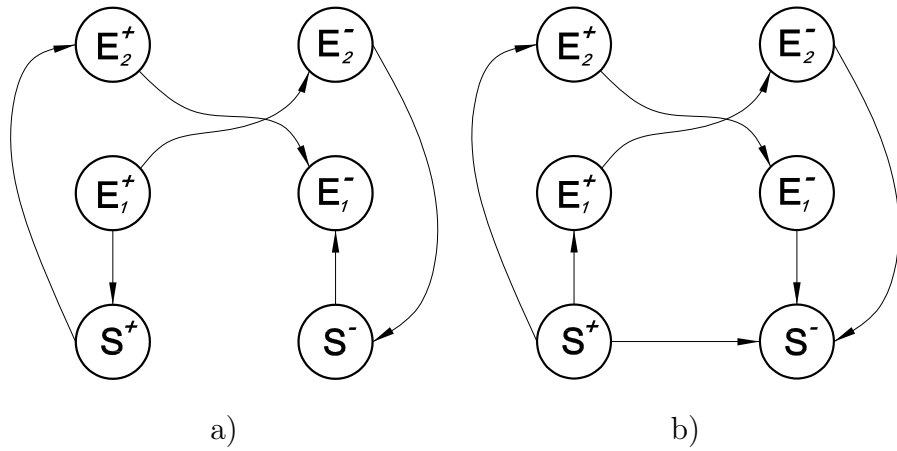
Figure 3.13: Feasible extremals and sequence of extremals from point in D(P): a) in Side and Lateral cases ($\frac{\delta}{2} < \Gamma \le \frac{\pi}{2}$). b) in Frontal case ($0 \le \Gamma \le \frac{\delta}{2}$).

points outside $C(P)$ can be easily obtained mapping through map F_Q all borders of regions inside $C(P)$.

Proposition 3.9 *Given a border* $\mathbf{B}$ *and* $Q \in \mathbf{B}$ *map* F_Q *transforms:*

1. $\mathbf{B} = C(P)$ *into itself;*

2. $\mathbf{B} = \partial SF_2(Q)$ *in* $\partial SB_1(f_Q(P))$

3. $\mathbf{B} = \partial SF_1(Q)$ *in* $\partial SB_2(f_Q(P))$

4. $\mathbf{B} = E_i$ *in arcs of the same type* $(i = 1, 2)$

Proof: The proof of this proposition, equivalent to proposition 2.16, can be found in chapter 2, section 2.5. ∎

In order to simplify the analysis, I will consider separately three cases: Frontal Case, Side Case, and Lateral Case.

3.4.1 Frontal Case

As discuss in chapter 1, the finite alphabet is $\mathcal{A}_{0<\Gamma<\frac{\delta}{2}} = \{*, S^+, S^-,$
$T_1^{L+}, T_1^{L-}, T_2^{R+}, T_2^{R-}\}$ (see also figure 3.2a). As a consequence of
theorem 3.4, it is sufficient to study the length of extremal paths of
type $S^+ T_1^{L+} * T_2^{R-} S^-$ only from points $Q = (\rho_P, \psi_Q)$ on the semicircle
of $C(P)$ (denoted by CS) in the upper-half plane. Indeed, also in
this case, up to a rotation of ψ_Q, optimal paths of type $S^+ T_2^{R+} *$
$T_1^{L-} S^-$ from $Q' = (\rho_P, -\psi_Q)$ in the lower-half plane is easily obtained.
Referring to figure 3.14, let the switching points of the optimal path
be denoted by N, M_1 and M_2. Moreover, in order to do the analysis,
it is useful to parameterize the family by the angular value α_{M_1} of
the switching point M_1 along the arc $C_2(P)$ between P and O_w and
the angular value α_{M_2} of the switching point M_2 along the arc $C_1(Q)$
between Q and O_w.

Theorem 3.5 *For any point $Q \in CS$, length L of a path $\gamma \in \mathcal{P}_Q$ of
type $S^+ T_1^{L+} * T_2^{R-} S^-$ is:*

$$
\begin{aligned}
L = {} & \rho_P \left(\frac{\cos \alpha_{M_1}}{\cos \phi_1} + \frac{\cos \alpha_{M_2}}{\cos \phi_2} \right) + \\
& - \rho_P \frac{\cos \phi_1 + \cos \phi_2}{\cos \phi_1 \cos \phi_2} \left[\rho_P \frac{\sin(\phi_1 - \alpha_{M_1})}{\sin \phi_1} \right]^{\frac{t_2}{t_1 + t_2}} \cdot \\
& \cdot \left[\rho_P \frac{\sin(\phi_2 - \alpha_{M_2})}{\sin \phi_2} \right]^{\frac{t_1}{t_1 + t_2}} e^{\left(\alpha_{M_1} + \alpha_{M_2} - \psi_Q \right) \frac{t_1 t_2}{t_1 + t_2}} , \quad (3.3)
\end{aligned}
$$

*when both $|\phi_1|$ and $|\phi_2|$ belong to $]0, \frac{\pi}{2}[$, with $t_1 = 1/\tan \phi_1$ and
$t_2 = 1/\tan \phi_2$. In the extreme cases $\phi_1 = \phi_2 = 0$ and $|\phi_1| = |\phi_2| = \frac{\pi}{2}$,
we have $L = 2\rho_P$ and $L = 2\rho_P \sin \frac{\psi_Q}{2}$, respectively.*

Proof: Recalling that $P = (\rho_P, 0)$, $Q = (\rho_P, \psi_Q)$, and $M_1 \in C_1(Q)$,
by the sine rule we have

$$
\rho_{M_1} = \rho_P \frac{\sin(\phi_1 - \alpha_{M_1})}{\sin \phi_1}, \quad (3.4)
$$
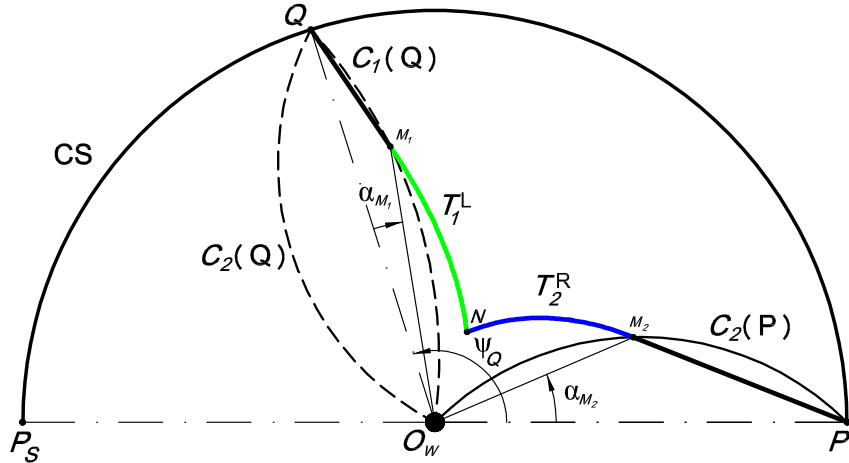
Figure 3.14: Path of type $S^+T_1^{L+} * T_2^{R-}S^-$ from $Q \in CS$.

On the other hand, point $M_2 \in C_2(P)$ and by the sine rule we have

$$\rho_{M_2} = \rho_P \frac{\sin(\phi_2 - \alpha_{M_2})}{\sin \phi_2}, \tag{3.5}$$

Moreover, the lengths of segments S^+ and S^- are

$$\overline{QM_1} = \rho_P \frac{\sin \alpha_{M_1}}{\sin \phi_1}, $$
$$\overline{PM_2} = \rho_P \frac{\sin \alpha_{M_2}}{\sin \phi_2}. \tag{3.6}$$

Setting $t_2 = \frac{\cos \phi_2}{\sin \phi_2}$, the right logarithmic spiral passing through M_2 (denoted with $T_{2M_2}^R$) is given by

$$T_{2M_2}^R : \left(\rho_{M_2} e^{(\alpha_{M_2} - \psi)t_2}, \psi \right).$$

Similarly, setting $t_1 = \frac{\cos \phi_1}{\sin \phi_1}$, the left spiral for M_1 (denoted with $T_{1M_1}^L$) is given by

$$T_{1M_1}^L : \left(\rho_{M_1} e^{-(\psi_Q - \alpha_{M_1} - \psi)t_1}, \psi \right).$$

The intersection point between the spirals $T_{M_1}^L$ and $T_{M_2}^R$ is $N = (\rho_N, \psi_N)$, where

$$\rho_N = \rho_P \, e^{\left(\alpha_{M_1} - \psi_Q + \alpha_{M_2}\right)\frac{t_1 t_2}{t_1 + t_2}} \left(\frac{\sin(\phi_1 - \alpha_{M_1})}{\sin \phi_1}\right)^{\frac{t_2}{t_1 + t_2}} \left(\frac{\sin(\phi_2 - \alpha_{M_2})}{\sin \phi_2}\right)^{\frac{t_1}{t_1 + t_2}}$$

(3.7)

$$\psi_N = \alpha_{M_1} \frac{t_1}{t_1 + t_2} + (\psi_Q - \alpha_{M_2})\frac{t_2}{t_1 + t_2} + \frac{1}{t_1 + t_2} \ln\left(\frac{\sin(\phi_1 - \alpha_{M_1})\sin \phi_2}{\sin(\phi_2 - \alpha_{M_2})\sin \phi_1}\right).$$

(3.8)

Notice that, for $\phi_1 = \phi_2 = \frac{\pi}{2}$ we have $M_1 \equiv M_2 \equiv N$ and spiral arcs have zero length. Hence, from (3.6) and (3.8), $L = 2\rho_P \sin \frac{\psi_Q}{2}$.

For $\phi_1 \in \left]0, -\frac{\pi}{2}\right[$ and $\phi_2 \in \left]0, \frac{\pi}{2}\right[$, the length of the spiral arcs T_1^L from M_1 to N and T_2^R from M_2 to N are given by

$$\overline{M_1 N} = \frac{\rho_{M_2} - \rho_N}{\cos \phi_1} \,,$$

$$\overline{M_2 N} = \frac{\rho_{M_2} - \rho_N}{\cos \phi_2} \,.$$

Adding up, after some simplifications, the total length L is therefore as reported in (3.3).

When $\phi_1 = \phi_2 = 0$, $M_1 \equiv M_2 \equiv O_w$ and spiral arcs have zero length, hence $L = 2\rho_P$. ∎

Having the path's length as a function of three parameters α_{M_1}, α_{M_2} and ψ_Q, I am now in a position to minimize the length within the sufficient family. Notice that I need only to consider $\alpha_{M_2} \in [0, \phi_2]$ (because the problem is symmetric w.r.t. X_w), and $\alpha_{M_1} \in [0, -\phi_1]$ for the geometrical considerations above on $C_2(Q)$ (see remark 3.2 and figure 3.5).

Theorem 3.6 *Given* $Q = (\rho_P, \psi_Q) \in CS$, *with both* $|\phi_1|$ *and* $|\phi_2|$ *belong to* $]0, \pi/2[$, *referring to figure 3.15,*

- *for* $0 < \psi_Q \leq \psi_M \triangleq -\frac{\sin(\phi_1 + \phi_2)}{\cos \phi_1 \cos \phi_2} \ln\left(\frac{\sin \phi_2 \sin(\phi_1 + \phi_2)}{\cos \phi_1 + \cos \phi_2}\right)$, *the optimal path is of type* $T_1^{L+} * T_{2P}^{R-}$;

- *for $\psi_M < \psi_Q \leq \psi_F \triangleq \phi_2 - \phi_1 + \psi_M - \frac{\sin(\phi_1 + \phi_2)}{\cos\phi_1 \cos\phi_2} \ln\left(\frac{\sin\phi_1 \sin(\phi_1 + \phi_2)}{\cos\phi_1 + \cos\phi_2}\right)$, the optimal path is of type $T_1^{L+} * T_2^{R-} S^-$;*

- *for $\psi_F < \psi_Q < \psi_V \triangleq 2\phi_1 + \psi_F$, the optimal path is of type $S^+ T_1^{L+} * T_2^{R-} S^-$;*

- *for $\psi_V \leq \psi_Q < \pi$, the optimal path is of type $S^+ * S^-$*

In a similar procedure followed in chapter 2, previous results have been obtained computing first and second derivatives of L and nonlinear minimization techniques.

I am now interested in determining the locus of switching points between extremals in optimal paths from $D(P)$. Based on a similar procedure followed in propositions 2.12 and 2.13, the loci of switching points are:

- For $Q \in C(P)$ with $0 \leq \psi_Q \leq \psi_M$, the switching locus is the arc of T_{2P}^R within the extreme points P and $m_1 = \left(\rho_P \frac{\sin(\phi_1 + \phi_2)\sin\phi_2}{\cos\phi_1 + \cos\phi_2}\right.$, $\left. \frac{1}{t_2}\ln\left(\frac{\cos\phi_1 + \cos\phi_2}{\sin(\phi_1 + \phi_2)\sin\phi_2}\right)\right)$ (included). On the other hand, in the lower half-plane, for $Q \in C(P)$ with $0 \leq \psi_Q \leq \psi_{\bar{M}} = -\psi_M$, the switching locus is the arc of T_{1P}^L within the extreme points P and $m_2 = \left(\rho_P \frac{\sin(\phi_1 + \phi_2)\sin\phi_1}{\cos\phi_1 + \cos\phi_2}\right.$, $\left.\frac{1}{t_1}\ln\left(\frac{\cos\phi_1 + \cos\phi_2}{\sin(\phi_1 + \phi_2)\sin\phi_1}\right)\right)$ (included).

- For $Q \in C(P)$ with $\psi_F < \psi_Q < \psi_V$, the loci of switching points M_1, N, and M_2 are the arcs $C_2(G_1)$, $C_2(m_1)$, and $C_2(P)$ with $G_1 = (\rho_P \frac{\sin\phi_2}{\sin\phi_1}, \psi_V - \phi_1 - \phi_2)$, respectively. On the other hand, in the lower half-plane, for $Q \in C(P)$ with $-\psi_F = \psi_{\bar{F}} < \psi_Q < \psi_{\bar{V}} = -\psi_V$, the loci of switching points $\bar{M}_1$, $\bar{N}$, and $\bar{M}_2$ are the arcs $C_1(G_2)$, $C_1(m_2)$, and $C_1(P)$ with $G_2 = (\rho_P \frac{\sin\phi_1}{\sin\phi_2}, \psi_{\bar{V}} + \phi_1 + \phi_2)$, respectively.

- For $Q \in C(P)$ with $\psi_M < \psi_Q \leq \psi_F$, the loci of switching points M_2, N are the arcs $C_2(P)$, $C_2(m_1)$, respectively; whereas, in

Region	Optimal Path
I $\cup$ I$_c$	S^-
II	$T_1^{L+} * T_2^{R-}$
II$'$	T_{2P}^{R-}
III $\cup$ III$_c$	$S^+ * S^-$
IV	$S^+ T_1^{L+} * T_2^{R-} S^-$
V	$T_1^{L+} * T_2^{R-} S^-$
VI	$T_2^{R-} S^-$
II$_c$	$T_2^{R+} * T_1^{L-}$
II$'_c$	T_{1P}^{R-}
IV$_c$	$S^+ T_2^{R+} * T_1^{R-} S^-$
V$_c$	$T_2^{R+} * T_1^{L-} S^-$
VI$_c$	$T_1^{L-} S^-$
V$_s$	$S^+ T_2^{R+} * T_{1P}^{L-}$

Table 3.1: Optimal synthesis in the disc $D(P)$.
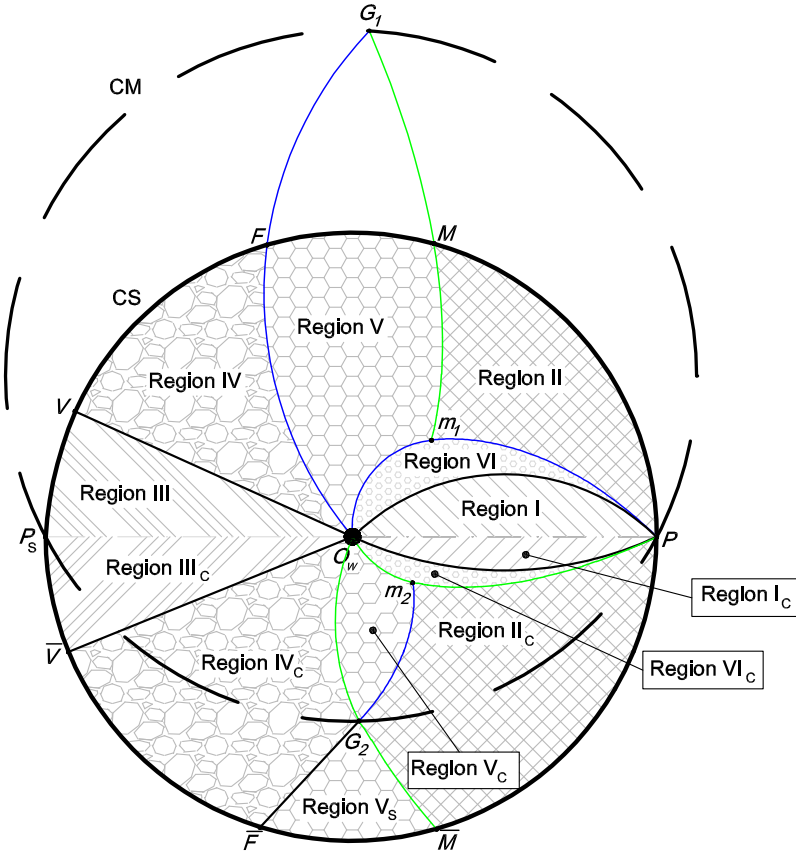
Figure 3.15: Partition of $D(P)$.

the lower half-plane, for $Q \in C(P)$ with $\psi_{\bar{M}} < \psi_Q < \psi_{\bar{F}}$, the switching loci are the arcs T_{1P}^L between P and m_2 (included), and $T_{1\bar{M}}^L$ between $\bar{M}$ and $G_2 = (\rho_P \frac{\sin \phi_1}{\sin \phi_2}, \psi_{\bar{V}} + \phi_1 + \phi_2)$.

- Finally, for $Q \in C(P)$ with $\psi_V \leq \psi_Q \leq \pi$ and $\psi_{\bar{V}} \leq \psi_Q \leq -\pi$, the loci of switching points is point O_w.

Having solved the optimal synthesis for points on $C(P)$, I now address optimal paths for internal points by using the following simple idea: for any $Q \in D(P) \setminus \partial D(P)$, find a point $S \in \partial D(P)$ such that

an optimal path γ from S to P goes through Q. By Bellmann's optimality principle [50], the sub-path from Q to P is also optimal. Figure 3.15 shows the partition of $D(P)$ in regions, whereas table 3.1 describes the optimal path from point Q belongs to each region.

Regions of the partition are generalized polygonals whose vertices are the characteristic points in $D(P)$ and whose boundaries belong either to the extremal curves, to the switching loci, or to $\partial D(P)$. All regions have three vertices, except Region I which has two. The boundary arc T_{2P}^{R} (T_{1P}^{L}) between Region II and Region VI (between Region II$_c$ and Region VI$_c$) is a degenerate case of measure zero in $D(P)$, and will be denoted as Region II$'$ (II$'_c$) (see table 3.1).

For points outside $C(P)$, function F_Q has been defined in (3.2) in order to transform paths starting from Q inside $C(P)$ in paths starting from $f_Q(P) = \left(\frac{\rho_P^2}{\rho_Q}, -\psi_Q \right)$ outside $C(P)$.

From other properties of F_Q, such as proposition 3.1, an optimal path is mapped into an optimal path. Hence, the optimal synthesis from points outside $C(P)$ can be easily obtained mapping through map F_Q all borders of regions inside $C(P)$.

Remark 3.6 *Referring to figure 3.15, points P, G_1, P_s and G_2 belong to a circle, named CM in figure. This circle is centered in a point whose cartesian coordinates are $(0, \alpha)$ where*

$$\alpha = \rho_P \frac{\sin^2 \phi_1 - \sin^2 \phi_2}{2 \sin \theta_{12} \sin \phi_1 \sin \phi_2} ,$$

and radius

$$R = \frac{\rho_P}{2 \sin \theta_{12}} \sqrt{\frac{\sin^2 \phi_1}{\sin^2 \phi_2} + \frac{\sin^2 \phi_2}{\sin^2 \phi_1} - 2 \cos(2\theta_{12})} ,$$

where

$$\theta_{12} = \frac{1}{t_1} \ln \left(\frac{\cos \phi_1 + \cos \phi_2}{\sin(\phi_1 + \phi_2) \sin \phi_1} \right) + \frac{1}{t_2} \ln \left(\frac{\cos \phi_1 + \cos \phi_2}{\sin(\phi_1 + \phi_2) \sin \phi_2} \right) .$$

It would be notice that if $\phi_1 = \phi_2 = \phi$ circle CM become circle $C(P)$, whereas if $\phi_1 = 0$ ($\phi_2 = 0$) circle CM degenerates in X_w, i.e., a circle with infinite radius.

Finally, the result of this analysis is the optimal synthesis of the entire motion plane shown in figure 3.16 and described in table 3.2.

Notice that, the subdivision of circle CM is similar to the subdivision of circle $C(P)$ for the Symmetric Frontal case, i.e., for $\Gamma = 0$. Indeed, for $Q \in CM$ on the upper half-plane, if $0 \le \psi_Q \le \psi_{G_1}$ the optimal path is of type $T_1^{L+} * T_2^{R-}$, if $\psi_{G_1} < \psi_Q < \psi_{V_1}$ the optimal path is of type $S^+ T_1^{L+} * T_2^{R-} S^-$ and, finally, if $\psi_{V_1} \le \psi_Q \le \pi$ the optimal path is of type $S^+ * S^-$. The same occur for point $Q \in C(P)$ in the lower half-plane. In particular, if $0 \le \psi_Q \le \psi_{G_2}$ the optimal path is of type $T_2^{R+} * T_1^{L-}$, if $\psi_{G_2} < \psi_Q < \psi_{V_2}$ the optimal path is of type $S^+ T_2^{R+} * T_1^{L-} S^-$ and, finally, if $\psi_{V_2} \le \psi_Q \le \pi$ the optimal path is of type $S^+ * S^-$.

3.4.2 Side and Lateral Cases

For the Side case, as discuss in chapter 1, the finite alphabet is $\mathcal{A}_{\frac{\delta}{2}<\Gamma<\frac{\pi-\delta}{2}} = \{*, S^+, S^-, T_1^{R+}, T_1^{R-}, T_2^{R+}, T_2^{R-}\}$ (see also figure 3.3d). As a consequence, based on theorem 3.4, it is sufficient to study the length of extremal paths of type $T_1^{R+} * T_2^{R-} S^- T_1^{R-}$ only from points $Q = (\rho_P, \psi_Q)$ on the semicircle of $C(P)$ (denoted by CS) in the upper-half plane. Indeed, up to a rotation of ψ_Q, optimal paths of type $T_1^{R+} S^+ T_2^{R+} * T_1^{R-}$ from $Q' = (\rho_P, -\psi_Q)$ in the lower-half plane is easily obtained. Referring to figure **??**, let the switching points of the optimal path be denoted by N, M_1 and M_2 or $\bar{N}$, $\bar{M}_1$ and $\bar{M}_2 \equiv P$, respectively, depending on the angular values α_{M_1} or $\alpha_{\bar{M}_1}$. Moreover, in order to do the analysis, it is useful to parameterize the family by the angular value $\alpha_{\bar{M}_1}$ of the switching point $\bar{M}_1$ along the arc $C_2(P)$ between P and P_F or the angular value α_{M_1} of the switching point M_1 along the extremal E_1 between P_F and O_w.

Region	Optimal Path
I $\cup$ I$_c$	S^-
I$_s$ $\cup$ I$_{cs}$	S^+
II $\cup$ II$_{cs}$	$T_1^{L+} * T_2^{R-}$
II$'$	T_{2P}^{R-}
II$'_s$	T_{2P}^{R+}
III $\cup$ III$_c$ $\cup$ III$_s$ $\cup$ III$_{cs}$	$S^+ * S^-$
IV $\cup$ IV$_{cs}$	$S^+ T_1^{L+} * T_2^{R-} S^-$
V	$T_1^{L+} * T_2^{R-} S^-$
VI	$T_2^{R-} S^-$
II$_c$ $\cup$ II$_s$	$T_2^{R+} * T_{1P}^{L-}$
II$'_c$	T_{1P}^{L-}
II$'_{cs}$	T_{1P}^{L+}
IV$_c$ $\cup$ IV$_s$	$S^+ T_2^{R+} * T_1^{R-} S^-$
V$_c$	$T_2^{R+} * T_1^{L-} S^-$
VI$_c$	$T_1^{L-} S^-$
V$_s$	$S^+ T_2^{R+} * T_{1P}^{L-}$
V$_{cs}$	$S^+ T_1^{L+} * T_{2P}^{R-}$
VI$_s$	$S^+ T_{2P}^{R+}$
VI$_{cs}$	$S^+ T_{1P}^{L+}$

Table 3.2: Optimal synthesis for all points of the motion plane.
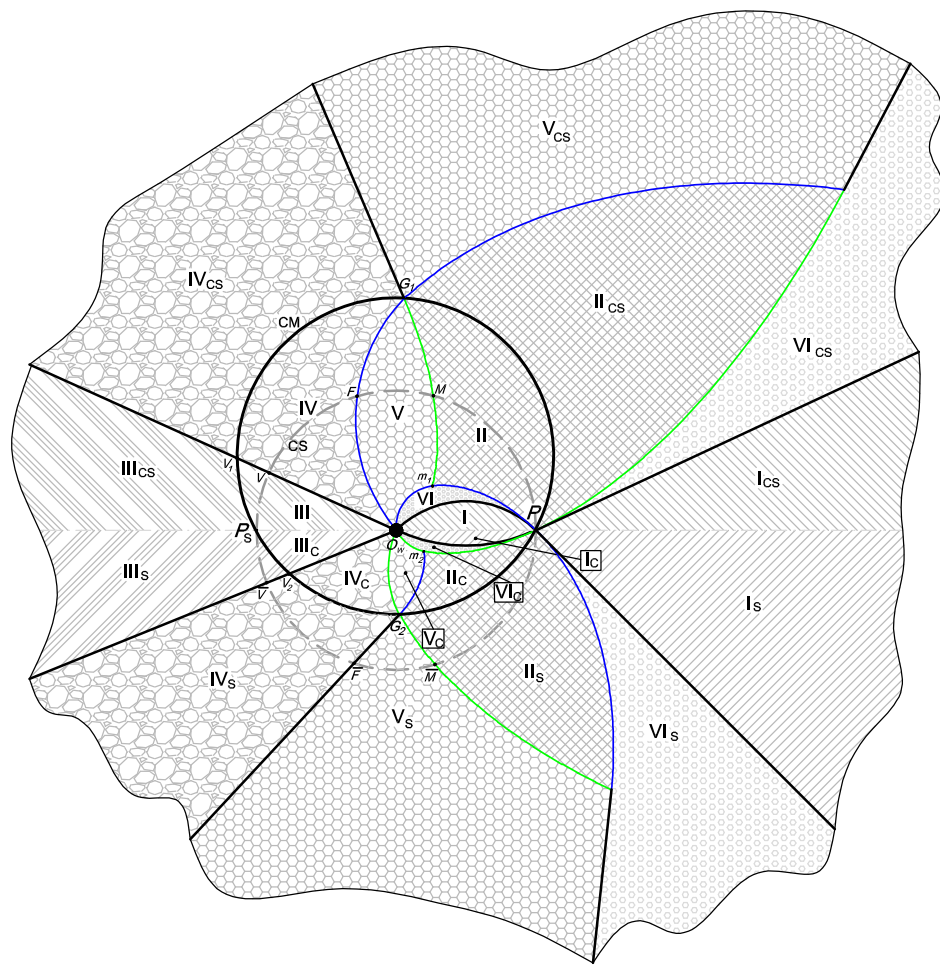
Figure 3.16: Partition of the motion plane for $0 \leq \Gamma < \frac{\delta}{2}$, i.e., the Frontal case.

Theorem 3.7 *For any point* $Q \in CS$, *length* L *of a path* $\gamma \in \mathcal{P}_Q$ *(see figure 3.17) of type* $T_1^{R+} * T_2^{R-} S^- T_1^{R-}$ *is:*

- *for* $0 \leq \alpha_{\bar{M}_1} \leq \phi_2 - \phi_1$, *i.e., from* P *to* P_F *(notice that the last arc has zero length):*

$$L = \rho_P \left\{ \frac{\cos \alpha_{\bar{M}_1}}{\cos \phi_2} + \frac{1}{\cos \phi_1} + \right.$$

$$\left. - \frac{\cos \phi_1 + \cos \phi_2}{\cos \phi_1 \cos \phi_2} e^{\left(\psi_Q - \alpha_{\bar{M}_1}\right)\frac{t_1 t_2}{t_2 - t_1}} \left(\frac{\sin \left(\phi_2 - \alpha_{\bar{M}_1}\right)}{\sin \phi_2} \right)^{-\frac{t_1}{t_2 - t_1}} \right\},$$

$$(3.9)$$

- *for $\alpha_{M_1} \geq \phi_2 - \phi_1$, i.e., from P_F to O_w:*

$$L = \rho_P \left\{ \frac{2}{\cos \phi_1} + e^{-\alpha_{M_1} t_1} \left[\frac{\cos(\phi_2 - \phi_1)}{\cos \phi_2} - \frac{1}{\cos \phi_1} + \right. \right.$$

$$\left. \left. - \frac{\cos \phi_1 + \cos \phi_2}{\cos \phi_1 \cos \phi_2} e^{[\psi_Q - (\phi_2 - \phi_1)]\frac{t_1 t_2}{t_2 - t_1}} \left(\frac{\sin \phi_1}{\sin \phi_2} \right)^{-\frac{t_1}{t_2 - t_1}} \right] \right\},$$

$$(3.10)$$

with $t_1 = 1/\tan \phi_1$ and $t_2 = 1/\tan \phi_2$.

Proof: Recalling that $P = (\rho_P, 0)$, $Q = (\rho_P, \psi_Q)$, when $0 \leq \alpha_{\bar{M}_1} \leq \phi_2 - \phi_1$, $\bar{M}_1 \in \partial SF_2(P)$ (see proposition 3.4), by the law of sines we have

$$\rho_{\bar{M}_1} = \rho_P \frac{\sin(\phi_2 - \alpha_{\bar{M}_1})}{\sin \phi_2}, \qquad (3.11)$$

and the length of segments S^- is

$$\overline{P\bar{M}_1} = \rho_P \frac{\sin \alpha_{\bar{M}_1}}{\sin \phi_2}, \qquad (3.12)$$

(cf. figure 3.17).

From (1.13), setting $t_2 = \frac{\cos \phi_2}{\sin \phi_2}$, the right logarithmic spiral passing through $\bar{M}_1$ (denoted with $T^R_{2\bar{M}_1}$) is given by

$$T^R_{2\bar{M}_1} : \left(\rho_{\bar{M}_1} e^{(\alpha_{\bar{M}_1} - \psi)t_2}, \psi \right).$$

Similarly, setting $t_1 = \frac{\cos \phi_1}{\sin \phi_1}$ the right spiral through Q (denoted as T_{1Q}^R) is given by

$$T_{1Q}^R : \left(\rho_Q e^{(\psi_Q - \psi)t_1}, \psi \right).$$

The intersection point between the spirals $T_{2\overline{M}_1}^R$ and T_{1Q}^R is $\overline{N} = (\rho_{\overline{N}}, \psi_{\overline{N}})$, where

$$\rho_{\overline{N}} = \rho_P \ e^{\left(\psi_Q - \alpha_{\overline{M}_1} \right) \frac{t_1 t_2}{t_2 - t_1}} \left(\frac{\sin \left(\phi_2 - \alpha_{\overline{M}_1} \right)}{\sin \phi_2} \right)^{-\frac{t_1}{t_2 - t_1}} \quad (3.13)$$

$$\psi_{\overline{N}} = \psi_Q \frac{t_1}{t_2 - t_1} - \alpha_{\overline{M}_1} \frac{t_2}{t_2 - t_1} - \frac{1}{t_2 - t_1} \ln \left(\frac{\sin \left(\phi_2 - \alpha_{\overline{M}_1} \right)}{\sin \phi_2} \right). \quad (3.14)$$

The length of the spiral arcs $T_{2\overline{M}_1}^R$ and T_{1Q}^R from $\overline{M}_1$ and Q to $\overline{N}$, respectively, are:

$$L_{\overline{M}_1 \overline{N}} = \frac{\rho_{\overline{M}_1} - \rho_{\overline{N}}}{\cos \phi_2},$$

$$L_{Q \overline{N}} = \frac{\rho_P - \rho_{\overline{N}}}{\cos \phi_1}.$$

Adding up, after some simplifications, the total length L is therefore as reported in (3.9).

When $\alpha_{M_1} \geq \phi_2 - \phi_1$, the optimal path is of type $T_1^{R+} * T_2^{R-} S^- T_1^{R-}$, where the last arc is a spiral arc passing through P, $i.e.$ T_{1P}^{R-}. As a consequence, the switching point M_2 belongs to T_{1P}^{R-} (cf. figure 3.17). Moreover, from results of theorem **??** (see also figure 3.9), $M_1 \equiv M_{2F}$ and for simple geometrical considerations, $M_1 \in T_{1P_F}^R$. For this reasons, coordinates of point $M_2 = (\rho_{M_2}, \psi_{M_2})$ are

$$M_2 : \left(\rho_P \ e^{(\phi_2 - \phi_1 - \alpha_{M_1})t_1}, \ \alpha_{M_1} - (\phi_2 - \phi_1) \right), \quad (3.15)$$

and coordinates of point $M_1 = (\rho_{M_1}, \psi_{M_1})$ are

$$M_1 : \left(\rho_P \frac{\sin \phi_1}{\sin \phi_2} e^{(\phi_2 - \phi_1 - \alpha_{M_1})t_1}, \ \alpha_{M_1} \right). \quad (3.16)$$

The right logarithmic spiral $T^R_{2M_1}$ passing through M_1 is given by

$$T^R_{2M_1} : \left(\rho_{M_1}\ e^{(\alpha_{M_1}-\psi)t_2}, \psi\right) .$$

Similarly, the right logarithmic spiral through Q, denoted as T^R_{1Q} is given by

$$T^R_{1Q} : \left(\rho_P\ e^{(\psi_Q-\psi)t_1}, \psi\right) .$$

The intersection point between spirals T^R_{1Q} and $T^R_{2M_1}$ is point $N = (\rho_N, \psi_N)$, where

$$\rho_N = \rho_P\ e^{\psi_Q \frac{t_1 t_2}{t_2-t_1}}\ e^{-\alpha_{M_1} t_1}\ e^{-(\phi_2-\phi_1)\frac{t_1^2}{t_2-t_1}} \left(\frac{\sin\phi_1}{\sin\phi_2}\right)^{-\frac{t_1}{t_2-t_1}} , \qquad (3.17)$$

$$\psi_N = \alpha_{M_1} + (\phi_2-\phi_1)\frac{t_1}{t_2-t_1} - \psi_Q\frac{t_1}{t_2-t_1} + \frac{1}{t_2-t_1}\ln\left(\frac{\sin\phi_1}{\sin\phi_2}\right) . \quad (3.18)$$

The length of the arc of spiral T^{R-}_{1P} between P and M_2 is

$$L_{PM_2} = \frac{\rho_P - \rho_{M_2}}{\cos\phi_1} = \frac{\rho_P}{\cos\phi_1}\left(1 - e^{(\phi_2-\phi_1-\alpha_{M_1})t_1}\right) ,$$

the length of arc S^- from M_1 to M_2 is

$$\overline{M_1 M_2} = \rho_P \frac{\sin(\phi_2 - \phi_1)}{\sin\phi_2}\ e^{(\phi_2-\phi_1-\alpha_{M_1})t_1}$$

and the length of the spiral arcs T^R_{1Q} and $T^R_{2M_1}$ from M_1 and Q to N, respectively, are

$$L_{M_1 N} = \frac{\rho_P - \rho_N}{\cos\phi_1} ,$$

$$L_{QN} = \frac{\rho_{M_1} - \rho_N}{\cos\phi_2} .$$

Adding up, after some simplifications, the total length L is obtained, as reported in (3.10). ∎

Having the path's length as a function of two parameters α_{M_1} or $\alpha_{\bar{M}_1}$ and ψ_Q, I am now in a position to minimize the length within the sufficient family.
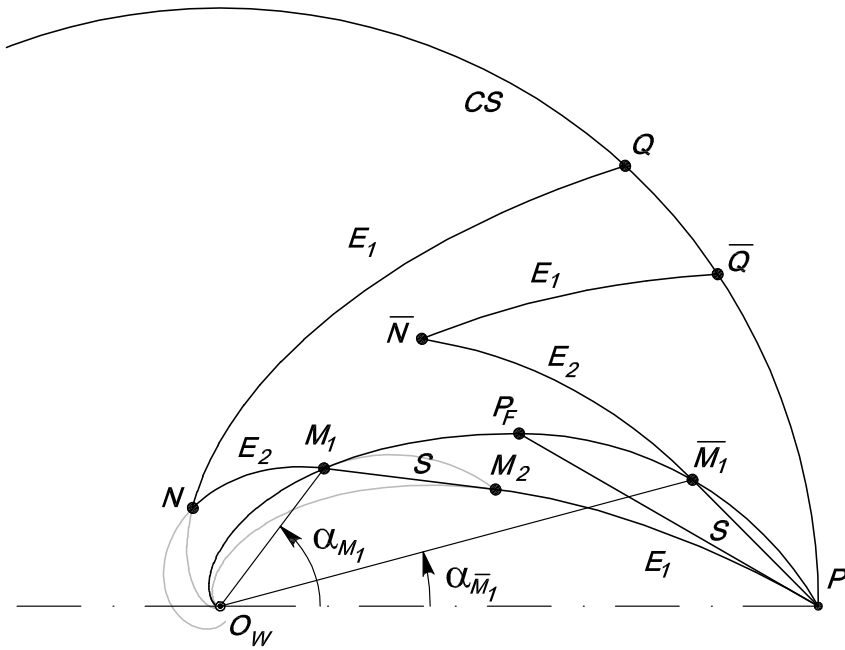
Figure 3.17: Path of type $T_1^{R+} * T_2^{R-} S^- T_1^{R-}$ or the degenerate case of type $T_1^{R+} * T_2^{R-} S^-$ from $Q \in CS$.

Theorem 3.8 *Given a point $Q \in CS$,*

- *for $0 \le \psi_Q \le \psi_{R_1} := \frac{\sin(\phi_2-\phi_1)}{\cos\phi_1\cos\phi_2} \ln\left(\frac{\cos\phi_1+\cos\phi_2}{\sin\phi_2\sin(\phi_2-\phi_1)}\right)$, optimal path is of type $T_1^{R+} * T_2^{R-}$;*

- *for $\psi_{R_1} \le \psi_Q \le \psi_{R_2}$ with $\psi_{R_2} := (\phi_2-\phi_1)+\psi_{R_1}+\tan\phi_2 \ln\left(\frac{\sin\phi_1}{\sin\phi_2}\right)$, optimal path is of type $T_1^{R+} * T_2^{R-} S^-$;*

- *for $\psi_{R_2} \le \psi_Q \le \pi$ the optimal path is $T_1^{R+} * T_1^{R-}$ through O_w.*

Moreover, for $\psi_Q = \psi_{R_2}$, any optimal path of type $T_1^{R+} * T_2^{R-} S^- T_1^{R-}$ turns out to have the same length ℓ of optimal path $T_1^{R+} * T_1^{R-}$. Hence, for $\psi_Q = \psi_{R_2}$ also $T_1^{R+} * T_2^{R-} S^- T_1^{R-}$ is optimal.

Previous results have been obtained computing first and second derivatives of L and nonlinear minimization techniques.

I am now interested in determining the locus of switching points between extremals in optimal paths.

Proposition 3.10 *For $Q \in CS$ with $0 < \psi_Q \leq \psi_{R_1}$, the switching locus is the arc of E_2 between P $M = (\rho_P \frac{\sin \phi_2 \sin(\phi_2 - \phi_1)}{\cos \phi_1 + \cos \phi_2}, \psi_M)$ (included), where $\psi_M = \tan \phi_2 \ln \left(\frac{\rho_P}{\rho_M} \right)$.*

Proof: From theorem 3.8, the optimal path from $Q \in CS$ to P is of type $T_1^{R+} * T_2^{R-}$ (see figure 3.18), with $T_2^{R-} \equiv T_{2P}^{R-}$, hence the switch occurs on T_{2P}^{R-}. For $\psi_Q = \psi_{R_1}$ the intersection between T_1^{R+} and T_2^{R-} is M (see figure 3.18). ∎

Proposition 3.11 *For $Q \in CS$ with $\psi_{R_1} < \psi_Q < \psi_{R_2}$, the loci of switching points M_2 and N are the $\partial SF_2(P)$ and $\partial SF_2(M)$.*

Proof: For $Q \in CS$ with $\psi_{R_1} < \psi_Q < \psi_{R_2}$, from theorem 3.8 we have $\overline{M}_1 \in \partial SF_2(P)$ (see figure 3.18). Furthermore, substituting the optimal values of α_{M_1} coordinates, obtained computing first and second derivatives of L, in equations (3.13) and (3.14) of the intersection point $\overline{N}$ between $E_1 \equiv T_1^{R+}$ through Q and $E_2 \equiv T_2^{R-}$ through $\overline{M}_1$ we obtain $\overline{N} \in \partial SF_2(m)$ (see proof of theorem 3.7). ∎

Finally, for $Q \in CS$ with $\psi_{R_2} \leq \psi < \pi$, the switching locus reduces to the origin O_w since two extremals T_i and intersect only in the origin for $i = 1, 2$.

The synthesis on $C(P)$ induce a partition in regions of $D(P)$. Indeed, for any $Q \in D(P)$, there exists a point $V \in C(P)$ such that the optimal path γ from V to P goes through Q. The Bellmann's optimality principle ensure the optimality of the sub-path from Q to P. Based on this construction the partition of $C(P)$ is reported in figure 3.18 and table 3.3.

For points outside $C(P)$, function F_Q has been defined in (3.2) in order to transform paths starting from Q inside $C(P)$ in paths starting from $f_Q(P) = \left(\frac{\rho_P^2}{\rho_Q}, -\psi_Q \right)$ outside $C(P)$.
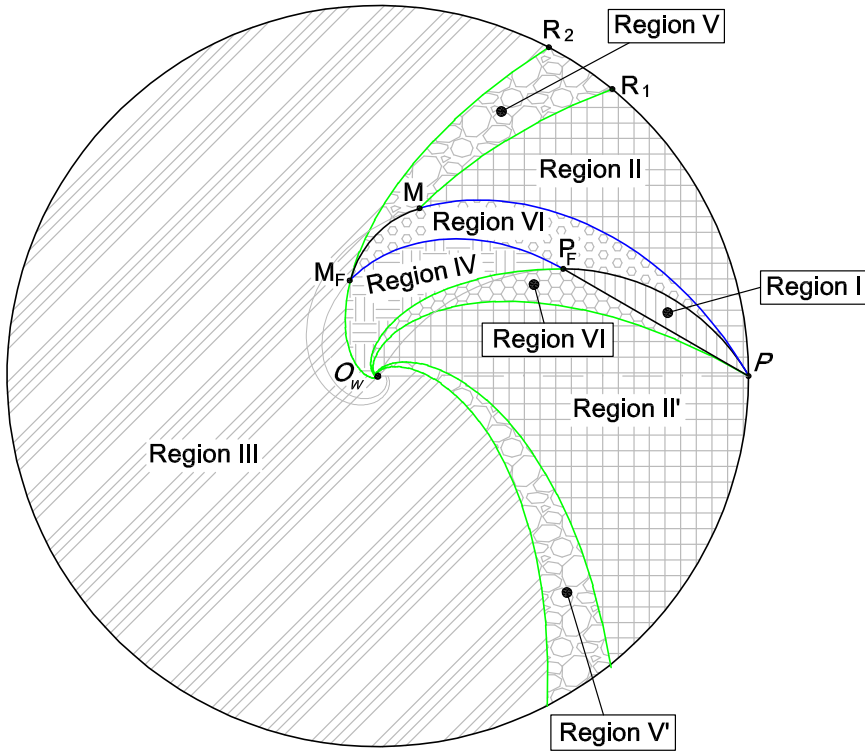
Figure 3.18: Partition of $D(P)$.

Based on proposition 3.9, the optimal synthesis of the entire motion plane is reported in figure 3.19.

The particular cases with $\Gamma = \frac{\delta}{2}$ and $\Gamma = \frac{\pi - \delta}{2}$, i.e., Borderline Frontal and Borderline Side cases can be easy obtained.

We first obtain the synthesis of the Borderline Frontal case whose finite alphabet is $\mathcal{A}_{\Gamma = \frac{\delta}{2}} = \left\{ *, S^+, S^-, H^+, H^-, T_2^{R+}, T_2^{R-} \right\}$, reported in figure 3.20 from the one obtained in the previous section. Notice that, $E_1 = T_1^R$ of the Side case degenerates in a straight line H through O_w for $\Gamma = \frac{\delta}{2}$, i.e., the Borderline Frontal case, and the finite alphabet is $\mathcal{A}_{\Gamma = \frac{\delta}{2}} = \left\{ *, S^+, S^-, H^+, H^-, T_2^{R+}, T_2^{R-} \right\}$. Indeed, referring to figure 3.18, points M_F and P_F degenerate on O_w. As a

Region	Optimal Path
I	S^-
II	$T_1^+ * T_2^-$
II$'$	$T_2^+ * T_1^-$
III	$T_1^+ * T_1^-$
IV	$T_2^- S^- T_1^-$
V	$T_1^+ * T_2^- S^-$
V$'$	$S^+ T_2^+ * T_1^-$
VI	$S^- T_1^-$

Table 3.3: Optimal synthesis in the disc $D(P)$.

consequence, Region IV, IV and VI' while coordinates Ψ_{R_1} and Ψ_{R_2} of points R_1 and R_2 can be obtained from values in 3.8 replacing $\phi_1 = 0$.

Referring again to figure 3.18, in the Borderline Side case, i.e., the left sensor border is aligned with the axle direction, $E_2 = T_2^R$ degenerates in a circumference C centered in O_w and the finite alphabet is $\mathcal{A}_{\Gamma = \frac{\pi - \delta}{2}} = \left\{ *,\ S^+,\ S^-,\ T_1^{R+},\ T_1^{R-},\ C^+,\ C^- \right\}$. Points $R_1 \equiv M$ and R_2 lays on $C(P)$ with $\Psi_{R_1} = \frac{1 + \sin\phi_1}{\cos\phi_1}$ and $\Psi_{R_2} = \frac{\pi}{2} - \phi_1 + \Psi_{R_1} + \tan\phi_1 \ln(\sin\phi_1)$. The obtained synthesis is reported in figure 3.21.

For the Lateral case the synthesis can be obtained from the one in figure 3.21 and it is reported in figure 3.22. Finally, the synthesis of the Symmetric Lateral case with $\Gamma = \pi/2$, i.e., axis Z_c of the sensor is aligned with axial direction, is reported in figure 3.23.

For completeness figure 3.24 shows the subdivision of the motion plane in case of $\delta = \frac{\pi}{2}$ and $\Gamma = \frac{\delta}{2}$, i.e., the right sensor border is aligned with robot's forward direction, whereas left sensor border is aligned with axial direction.
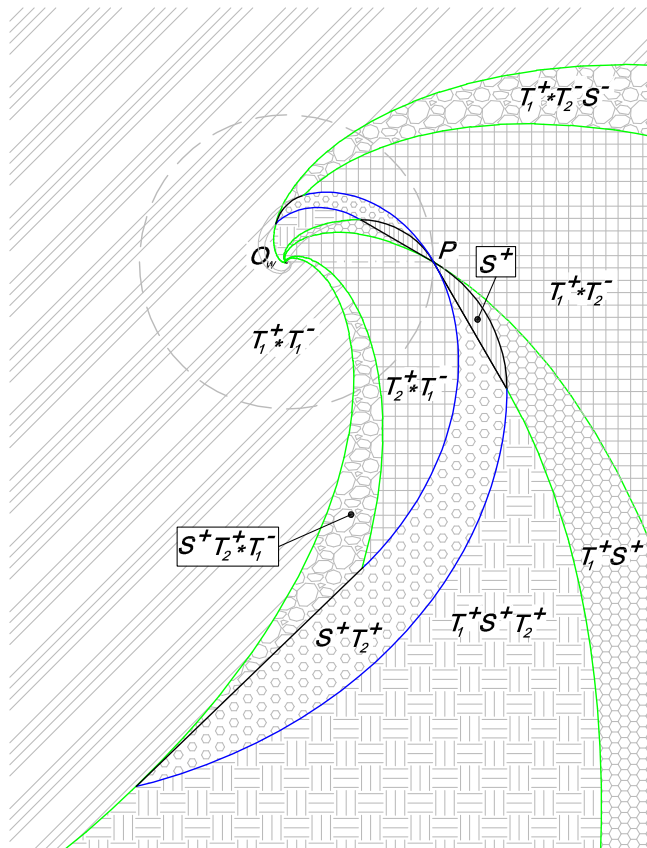
Figure 3.19: Partition of the motion plane for $\frac{\delta}{2} < \Gamma < \frac{\pi-\delta}{2}$.

3.5   Conclusion

In this chapter, a complete characterization of shortest paths for unicycle nonholonomic mobile robots equipped with a side sensor systems with limited field-of-view has been proposed, and hence a generalization of results obtained in previous chapter 2 to arbitrarily FOVs. In particular, the forward direction is not necessarily included inside the sensor FOV. This leads to a more complex analysis of the reduction to a finite and sufficient family of optimal paths by excluding particular
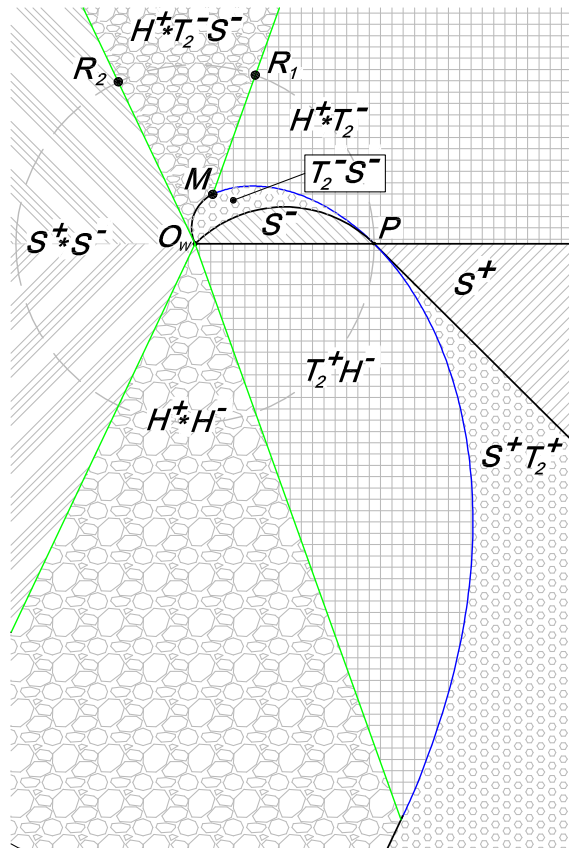
Figure 3.20: Partition of the motion plane for $\Gamma = \delta/2$ (i.e., the right sensor border is aligned with the robot motion direction, Borderline Frontal).

types of path. Nevertheless, also in this case, a finite sufficient family of optimal paths has been determined based on geometrical properties of the considered problem and a complete shortest path synthesis to reach a point keeping a feature in sight has been provided.
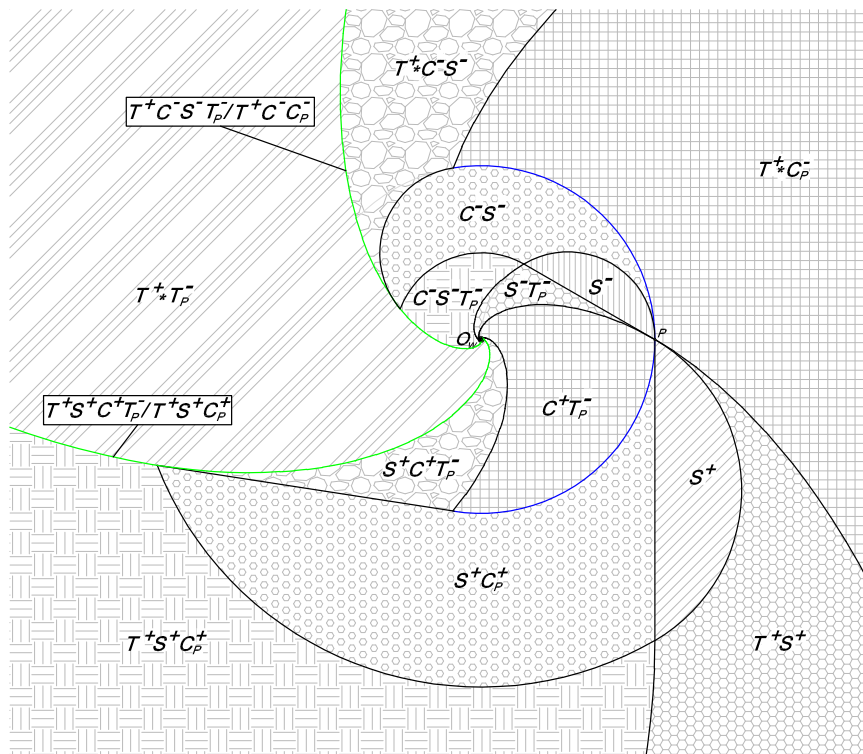
Figure 3.21: Partition of the motion plane for $\Gamma = \frac{\pi - \delta}{2}$ (i.e., the left sensor border is aligned with the axle direction, Borderline Side).
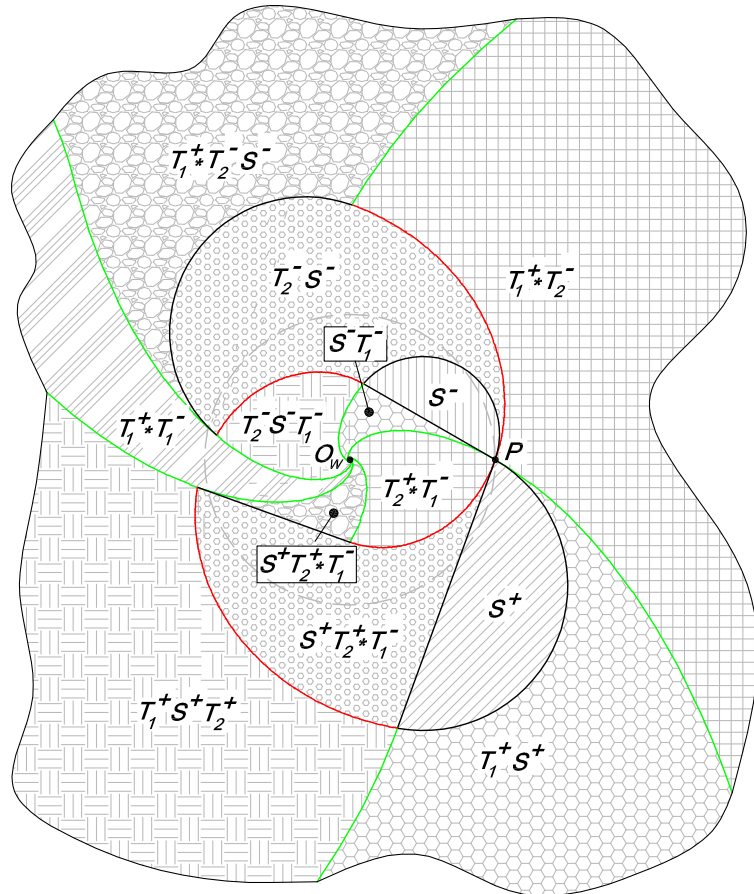
Figure 3.22: Partition of the motion plane for $\frac{\pi-\delta}{2} \leq \Gamma < \frac{\pi}{2}$ (i.e. axle direction is included inside the SR).
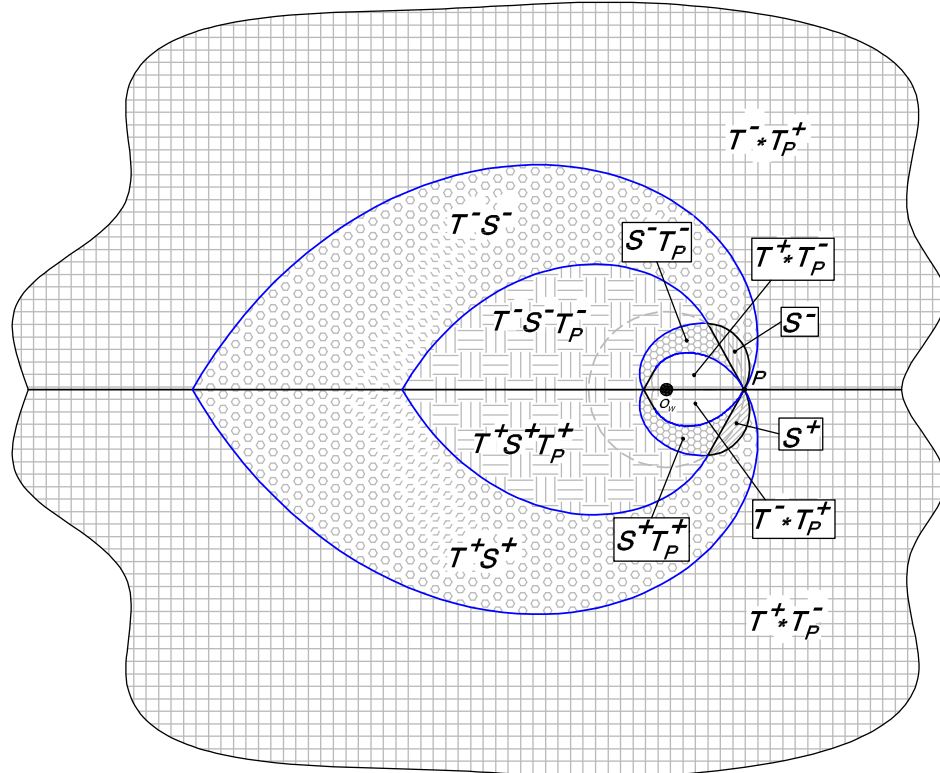
Figure 3.23: Partition of the motion plane for $\Gamma = \frac{\pi}{2}$ (i.e. axle direction is aligned with axis Z_c.
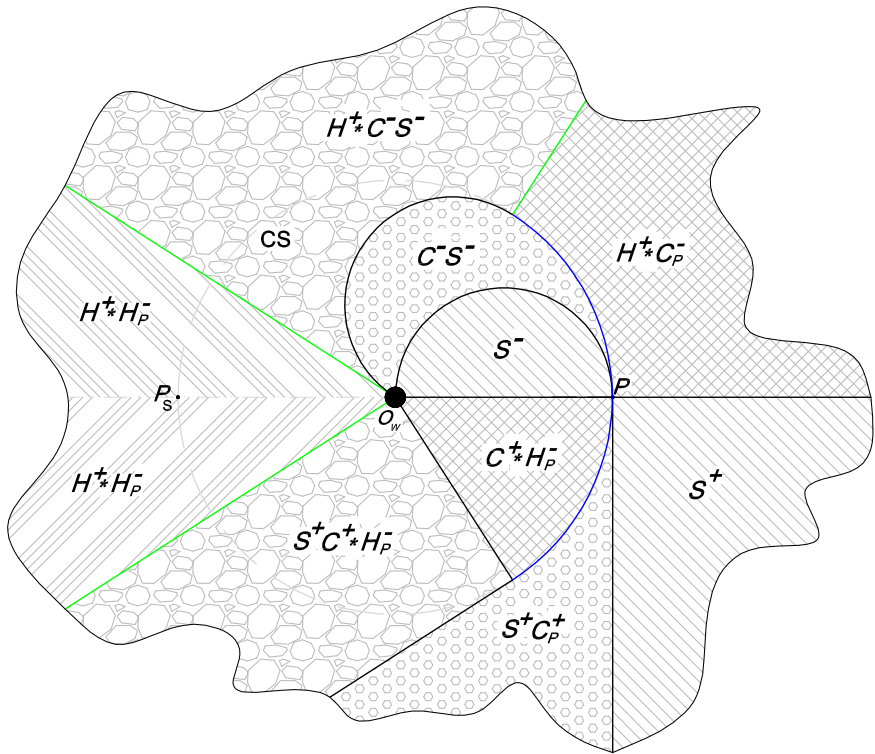
Figure 3.24: Partition of the motion plane in case of $\delta = \frac{\pi}{2}$ and $\Gamma = \frac{\delta}{2}$ (i.e., the right sensor border is aligned with robot's forward direction, whereas left sensor border is aligned with axial direction.

Part II

Optimal Visual Servoing
With Limited Field-Of-View

THIS PART presents an optimal feedback control scheme to drive a vehicle equipped with a limited Field-Of-View camera towards a desired position following the shortest path and keeping a given landmark in sight. Indeed, towards the practical application of the results of previous chapters, a crucial step is to translate the optimal trajectories (which are evaluated from any initial condition as plans to be executed in open-loop) into feedback control laws, i.e., to write laws which determine the control inputs (the vehicle velocities) as a function of the current state of the system only. Only when such a feedback control law is derived, it will be possible to make the system reach the desired posture with robustness against disturbances and uncertainties, i.e., it will be possible to show *stability* of the system at the desired configuration.

Chapter 4 presents optimal feedback control laws and a proof of stability for the controlled system, whereas chapter 5 reports simulations to show the effectiveness of the proposed technique in a visual control scheme where a combination of position-based visual servoing and image-based visual servoing are merged.

Chapter 4

Optimal Feedback Control with Planar Limited FOV

THIS CHAPTER presents an optimal feedback control scheme to drive a vehicle equipped with a limited Field-Of-View camera towards a desired position following the shortest path and keeping a given landmark in sight. Based on the shortest path synthesis obtained in chapter 2, feedback control laws are defined for any point on the motion plane exploiting geometric properties of the synthesis itself. Moreover, by using a slightly generalized stability analysis setting, which is that of stability on a manifold, a proof of stability is given. Results reported in this chapter can be found in paper [A4].

4.1 Introduction

In this chapter, I consider the problem of visual servo control for a unicycle-like vehicle equipped with a monocular fixed camera. The system, subject to nonholonomic constraints imposed by the vehicle kinematics and to FOV constraints imposed by camera, must reach a desired position on the motion plane following the optimal (shortest) path. In order to localize itself and to compute a visual servo control,

the robot must keep at least three features in view. Indeed, given three or more features both in the current image and in the desired one, by using the estimation technique proposed in [30], state variables of the vehicle are available up to a scale factor. A first step toward the solution of this problem has been done in this thesis considering a single feature to be kept in sight. In chapter 2, a globally valid shortest path synthesis has been provided, i.e., a partition of the motion plane into regions completely describing the shortest path type from any starting point in that region to the goal point. An optimal synthesis in case of three or more features in view is still under study.

Based on the geometric properties of the optimal synthesis described in chapter 2 and available also in [A2], next sections are dedicated to define optimal feedback control laws for any point on the motion plane and give a proof of stability of the controlled system. These laws are provided in explicit form as simple algebraic functions of the current state only, which can be easily computed to give in real time the velocity input to be used, thus requiring no replanning procedure, and being intrinsically more robust.

4.1.1 Shortest Path Synthesis: A Summary of Chapter 2

In this section, I report main results of chapter 2 referring to this chapter for further details.

As a first result, based on the theory of optimal control with state and control constraints [47], extremal maneuvers of the optimal problem (i.e., maneuvers that satisfy necessary conditions for optimality) are rotation on the spot (corresponding to $\nu = 0$ and denoted by $*$), straight line (corresponding to $\omega = 0$ and denoted by S), and two logarithmic spirals with characteristic angle ϕ, clockwise and counterclockwise rotating around the feature (i.e., O_w) and denoted by T^L and T^R, respectively. Moreover, as extremal arcs can be executed by the vehicle in either forward or backward direction, I use superscripts $+$ and $-$ to make this explicit (e.g., S^- stands for a straight
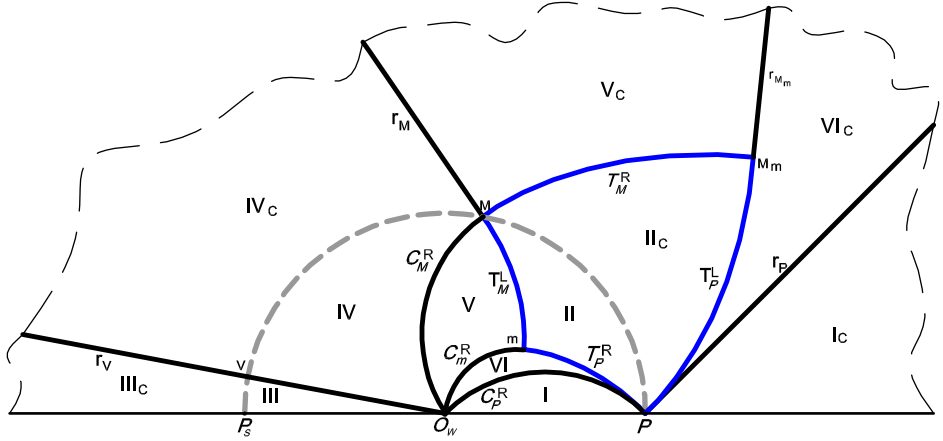
Figure 4.1: Partition of the upper half plane with $\phi = \pi/4$.

line executed backward w.r.t. the heading angle). In conclusion, extremal paths consist of sequences, or *words*, comprised of symbols in the alphabet $\left\{ *, S^+, S^-, T^{R+}, T^{R-}, T^{L+}, T^{L-} \right\}$. Rotations on the spot ($*$) have zero length, but may be used to properly connect other maneuvers.

Symmetries and invariants of the problem have been exploited to determine optimal paths from any point of the motion plane to the goal, providing a complete partition of the motion plane in regions as shown in figure 4.1 and described in table 2.4. Despite that every optimal path may begin and end with a turn on the spot, in table 2.4, I omit explicit mention of initial and final rotation in place to simplify notation. Let us also introduce here a further result of chapter 2 which will turn out to be a useful tool in the following sections. For any point Q, let us consider region C_Q delimited by two circle arcs C_Q^R and C_Q^L between Q and O_w such that $\forall V \in C_Q^R (C_Q^L)$, angle $\widehat{QVO}_w = \pi - \phi$ in the half-plane on the right (left) of $\overline{QO}_w$. We will refer to $C_Q^R (C_Q^L)$ as the right (left) ϕ-arc in Q. Moreover, let $r_Q^R (r_Q^L)$ denote the half-line from Q forming an angle $\psi_Q + \phi$ ($\psi_Q - \phi$) with the X_w axis. Also, let Γ_Q denote the cone delimited by r_Q^R and r_Q^L. We will refer to $r_Q^R (r_Q^L)$ as

the right (left) ϕ-radius in Q. By elementary geometric arguments, all points of C_Q and Γ_Q are reachable by a straight line without violating the FOV constraints. Moreover, we have the following result whose proof can be found in chapter 2:

Proposition 4.1 *If an optimal path from Q includes a segment of the type S^+ (S^-), with extremes in A and B (B and A), then either $B = P \in C_A$ ($A = P \in C_B$) or $B \in C_A^R \cup C_A^L$ ($A \in r_B^R \cup r_B^L$).*

Before starting toward desired position P, vehicle needs to localize itself in the motion plane, that is to deduce the region it belongs to, in order to select the optimal path. For any point $Q = (\rho, \psi)$, i.e., the current robot position, table 2.4 in chapter 2 describes the criteria to deduce the region Q belongs to, based on ratio ρ/ρ_P and angle ψ and in term of a number of elementary inequalities. The computation of these parameters requires at least two corresponding features in the current image and in the desired one in addition to the one that must be maintained inside FOV during all maneuvers that vehicle performs from Q to P, along shortest path. Indeed, in [51] authors show that, by taking the planar motion constraint of the mobile robot into account, robot position can be directly computed using three feature points in a non singular configuration, up to a common scale factor arbitrarily chosen within the set of state variable (for example, the hight of one feature w.r.t. $\langle C \rangle$ frame). Moreover, given any initial position Q inside CS, i.e., semicircle in the upper-half plane centered in O_w and radius ρ_P, algorithm reported in algorithm 4.1 returns the Region in which Q lays. For an external point Q ($\rho_Q > \rho_P$), the procedure is applied to $F(Q)$, i.e., replacing ρ_Q with $\frac{\rho_P^2}{\rho_Q}$ and complementing the output region.

Remark 4.1 *The region in which $Q = (\rho_Q, \psi_Q)$ lays can be determined verifying at most 6 inequalities on ρ_Q and ψ_Q. Indeed, the first inequality is the test $\rho_Q \gtrless \rho_P$, while algorithm reported in figure 4.1 consists in at most 5 inequality tests.*

Algorithm 4.1 Region Test Algorithm for points inside CS

1: **procedure** $\textsc{RegionTest}(\rho_Q,\ \psi_Q)$
2:     **Constant Parameters:** $\phi,\ \rho_P$
3:     **if** $\psi_Q \leq \psi_m$ **then**
4:         **if** $\rho_Q \leq \rho_P \dfrac{\sin\left(\phi - \psi_Q\right)}{\sin\phi}$ **then** $\left\{Q \text{ is below or on } C_P^R\right\}$
5:           **return** Region I
6:         **else if** $\rho_Q < \rho_P\, e^{-\psi_Q t}$ **then** $\left\{Q \text{ is below } T_P^R\right\}$
7:           **return** Region VI
8:         **else if** $\rho_Q = \rho_P\, e^{-\psi_Q t}$ **then** $\left\{Q \text{ is on } T_P^R\right\}$
9:           **return** Region II$'$
10:         **else**
11:           **return** Region II
12:         **end if**
13:     **else if** $\psi_Q \leq \psi_M$ **then**
14:         **if** $\rho_Q \leq \rho_P \sin\phi \sin\left(\phi - \psi_Q\right)$ && $\psi_Q \leq \psi_m + \phi$ **then** $\{Q$ is below or on $C_m^R\}$
15:           **return** Region VI
16:         **else if** $\rho_Q \leq \rho_P\, e^{\left(\psi_Q - \psi_M\right)t}$ **then** $\left\{Q \text{ is below or on } T_M^L\right\}$
17:           **return** Region V
18:         **else**
19:           **return** Region II
20:         **end if**
21:     **else if** $\psi_Q \leq \psi_V$ **then**
22:         **if** $\rho_Q \leq \rho_P \dfrac{\sin\left(\phi - \psi_Q\right)}{\sin\phi}$ && $\psi_Q \leq \psi_M + \phi$ **then** $\{Q$ is below or on $C_M^R\}$
23:           **return** Region V
24:         **else**
25:           **return** Region IV
26:         **end if**
27:     **else**
28:         **return** Region III
29:   **end if**
30: **end procedure**
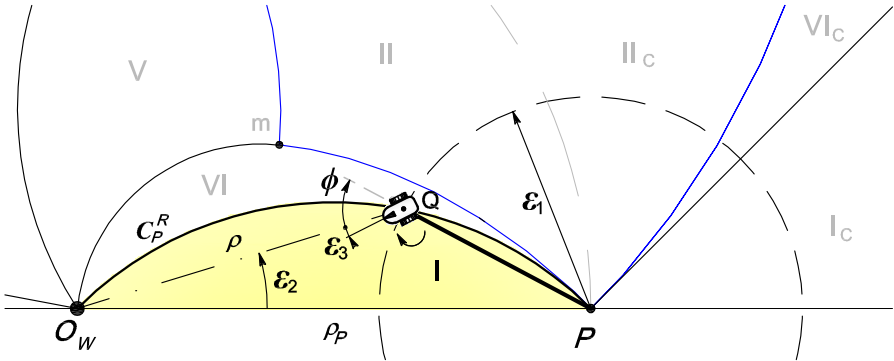
Figure 4.2: An example to show that point P is not stable for the optimality controlled system, in the sense of Lyapunov.

4.2 Optimal Feedback Control Laws

In this section, I define feedback control laws $u(\eta) = [\nu(\eta), \omega(\eta)]^T$ for any initial configuration $\eta = [\rho, \psi, \beta]^T$ of the vehicle. In this regard, it should be noticed that the shortest path synthesis in table 2.4 is completely defined in terms of variables ρ/ρ_P and ψ only, but it is independent from β. Indeed, the synthesis is obtained minimizing cost functional (1.9) which does not weigh β. For this reason, the cost functional does not constrain β to be decreasing, as shown in the following remark.

Remark 4.2 *Consider a vehicle position Q, on the boundary C_P^R between Region I and Region VI (see figure 4.2), arbitrarily close to the desired position P w.r.t. states ρ, ψ, and β. In other words, let $\eta = (\rho_P - \varepsilon_1, \varepsilon_2, \varepsilon_3)$ where ε_1, ε_2 and ε_3 are arbitrarily small (see figure 4.2). In order to perform an optimal path, the vehicle must turn on the spot in Q, and β goes as far as ϕ before converging to zero. This happens for any robot configuration on C_P^R. Thus, strictly speaking, point P is not stable in the sense of Lyapunov for the system controlled with the optimal synthesis in chapter 2.*
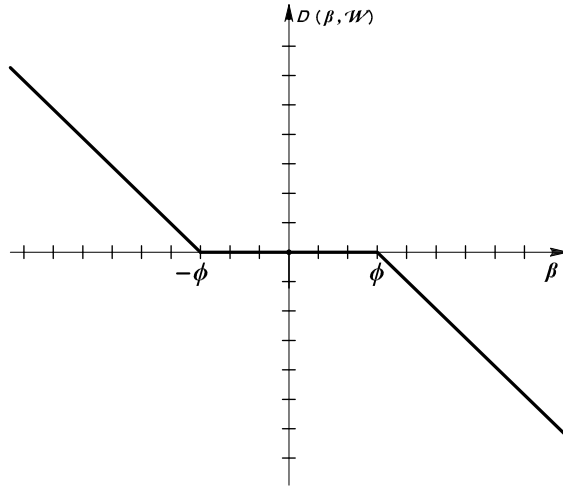
Figure 4.3: Function $D(\beta, \mathcal{W})$.

Despite the previous remark, the proposed optimal feedback control scheme clearly exhibits convergence and boundedness of trajectories, which can be formalized and proved in a slightly generalized stability analysis setting, which is that of stability on a manifold ([44]). In this regard, let a function $V : \mathbb{R}^3 \to \mathbb{R}$ be defined as

$$V(\eta) = \frac{1}{2}\left(\frac{\rho}{\rho_P} - 1\right)^2 + \frac{\psi^2}{2} + \frac{1}{2}D^2(\beta, \mathcal{W}), \qquad (4.1)$$

where $D(\beta, \mathcal{W})$ is defined as (see also figure 4.3)

$$D(\beta, \mathcal{W}) = \begin{cases} -\beta - \phi & \text{if } \beta < -\phi, \\ 0 & \text{if } \beta \in \mathcal{W} = [-\phi, \phi], \\ \phi - \beta & \text{if } \beta > \phi. \end{cases} \qquad (4.2)$$

Notice that, (4.1) is a continuously differentiable function such that $V(\eta) = 0$ on manifold $M = \{\eta \in \mathbb{R}^3 | \rho = \rho_P, \psi = 0, \beta \in \mathcal{W}\}$, whereas set

$$\Omega_\ell = \{\eta \in \mathbb{R}^3 : V(\eta) \leq \ell\}$$

is bounded for every $\ell > 0$. In the following, I consider a value ℓ such that set $\{\beta| -\pi/2 < \beta < \pi/2\}$ is included inside Ω_ℓ. The time derivative of (4.1) along the trajectories of the system is given by

$$\dot{V}(\eta) = \frac{1}{\rho_P} \left[-\left(\frac{\rho}{\rho_P} - 1 \right) \cos\beta + (\psi - D(\beta, \mathcal{W})) \frac{\rho_P \sin\beta}{\rho} \right] \nu + D(\beta, \mathcal{W}) \omega,$$

(4.3)

where ν and ω are robot's control inputs. As the vehicle has to be always aligned with the optimal path, ω is determined by geometrical conditions deduced by the synthesis itself. On the other hand, as the vehicle has to reach point P along the shortest path without any time constraint, ν can be chosen in order to make $\dot{V}$ at least negative semidefinite, e.g.,

$$\nu = \bar{\nu} = -K_\nu \left[-\left(\frac{\rho}{\rho_P} - 1 \right) \cos\beta + (\psi - D(\beta, \mathcal{W})) \frac{\rho_P \sin\beta}{\rho} \right].$$

(4.4)

Finally, let us define R as the set of all points in Ω_ℓ where $\dot{V} = 0$.

Next sections are dedicated to define the optimal control laws, ν and ω, for any point on the motion plane, and to prove stability properties of the optimal feedback control scheme on the manifold M by using LaSalle's invariance principle, i.e., to prove that the largest invariant set in R is M itself.

4.2.1 Control Laws

The key idea behind the control laws defined in this section, is to establish geometric conditions that have to be respected to keep the vehicle aligned with optimal path in each point Q on the motion plane.

Although the optimal synthesis is completely defined in terms of only the state variables ρ and ψ, control laws are defined in terms of ρ, ψ and β, where $\beta \in \mathcal{W} = [-\phi, \phi]$. We will use superscript $\mathcal{W}$ to make this explicit, (e.g., $\mathrm{I}^{\mathcal{W}}$ corresponds to robot configuration $\eta = (\rho, \psi, \beta)$ such that point (ρ, ψ) belongs to Region I and angle $\beta \in \mathcal{W}$). Moreover, as control laws defined in next sections depend on
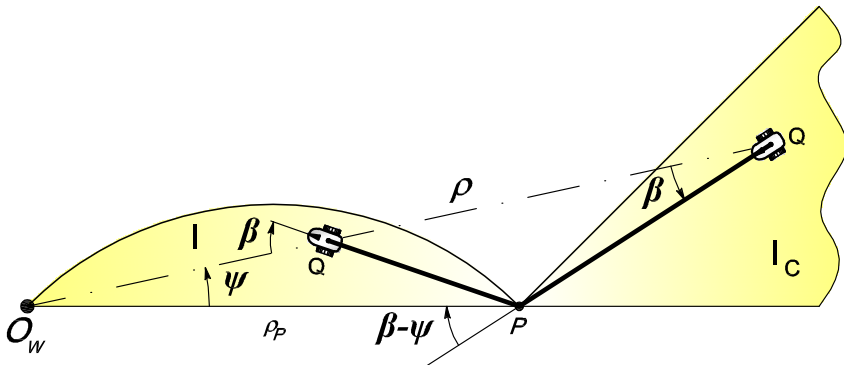
Figure 4.4: Geometric construction to determine control law in Region I and I$_c$.

geometrical properties of the optimal synthesis, they are not valid for values of $\beta \notin \mathcal{W}$ and, hence, it could not guarantee stability outside $\mathcal{W}$. For this reason, for η such that $\beta \notin \mathcal{W}$ and, hence $D(\beta, \mathcal{W}) \neq 0$, we consider the following control laws:

$$u(\eta) = \begin{cases} \nu = 0, \\ \omega = -K_\omega D(\beta, \mathcal{W}) \end{cases} \tag{4.5}$$

where K_ω is a positive control gain.

Finally, due to the symmetry of the optimal synthesis, I consider Q in the upper half plane (see figure 2.14), taking into account that a similar procedure can be followed to design control laws in each corresponding symmetric region.

4.2.1.1 Control Law for Configuration $\eta \in \mathbf{I}^{\mathcal{W}} \cup \mathbf{I}_c^{\mathcal{W}}$

For these robot configurations (see table 2.4), the optimal path to P is a straight line. From proposition 4.1, as for any point $Q \in \mathrm{I}$ ($Q \in \mathrm{I}_c$), point $P \in C_Q$ ($P \in \Gamma_Q$), vehicle follows optimal path if it is anytime aligned with segment $\overline{QP}$. Hence, based on figure 4.4, and by using

the sine rule, we obtain the following alignment condition

$$F_{\mathrm{I}^{\mathcal{W}} \cup \mathrm{I}^{\mathcal{W}}_c}(\eta) = \frac{\rho}{\rho_P} \sin \beta - \sin (\beta - \psi) = 0 \tag{4.6}$$

Notice that, (4.6) depends on ratio $\frac{\rho}{\rho_P}$. As a consequence, it is also valid for state variables whose values are scaled by a common factor.

Based on (4.6) I am now able to define control law $u(\eta)$:

$$\omega = K_\omega \left(\frac{\rho}{\rho_P} \sin \beta - \sin (\beta - \psi) \right), \quad \begin{cases} \nu = 0, & \text{if } F_{\mathrm{I}^{\mathcal{W}} \cup \mathrm{I}^{\mathcal{W}}_c}(\eta) \neq 0 , \\ \nu = \bar{\nu}, & \text{if } F_{\mathrm{I}^{\mathcal{W}} \cup \mathrm{I}^{\mathcal{W}}_c}(\eta) = 0 , \end{cases} \tag{4.7}$$

where K_ω is a positive control gain for points $Q \in \mathrm{I}^{\mathcal{W}}$ and negative for points $Q \in \mathrm{I}^{\mathcal{W}}_c$. In other words, the vehicle rotates on the spot until alignment condition $F_{\mathrm{I}^{\mathcal{W}} \cup \mathrm{I}^{\mathcal{W}}_c}(\eta) = 0$, and then follows straight line path toward P.

Remark 4.3 *Notice that, when $F_{\mathrm{I}^{\mathcal{W}} \cup \mathrm{I}^{\mathcal{W}}_c}(\eta) = 0$, I still compute ω in order to correct the orientation error due to noise or drift, as usual happens in reality. This also happens for the following control laws.*

4.2.1.2 Control Law for Configuration $\eta \in \mathrm{VI}^{\mathcal{W}}_c$

For these robot configurations, the optimal path to P is of type $S^+ T_P^{L+}$ (see table 2.4). For any $Q \in \mathrm{VI}_c$, based on proposition 4.1, robot must move straight toward G, intersection between C_Q^L and spiral T_P^L (see figure 4.6), that is, recalling that $Q = (\rho, \psi)$, a solution of

$$F_{\mathrm{VI}^{\mathcal{W}}_c}(\eta) = \frac{\rho}{\rho_P} \frac{\sin \beta}{\sin \phi} + e^{(\psi - \beta - \phi) t} = 0 , \tag{4.8}$$

in terms of β, where $t = 1/\tan \phi$. Based on (4.8), I am now able to define the control algorithm for points Q belonging to Region VI:

$$\omega = K_\omega \left(\frac{\rho}{\rho_P} \frac{\sin \beta}{\sin \phi} + e^{(\psi - \beta - \phi) t} \right), \quad \begin{cases} \nu = 0, & \text{if } F_{\mathrm{VI}^{\mathcal{W}}_c}(\eta) \neq 0 , \\ \nu = \bar{\nu}, & \text{if } F_{\mathrm{VI}^{\mathcal{W}}_c}(\eta) = 0 , \end{cases}$$

with $K_\omega > 0$.
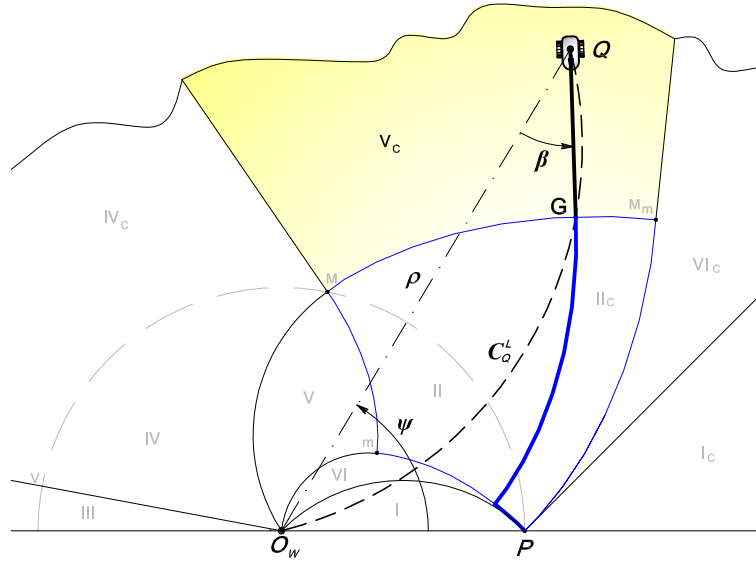
Figure 4.5: Geometric construction to determine control law in Region V_c.

4.2.1.3 Control Law for Configuration $\eta \in \mathbf{V}_c^{\mathcal{W}}$

If robot position is in regions V_c (see figure 2.14), with $\beta \in \mathcal{W}$, for these robot configurations, the shortest path to P is of type $S^+ T^{L+} *$ T_P^{R-} (see table 2.4). From points $Q \in V_c$, for proposition 4.1, vehicle must move toward the intersection point between spiral T_M^R and C_Q^L (see figure 4.5), that is a solution of

$$F_{V_c^{\mathcal{W}}}(\eta) = \frac{\rho}{\rho_P}\frac{\sin\beta}{\sin\phi} + \mathrm{e}^{(\psi_M - \psi + \beta + \phi)t} = 0 \, , \qquad (4.9)$$

in terms of β, where $\psi_M = -4\tan\phi\ln\sin\phi$ and $t = 1/\tan\phi$. Notice that, (4.9) is valid for state variables whose values are scaled by a common factor. Based on (4.9), I am now able to define the control algorithm for points Q belonging to Region V_c:

$$\omega = K_\omega \left(\frac{\rho}{\rho_P}\frac{\sin\beta}{\sin\phi} + \mathrm{e}^{(\psi_M - \psi + \beta + \phi)t} \right), \quad \begin{cases} \nu = 0, & \text{if } F_{V_c^{\mathcal{W}}}(\eta) \neq 0 \, , \\ \nu = \bar{\nu}, & \text{if } F_{V_c^{\mathcal{W}}}(\eta) = 0 \, , \end{cases}$$
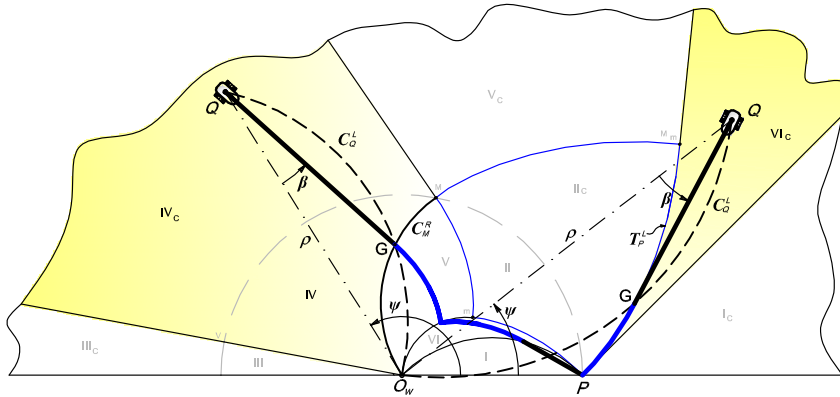
Figure 4.6: Geometric construction to determine control law in Region $\text{IV} \cup \text{IV}_c$ and Region VI_c.

where $K_\omega > 0$.

4.2.1.4 Control Law for Configuration $\eta \in \mathbf{IV}^{\mathcal{W}} \cup \mathbf{IV}_c^{\mathcal{W}}$

From these robot configurations, the optimal path to P is of type $S^+ T^{L+} * T^{R-} S^-$ (see table 2.4). Based on proposition 4.1, from these points, vehicle has to be aligned with segment $\overline{QG}$, where G is the intersection point between C_Q^L and C_M^R (see figure 4.6). In other words, given a point Q in Region $\text{IV} \cup \text{IV}_c$, alignment condition can be obtained as solution of

$$F_{\text{IV}^{\mathcal{W}} \cup \text{IV}_c^{\mathcal{W}}}(\eta) = \sin\left(2\phi + \psi_M + \beta - \psi\right) + \frac{\rho}{\rho_P}\sin\beta = 0, \qquad (4.10)$$

in terms of β, where $\psi_M = -4\tan\phi \ln\sin\phi$. Notice that, (4.10) is valid for state variables whose values are scaled by a common factor. Based on (4.10), I am now able to define the control laws:

$$\omega = K_\omega \left(\sin\left(2\phi + \psi_M + \beta - \psi\right) + \frac{\rho}{\rho_P}\sin\beta \right), \quad \begin{cases} \nu = 0, & \text{if } F_{\text{IV}^{\mathcal{W}} \cup \text{IV}_c^{\mathcal{W}}}(\eta) \neq 0, \\ \nu = \bar{\nu}, & \text{if } F_{\text{IV}^{\mathcal{W}} \cup \text{IV}_c^{\mathcal{W}}}(\eta) = 0, \end{cases}$$

where $K_\omega > 0$.

4.2.1.5   Control Law for Configuration $\eta \in \mathbf{II}_c' \cup \mathbf{II}^{\mathcal{W}} \cup \mathbf{II}_c^{\mathcal{W}} \cup \mathbf{V}^{\mathcal{W}}$

From these robot configurations, the robot must move along a T_Q^{L+} spiral arc. The vehicle is aligned with a left logarithmic spiral if angle β is equal to spiral's characteristic angle, i.e., $\beta = \phi$. Hence, the control laws for such points are

$$\omega = -K_\omega \left(\beta + \phi\right) + \frac{\sin\beta}{\rho}\,\nu, \quad \begin{cases} \nu = 0, & \text{if } \beta + \phi \neq 0\,, \\ \nu = \bar{\nu}, & \text{if } \beta + \phi = 0\,, \end{cases}$$

where $K_\omega > 0$. Unfortunately, for geometrical properties of the logarithmic spirals, it is not possible to move along spirals with a feedback control computed on state variables known up to a common scale factor (notice that this occurs also for a circumference). Hence, a further knowledge about feature position is necessary to perform this path, for example hight of the feature that is kept in sight during motion.

4.2.1.6   Control Law for Configuration $\eta \in \mathbf{II}'^{\mathcal{W}} \cup \mathbf{VI}^{\mathcal{W}}$

If robot configuration η is such that point $Q = (\rho,\,\psi)$ belongs to regions $\mathbf{II}'^{\mathcal{W}} \cup \mathbf{VI}^{\mathcal{W}}$, with $\beta \in \mathcal{W}$, from these robot configurations, the robot must move along a T_Q^{R-} spiral arc. The vehicle is aligned with a right logarithmic spiral if angle β is equal to spiral's characteristic angle, i.e., $\beta = -\phi$. Hence, the control laws for such points are

$$\omega = -K_\omega \left(\beta - \phi\right) + \frac{\sin\beta}{\rho}\,\nu, \quad \begin{cases} \nu = 0, & \text{if } \beta - \phi \neq 0\,, \\ \nu = \bar{\nu}, & \text{if } \beta - \phi = 0\,, \end{cases}$$

where $K_\omega > 0$.

4.2.1.7   Control Law for Configuration $\eta \in \mathbf{III}^{\mathcal{W}} \cup \mathbf{III}_c^{\mathcal{W}}$

If robot configuration η is such that point $Q = (\rho,\,\psi)$ belongs to regions $\mathbf{III}^{\mathcal{W}} \cup \mathbf{III}_c^{\mathcal{W}}$, with $\beta \in \mathcal{W}$, in this particular case, the robot

must move toward feature position O_w. The vehicle is aligned with the straight line from Q to O_w if $\beta = 0$; hence, control laws are

$$\omega = K_\omega \beta, \quad \begin{cases} \nu = 0, & \text{if } \beta \neq 0, \\ \nu = \bar{\nu}, & \text{if } \beta = 0, \end{cases}$$

where $K_\omega > 0$. Notice that, ν defined in (4.4), has a singularity in O_w. Indeed, in O_w variables β and ψ are not defined and $\rho = 0$. In this case is however still possible to define control laws that brings the robot in region VI (or I) without following the optimal path in order to avoid the crossing of O_w.

4.3 Stability Analysis

In this section, the stability of the control scheme previously presented is analyzed by means of LaSalle's invariance principle [45], showing that manifold $M = \{\eta \in \mathbb{R}^3 | \rho = \rho_P, \psi = 0, \beta \in \mathcal{W}\}$ is asymptotically stable for any initial configuration of the robot on the motion plane. The objective here is to prove that the largest invariant set in $R = \{\eta \in \mathbb{R}^3 | \dot{V}(\eta) = 0\}$ in Ω_ℓ is the manifold M. Next section are dedicated to characterized set R for each region and then determine the largest invariant set in Ω_ℓ. For the sake of clarity, for each region I consider only points in Ω_ℓ omitting this intersection in the following notation.

For points Q such that $\beta \notin \mathcal{W}$, i.e. $D(\beta, \mathcal{W}) \neq 0$, $\dot{V}(\eta) = -K_\omega D^2(\beta, \mathcal{W})$, that is negative semidefinite. Set of points Q such that $\dot{V}(\eta) = 0$ is given by $R_{\beta \notin \mathcal{W}} = \{D(\beta, \mathcal{W}) = 0, \forall \rho, \forall \psi\}$, i.e., set of points whose stability will now be analyzed.

For all points Q such that $\beta \in \mathcal{W}$, (4.3) becomes

$$\dot{V}(\eta) = \frac{1}{\rho_P} \left[-\left(\frac{\rho}{\rho_P} - 1\right) \cos \beta + \psi \frac{\rho_P \sin \beta}{\rho} \right] \nu, \qquad (4.11)$$

that depends only on input control ν. Notice that, since $D(\beta, \mathcal{W}) = 0$, the control input ν is the same for all the regions of the optimal

synthesis and

$$\dot{V}(\eta) = -\frac{K_\nu}{\rho_P} \left[-\left(\frac{\rho}{\rho_P} - 1 \right) \cos \beta + \psi \frac{\rho_P \sin \beta}{\rho} \right]^2 . \qquad (4.12)$$

The set of points Q with $\beta \in \mathcal{W}$ and such that $\dot{V}(\eta) = 0$ is $R_{\beta \in \mathcal{W}} = M \cup \left\{ \psi = 0, \, \beta = \pi/2, \, \forall \rho \right\} \cup \left\{ \beta = \arctan \left(\left(\frac{\rho}{\rho_P} - 1 \right) \frac{\rho}{\rho_P} \frac{1}{\psi} \right), \, \forall \psi, \, \forall \rho \right\}$.

The objective now is to characterize the largest invariant set contained in $R_{\beta \in \mathcal{W}}$.

Proposition 4.2 *The largest invariance set contained in $R = R_{\beta \notin \mathcal{W}} \cup R_{\beta \in \mathcal{W}}$ is $M = \left\{ \eta \in \mathbb{R}^3 | \rho = \rho_P, \, \psi = 0, \, \beta \in \mathcal{W} \right\}$.*

Proof: Previous results for point Q such that $\beta \in \mathcal{W}$ prove that starting from $R_{\beta \notin \mathcal{W}}$, the system evolves in $R_{\beta \in \mathcal{W}}$. Hence, $R_{\beta \notin \mathcal{W}}$ does not contain invariant sets.

For any Q such that $\beta = \arctan \left(\left(\frac{\rho}{\rho_P} - 1 \right) \frac{\rho}{\rho_P} \frac{1}{\psi} \right)$, we have $\dot{V}(\eta) = 0$ and hence $\nu = 0$. As a consequence, from the kinematic model, $\dot{\rho} = \dot{\psi} = 0$ and hence β should be constant. From the control laws defined previously, this happens only if β is such that the robot is aligned with the optimal path associated to the region it belongs to. It can be directly verified that such values of β do not verify alignment conditions reported above. Hence, the considered subset of R does not contain invariant sets.

Set $R_1 = \left\{ \psi = 0, \, \beta = \pi/2, \, \forall \rho \right\}$ is a subset of $\mathrm{I}^{\mathcal{W}} \cup \mathrm{I}_c^{\mathcal{W}}$. Hence, for any Q in R_1, (4.6) becomes $F_{\mathrm{I}^{\mathcal{W}} \cup \mathrm{I}_c^{\mathcal{W}}} = \frac{\rho}{\rho_P} - 1$. If $\rho \neq \rho_P$ the control laws are $\nu = 0$ and $\omega \neq 0$. Hence, $\dot{\beta} \neq 0$ and R_1 does not contain invariant sets.

If $Q \in R_1$ and $\rho_Q = \rho_P$ we have that Q is a particular point of M. Finally, notice that $M \subset \mathrm{I}^{\mathcal{W}}$, and for any $Q \in M$ $F_{\mathrm{I}^{\mathcal{W}} \cup \mathrm{I}_c^{\mathcal{W}}} = 0$. From control laws (4.7) we have $\nu = \omega = 0$ hence M is an invariant set. ■

As a consequence of proposition 4.2 and, by using LaSalle's invariance principle, manifold M is stable for the optimal feedback control laws previously defined.

4.4 Conclusion

A nonlinear optimal feedback control capable of maintaining the vehicle aligned with shortest path from any initial robot position to the desired one has been proposed. Moreover, a proof of stability has been given and realistic simulations, proving the effectiveness of our technique, have been reported. Moreover, the problem of keeping in sight, during motion, at least one feature has been taken into account. On the other hand, in order to obtain the current robot position, a least three features are needed. As a consequence, a generalization of the optimal synthesis used here to define the optimal control laws would be necessary, providing the shortest paths to a goal keeping in sight at least three features. Such extension to the proposed approach is still an open problem.

Chapter 5

Simulation results

T HIS CHAPTER presents simulation results showing the effectiveness of control laws proposed in previous chapter. For this purpose, a visual control scheme where a combination of position-based visual servoing and image-based visual servoing are merged, is used.

5.1 Introduction

Visual servoing techniques use visual information directly, by the computation of an image error signal, or indirectly, by the evaluation of the state of the vehicle (see [19] and [20]). These two approaches are often referred to as Image-Based Visual Servoing (IBVS) and Position-Based Visual Servoing (PBVS) ([21]). In particular, in IBVS the control error is defined directly in the image space, based on features extracted from image data, e.g., visual cues like points, planes or lines; on the other hand, PBVS computes the error in relation to a set of 3D parameters that are estimated from image measurements, e.g., robot position errors with respect to the desired position to reach. In the second case, position errors are usually computed in the robot Cartesian space and provided, as customary, to the control system. Robot position reconstruction is often referred to as robot localization. The
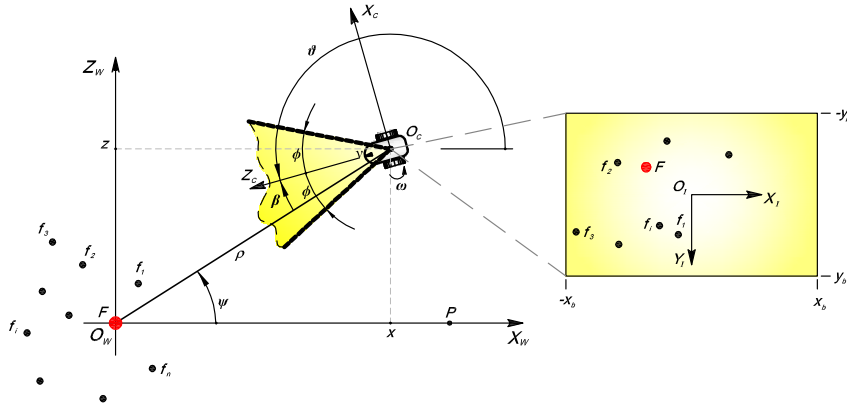
Figure 5.1: Mobile robot and system coordinates.

two vision-based schemes thus described should be regarded as the end-points of a range of different possibilities, whereby the raw sensorial information is gradually abstracted away to a more structured representation using some knowledge of the robot-environment model.

In this chapter, a combination of position-based visual servoing and image-based visual servoing, depending on which region of the optimal synthesis robot is in, is used as discuss in next sections.

5.2   Trajectories on Image Plane

Consider a unicycle-like nonholonomic mobile robot moving on a plane whose kinematic model in polar coordinates $\eta = [\rho, \, \psi, \, \beta]^T$ is given by

$$\begin{bmatrix} \dot{\rho} \\ \dot{\psi} \\ \dot{\beta} \end{bmatrix} = \begin{bmatrix} -\cos\beta & 0 \\ \frac{\sin\beta}{\rho} & 0 \\ \frac{\sin\beta}{\rho} & -1 \end{bmatrix} \begin{bmatrix} \nu \\ \omega \end{bmatrix}. \tag{5.1}$$

The vehicle is equipped with a rigidly fixed pinhole camera with a reference frame $\langle C \rangle = \{O_c, X_c, Y_c, Z_c\}$ such that the optical cen-

ter O_c corresponds to the robot's center and the optical axis Z_c is aligned with the robot's forward direction, i.e., $\Gamma = 0$ (see figure 5.1). Giving the motionless feature coordinates in the fixed frame $\langle W \rangle$ be expressed by $^wP = [^wx, {}^wy, {}^wz]^T$, letting ^cH_w be the transformation matrix between $\langle W \rangle$ and $\langle C \rangle$ and assuming a pinhole camera model, the corresponding image features points will be:

$$^Ip = \begin{bmatrix} ^Ix & {}^Iy \end{bmatrix}^T = \begin{bmatrix} \alpha_x \frac{^cx}{^cz} & \alpha_y \frac{^cy}{^cz} \end{bmatrix}^T \tag{5.2}$$

where $[^cP^T, 1]^T = [^cx, {}^cy, {}^cz, 1]^T = {}^cH_w[^wP^T, 1]^T$ are the feature coordinates in the camera frame, α_x and α_y are the focal lengths of the camera calibration matrix

$$K_c = \text{diag}(\alpha_x, \alpha_y, 0)\,, \tag{5.3}$$

and $^Ip = [^Ix, {}^Iy]^Y$ are the features coordinates in the image frame (measured in pixels) ([48]). The characteristic angle of the symmetric FOV is

$$\phi = \arctan\left(\frac{x_b}{\alpha_x}\right) \tag{5.4}$$

where x_b is the x image boundary.

The origin O_I of the image plane reference frame $\langle I \rangle = \{O_I, X_I, Y_I\}$ is assumed to be coincident with the principal point, i.e., the intersection of the camera axis (or Z_c) with the image plane (see figure 5.1).

In the visual servoing literature, whenever an eye-in-hand configuration is considered (as is a camera rigidly fixed on a moving platform), the objective of the control task is to stabilize the robot towards the desired position controlling the camera position ([19, 20, 52]). More precisely:

Definition 5.1 *Given the desired and the current robot positions, which correspond the desired $\langle C_d \rangle = \{O_{cd}, X_{cd}, Y_{cd}, Z_{cd}\}$ and the current $\langle C_c \rangle = \{O_{cc}, X_{cc}, Y_{cc}, Z_{cc}\}$ reference frames respectively, the stabilization in the desired position is accomplished if $\langle C_c \rangle \equiv \langle C_d \rangle$ at the end of the control task.*

Indeed, as is customary in the visual servoing literature, $\langle W \rangle \equiv \langle C_d \rangle$ (in our case $X_w = -Z_{cd}$, $Y_w = Y_{cd}$ and $Z_w = X_{cd}$), hence stabilizing the robot in the desired position corresponds to $\eta(t) \to (\rho_P, 0, 0)$ as $t \to +\infty$.

In this chapter, full camera calibration is assumed. Moreover, the robot is considered stabilized if definition 5.1 holds. More in depth, definition 5.1 is substituted with:

Definition 5.2 *Given n desired and current* image feature *positions,* $F_d = [{}^I x_{d_1}, {}^I y_{d_1}, {}^I x_{d_2}, \ldots, {}^I y_{d_n}]^T$ *and* $F_c = [{}^I x_{c_1}, {}^I y_{c_1}, {}^I x_{c_2}, \ldots, {}^I y_{c_n}]^T$ *respectively, the servoing task is accomplished if at the end of the control task is* $F_d = F_c \Rightarrow {}^I x_{d_i} = {}^I x_{c_i}$ *and* ${}^I y_{d_i} = {}^I y_{c_i}$, $\forall i = 1, \ldots, n$.

5.2.1   Optimal paths on the Image Plane

As shown in chapter 1, the optimal paths are words in a certain alphabet, whose elements depend on characteristic angles $\delta = |\phi_2 - \phi_1|$ and $\varepsilon = 2\hat{\phi}$ of the camera and angle Γ between axis Z_c and the robot's forward direction. Whereas the definition of the optimal language for 3-D paths induces a partition of the motion plane in regions, an analogous partition on the image plane is not immediate. However, a first step toward this objective is to define an equivalent finite optimal alphabet in the image space, i.e., to determine the trajectories of the feature that must be maintain in view from initial to desired position, along the shortest path (see also [A10] for further details). Let us consider the relationship between robot's control inputs ν and ω and feature velocities ${}^I \dot{x}$ and ${}^I \dot{y}$ on the image plane for a generic value of Γ, i.e.,

$$\begin{bmatrix} {}^I \dot{x} \\ {}^I \dot{y} \end{bmatrix} = \begin{bmatrix} \frac{{}^I y}{\alpha_y h} \left({}^I x \cos \Gamma - \alpha_x \sin \Gamma \right) & \frac{{}^I x^2 + \alpha_x^2}{\alpha_x} \\ \frac{{}^I y^2}{\alpha_y h} \cos \Gamma & \frac{{}^I x \, {}^I y}{\alpha_x} \end{bmatrix} \begin{bmatrix} \nu \\ \omega \end{bmatrix} = J \begin{bmatrix} \nu \\ \omega \end{bmatrix}, \quad (5.5)$$

where J is known as *Image Jacobian*.

A rotation on the spot, denoted by symbol $*$ in the optimal alphabet, is performed by the vehicle if $\nu = 0$. Without loss of generality,

(a) During a rotation on the spot feature moves on a conic.

(b) During a straight line motion, feature moves on a line through point $(-\alpha_y \tan \Gamma, 0)$.

(c) During a logarithmic spiral motion, feature moves on the left or right FOV's border.

(d) During a logarithmic spiral motion, feature moves on the left or right FOV's border.
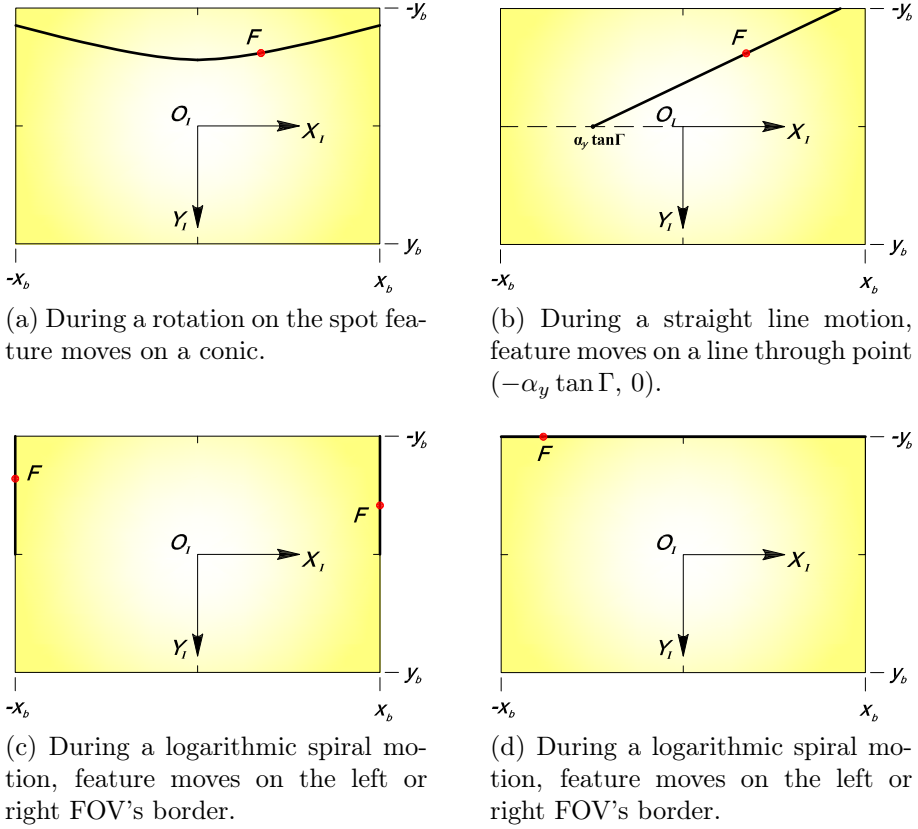
Figure 5.2: Feature trajectories on image plane.

consider $\omega = \bar{\omega} = \text{const.}$ and from (5.5), we have

$$
{}^I \dot{x} = \frac{{}^I x^2 + \alpha_x^2}{\alpha_x} \bar{\omega} \, ,
$$

$$
{}^I \dot{y} = \frac{{}^I x \, {}^I y}{\alpha_x} \bar{\omega} \, ,
$$

and by integration, we obtain

$$
{}^{I}y = \frac{{}^{I}y_i \cos\left(\arctan\left(\frac{{}^{I}x_i}{\alpha_x}\right)\right)}{\cos\left(\arctan\left(\frac{{}^{I}x}{\alpha_x}\right)\right)}, \tag{5.6}
$$

where ${}^{I}p_i = [{}^{I}x_i, {}^{I}y_i]^T$ is the initial feature position on image plane. Equation (5.6) represents a conic (see figure 5.2a), i.e., the intersection between the image plane and the cone with vertex in the camera center O_c (optical center) and base circumference passing through the 3-D feature position.

On the other hand, a straight line path, denoted by symbol S in the optimal alphabet, is performed by the vehicle if $\omega = 0$. Without loss of generality, consider $\nu = \bar{\nu} = \text{const.}$ and from (5.5), we have

$$
{}^{I}\dot{x} = \frac{{}^{I}y}{\alpha_y\, h}\left({}^{I}x\cos\Gamma - \alpha_x\sin\Gamma\right)\bar{\nu}\,,
$$

$$
{}^{I}\dot{y} = \frac{{}^{I}y^2}{\alpha_y\, h}\cos\Gamma\bar{\nu}\,,
$$

and by integration, we obtain

$$
{}^{I}y = \frac{{}^{I}y_i}{{}^{I}x_i - \alpha_y\tan\Gamma}\, x - \frac{\alpha_y\,{}^{I}y_i\tan\Gamma}{{}^{I}x_i - \alpha_y\tan\Gamma}\,. \tag{5.7}
$$

Equation (5.7) describes a straight line passing through initial feature position and point $(0, \alpha_y\tan\Gamma)$ (see figure 5.2b). Notice that, if $\Gamma = 0$, (5.7) represents a straight line passing through the principal point.

The logarithmic spiral, denoted generically by symbol T in the optimal alphabet, is completely determined by its characteristic angle $\phi = \arctan\left(\frac{|x_b|}{\alpha_x}\right)$. Since such an angle remains constant as the robot travels on the spiral, the coordinates of the image feature ${}^{I}x$ should be constant and equal to the image horizontal boundary $\pm x_b$. Therefore, the image plane trajectory for the logarithmic spiral will be simply a

straight line coincident with the right or left camera border depending on vehicle performs a left or right spiral (see figure 5.2c).

Finally, if the vehicle performs an involute of circle, feature moves on the upper or lower camera border. For this reason, the image plane trajectory is still a straight line but this time coincident with upper or lower camera border, i.e., $^{I}y = -y_b$ or $^{I}y = y_b$, respectively. Moreover, if $^{I}x > 0$ vehicle performs a left involute, if $^{I}x < 0$ vehicle performs a right involute, and if $^{I}x = 0$ vehicle is on the circumference with radius R_b and centered in O_w, i.e., the boundary of region Z_0, with $\beta = 0$ (see figure 5.2d).

5.3 Simulation Results

In this section, simulation results for the controlled system with optimal feedback control laws defined in previous chapter 4 are proposed. As described in table 5.1, these laws are provided in explicit form as simple algebraic functions of the current state only, which can be easily computed to give in real time the velocity input to be used. Moreover, trajectories of all features in view are reported showing that optimal path on image plane are a sequence of elementary trajectories obtained in previous section. A virtual framework is used where random 3-D points representing features of a virtual scene are generated. The 3-D points of the scene are projected in the image plane of a virtual camera whose size is 640×480 pixels. Moreover, the image frames are captured with 10 frames/second. The characteristic angle of the symmetric planar cone is $\delta = 2\phi = 37.76°$. The control laws proposed in previous chapter are designed to keep only one landmark in view. Nevertheless, before moving toward desired position P along the optimal path, vehicle needs to localize itself by the estimate of ψ and ratio ρ/ρ_P by using feature measurements on the image plane. In order to do this at least three features in view are needed. For this reason, I will generate several virtual points in the scene to guarantee this requirement anytime during all maneuvers

Region	Optimal Path	Control laws
$\mathrm{I}^{\mathcal{W}}$	S^-	$\omega = K_\omega \left(\dfrac{\rho}{\rho_P} \sin\beta - \sin(\beta - \psi) \right),$ $\nu = \begin{cases} 0, & \text{if } F_{\mathrm{I}^{\mathcal{W}} \cup \mathrm{I}_c^{\mathcal{W}}}(\eta) \neq 0, \\ \bar{\nu}, & \text{if } F_{\mathrm{I}^{\mathcal{W}} \cup \mathrm{I}_c^{\mathcal{W}}}(\eta) = 0. \end{cases}$
$\mathrm{I}_c^{\mathcal{W}}$	S^+	$\omega = -K_\omega \left(\dfrac{\rho}{\rho_P} \sin\beta - \sin(\beta - \psi) \right),$ $\nu = \begin{cases} 0, & \text{if } F_{\mathrm{I}^{\mathcal{W}} \cup \mathrm{I}_c^{\mathcal{W}}}(\eta) \neq 0, \\ \bar{\nu}, & \text{if } F_{\mathrm{I}^{\mathcal{W}} \cup \mathrm{I}_c^{\mathcal{W}}}(\eta) = 0. \end{cases}$
$\mathrm{II}^{\mathcal{W}} \cup \mathrm{II}_c^{\mathcal{W}}$	$T^{L+} * T_P^{R-}$	$\omega = -K_\omega (\beta - \phi) + \dfrac{\sin\beta}{\rho} \nu,$ $\nu = \begin{cases} 0, & \text{if } \beta - \phi \neq 0, \\ \bar{\nu}, & \text{if } \beta - \phi = 0. \end{cases}$
$\mathrm{II'}^{\mathcal{W}}$	T_P^{R-}	$\omega = -K_\omega (\beta - \phi) + \dfrac{\sin\beta}{\rho} \nu,$ $\nu = \begin{cases} 0, & \text{if } \beta - \phi \neq 0, \\ \bar{\nu}, & \text{if } \beta - \phi = 0. \end{cases}$
$\mathrm{II}_c'^{\mathcal{W}}$	T_P^{L+}	$\omega = -K_\omega (\beta + \phi) + \dfrac{\sin\beta}{\rho} \nu,$ $\nu = \begin{cases} 0, & \text{if } \beta + \phi \neq 0, \\ \bar{\nu}, & \text{if } \beta + \phi = 0. \end{cases}$
$\mathrm{III}^{\mathcal{W}} \cup \mathrm{III}_c^{\mathcal{W}}$	$S^+ * S^-$	$\omega = K_\omega \beta,$ $\nu = \begin{cases} 0, & \text{if } \beta \neq 0, \\ \bar{\nu}, & \text{if } \beta = 0. \end{cases}$
$\mathrm{IV}^{\mathcal{W}} \cup \mathrm{IV}_c^{\mathcal{W}}$	$S^+ T^{L+} * T^{R-} S^-$	$\omega = K_\omega \left(\sin(2\phi + \psi_M + \beta - \psi) + \dfrac{\rho}{\rho_P} \sin\beta \right),$ $\nu = \begin{cases} 0, & \text{if } F_{\mathrm{IV}^{\mathcal{W}} \cup \mathrm{IV}_c^{\mathcal{W}}}(\eta) \neq 0, \\ \bar{\nu}, & \text{if } F_{\mathrm{IV}^{\mathcal{W}} \cup \mathrm{IV}_c^{\mathcal{W}}}(\eta) = 0. \end{cases}$
$\mathrm{V}^{\mathcal{W}}$	$T^{L+} * T^{R-} S^-$	$\omega = -K_\omega (\beta + \phi) + \dfrac{\sin\beta}{\rho} \nu,$ $\nu = \begin{cases} 0, & \text{if } \beta + \phi \neq 0, \\ \bar{\nu}, & \text{if } \beta + \phi = 0. \end{cases}$
$\mathrm{V}_c^{\mathcal{W}}$	$S^+ T^{L+} * T_P^{R-}$	$\omega = K_\omega \left(\dfrac{\rho}{\rho_P} \dfrac{\sin\beta}{\sin\phi} + \mathrm{e}^{(\psi_M - \psi + \beta + \phi)t} \right),$ $\nu = \begin{cases} 0, & \text{if } F_{\mathrm{V}_c^{\mathcal{W}}}(\eta) \neq 0, \\ \bar{\nu}, & \text{if } F_{\mathrm{V}_c^{\mathcal{W}}}(\eta) = 0. \end{cases}$
$\mathrm{VI}^{\mathcal{W}}$	$T^{R-} S^-$	$\omega = -K_\omega (\beta - \phi) + \dfrac{\sin\beta}{\rho} \nu,$ $\nu = \begin{cases} 0, & \text{if } \beta - \phi \neq 0, \\ \bar{\nu}, & \text{if } \beta - \phi = 0. \end{cases}$
$\mathrm{VI}_c^{\mathcal{W}}$	$S^+ T_P^{L+}$	$\omega = K_\omega \left(\dfrac{\rho}{\rho_P} \dfrac{\sin\beta}{\sin\phi} + \mathrm{e}^{(\psi - \beta - \phi)t} \right),$ $\nu = \begin{cases} 0, & \text{if } F_{\mathrm{VI}_c^{\mathcal{W}}}(\eta) \neq 0, \\ \bar{\nu}, & \text{if } F_{\mathrm{VI}_c^{\mathcal{W}}}(\eta) = 0. \end{cases}$

Table 5.1: Optimal feedback control laws. In this table, K_ω is considered a positive control gain.

robot performs along the shortest path. Once the vehicle is localized, the associated controller is selected and performed. Control laws for configurations η in Regions $\text{I}^{\mathcal{W}}$, $\text{I}_c^{\mathcal{W}}$, $\text{VI}_c^{\mathcal{W}}$, $\text{V}_c^{\mathcal{W}}$, $\text{IV}^{\mathcal{W}} \cup \text{IV}_c^{\mathcal{W}}$ and $\text{III}^{\mathcal{W}} \cup \text{III}_c^{\mathcal{W}}$ are defined in terms of β and ratio ρ/ρ_P which can be determined by using directly image coordinates of only one feature. Indeed, let $^I p = [^I x, {}^I y]^T$ be the feature coordinates in the image plane, we have

$$\beta = \arctan\left(\frac{^I x}{\alpha_x}\right).$$

Moreover, let us introduce the following two state variables

$$\varrho_1 = \frac{\alpha_x}{\alpha_y}\frac{^I x}{^I y}, \quad \varrho_2 = \frac{\alpha_y}{^I y}.$$

By using (5.2), it is straightforward to obtain

$$\bar{\rho} = \sqrt{\varrho_1^2 + \varrho_2^2} = \frac{\sqrt{^c x^2 + {}^c z^2}}{h} = \frac{\rho}{h}.$$

where $h = {}^c y$, i.e., the feature height. On the other hand,

$$\bar{\rho}_P = \sqrt{\varrho_{1d}^2 + \varrho_{2d}^2} = \frac{\sqrt{^c x_d^2 + {}^c z_d^2}}{h} = \frac{\rho_P}{h},$$

where ϱ_{1d} and ϱ_{2d} are variable defined in (5.3) but computed in P, i.e., the desired robot position. As a consequence,

$$\frac{\rho}{\rho_P} = \frac{\sqrt{\varrho_1^2 + \varrho_2^2}}{\sqrt{\varrho_{1d}^2 + \varrho_{2d}^2}},$$

computable by using only image coordinates of only the feature placed on the axis through the origin O_w of frame $\langle W \rangle$ and perpendicular to the plane of motion.

On the other hand, state variable ψ can be determine as in [30] by using at least three image feature coordinates. Of course, for the sake of robustness and precision of calculation, more features are desirable. On the other hand, for control laws in Regions $\text{II}'^{\mathcal{W}}$, $\text{II}_c'^{\mathcal{W}}$,

$\text{II}^{\mathcal{W}}$, $\text{II}_c^{\mathcal{W}}$ and $\text{VI}^{\mathcal{W}}$, input ω is defined in terms of the absolute value of ρ which can be obtained by using directly image coordinates of only one feature but assuming that the height of the feature is known. For this reason, the visual servoing approach proposed here can be classified as a combination of Image-Based and Position-Based approach depending on which Region robot is in.

When robot reaches desired position P, the control law $u(\eta) = [0, K_\omega\beta]$ is performed in order to align the vehicle with the desired orientation.

Simulations reported here concern the optimal feedback control laws from points Q in Region I_c (see figure 5.3), Region VI_c (see figure 5.6), Region V_c (see figure 5.9) and Region $\text{IV} \cup \text{IV}_c$ (see figure 5.12). Moreover, figures 5.5, 5.8, 5.11 and 5.14 show also feature trajectories on image plane. Simulations are performed adding Gaussian image noise to the points with a standard deviation of $\sigma = 0.3$ pixel. Notice that, at least three features are in view along shortest path from Q to P, and hence, it is always possible to localize the vehicle. Finally, figures 5.4, 5.7, 5.10 and 5.13 show the evolution of state variables along shortest paths, both with and without noise.

5.4   Conclusion

In this chapter, realistic simulations, proving the effectiveness of optimal control laws previously defined, have been reported. The robot successfully reached the desired position while keeping a given feature always in view. It was shown that the method can work efficiently given a robust recognition system. The robustness of the overall algorithm could be increased, nevertheless this approach seems to be promising for an effective application in real world environments. The adoption of robust recognition systems, performant feature trackers and feature estimation filters may increase the applicability of the proposed technique. Robustness to uncalibrated camera parameters should also be considered.
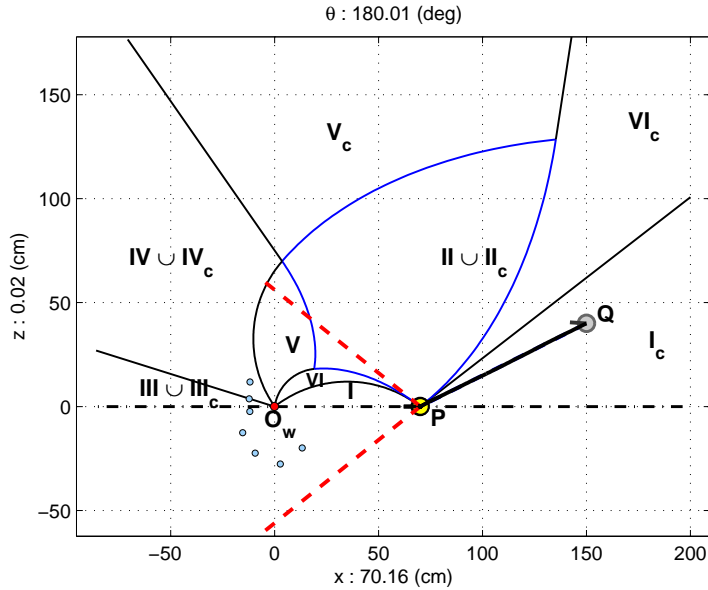
Figure 5.3: Optimal path from points Q in Region I_c (S^+ path) ($Q = [155.24, 15°, 19°]^T$ and $P = [70, 0°, 0°]^T$) (solid line the real robot trajectory, dashed line the ideal one. Notice that they are almost overlapping).


(a) Without noise.

(b) With gaussian noise.
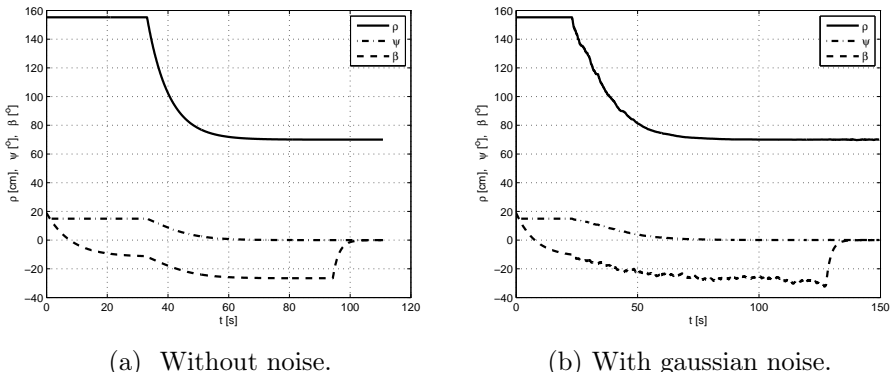
Figure 5.4: Evolution of state variables ρ, ψ and β along path S^+ from region I_c.
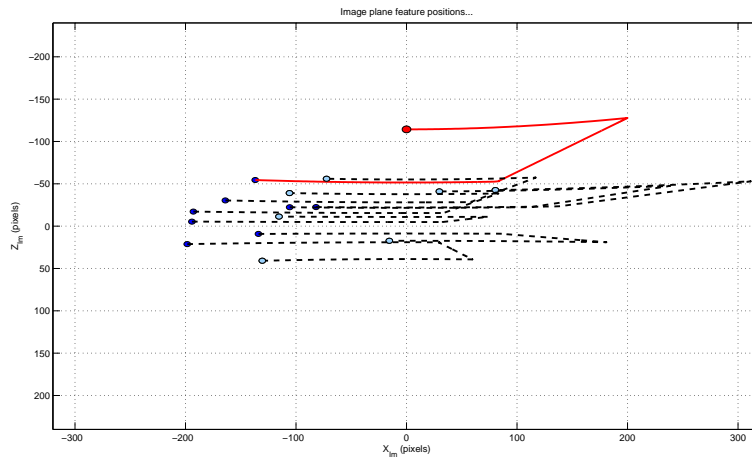
(a) Optimal path without noise.
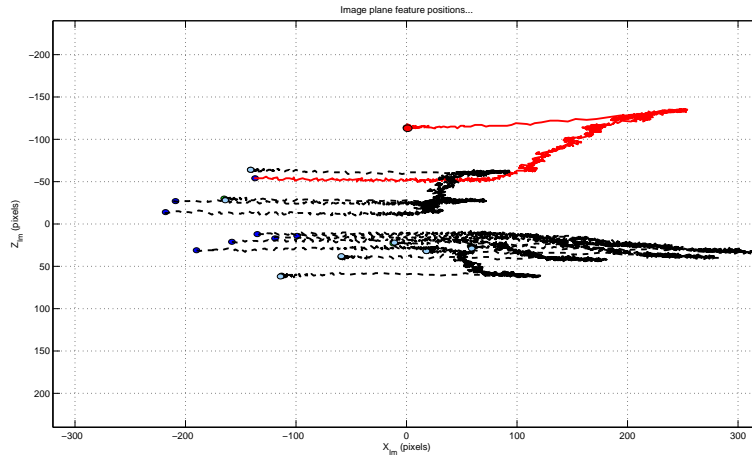
(b) Optimal path with gaussian noise.

Figure 5.5: Features trajectories on image plane (solid line for the feature in O_w, dashed line the other ones). Trajectories are composed of a piece of conic through initial feature position, a straight line through the principal point and a final conic until desired position.
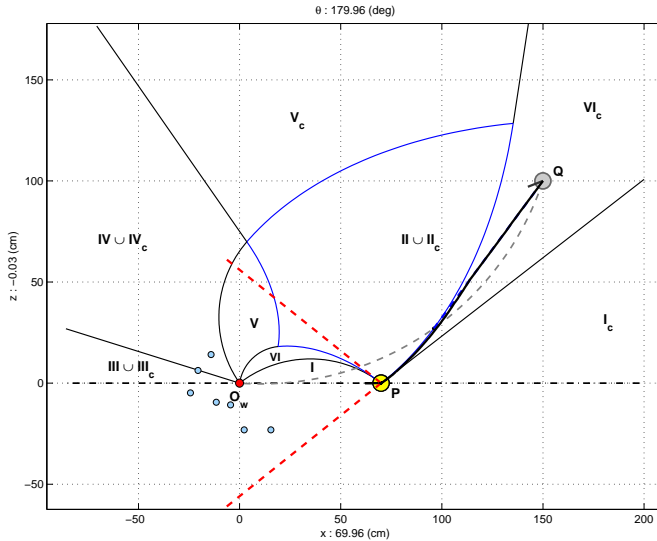
Figure 5.6: Optimal path from points Q in Region VI$_c$ ($S^+ T_P^{L+}$ path) ($Q = [180.27, 33.7°, 12.6°]^T$ and $P = [70, 0°, 0°]^T$) (solid line the real robot trajectory, dashed line the ideal one. Notice that when vehicle is near to spiral T_P^L, due mainly to localization problem caused by gaussian noise, the vehicle trajectory deviates slightly from ideal one).


(a) Without noise.

(b) With gaussian noise.
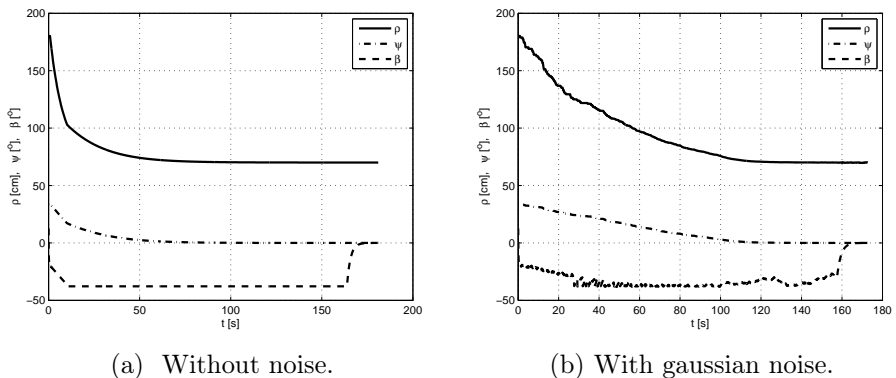
Figure 5.7: Evolution of state variables ρ, ψ and β along path $S^+ T_P^{L+}$ from region VI$_c$.
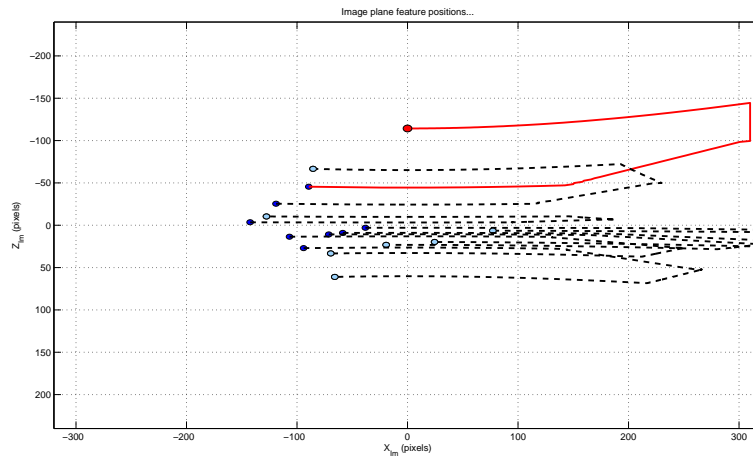
(a) Optimal path without noise.
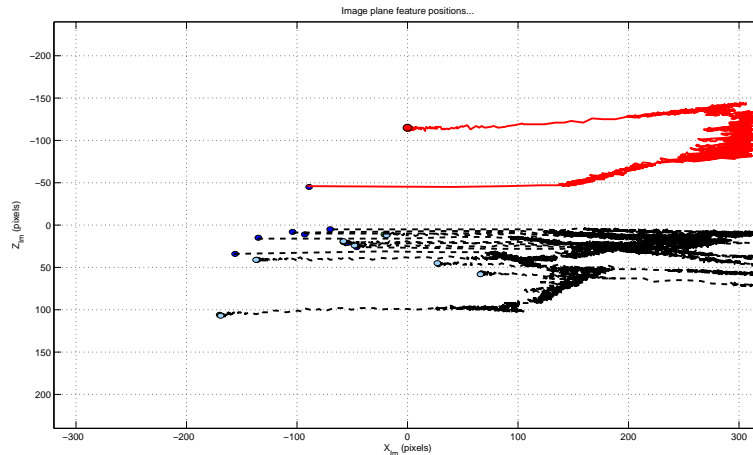
(b) Optimal path with gaussian noise.

Figure 5.8: Features trajectories for path $S^+ T_P^{L+}$ on image plane (solid line for the feature in O_w, dashed line the other ones). The trajectory of feature O_w is composed of a piece of conic through initial feature position, straight line through the principal point, a straight line coincident with the image border and a final conic until desired position.
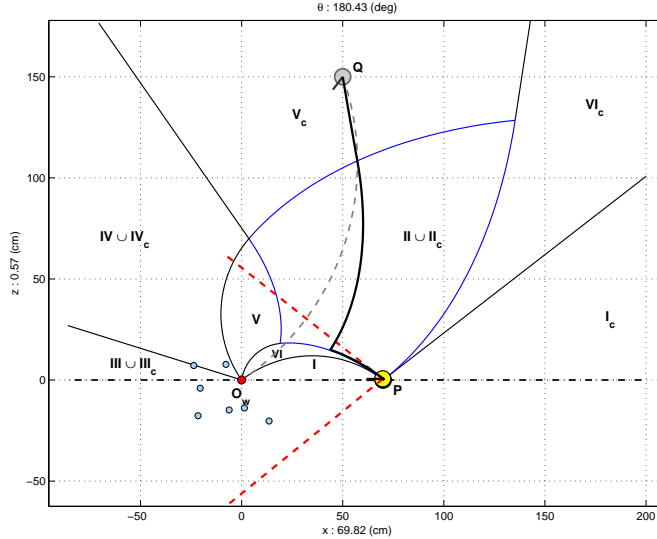
Figure 5.9: Optimal path from points Q in Region V$_c$ ($S^+T^{L+} * T_P^{R-}$ path) ($Q = [158.11, 71.56°, 18.9°]^T$ and $P = [70, 0°, 0°]^T$) (solid line the real robot trajectory, dashed line the ideal one. Notice that due mainly to localization problem caused by noise, final arc T_P^{R-} is not followed exactly and the parking error is slightly bigger than in previous simulations).

(a) Without noise.

(b) With gaussian noise.
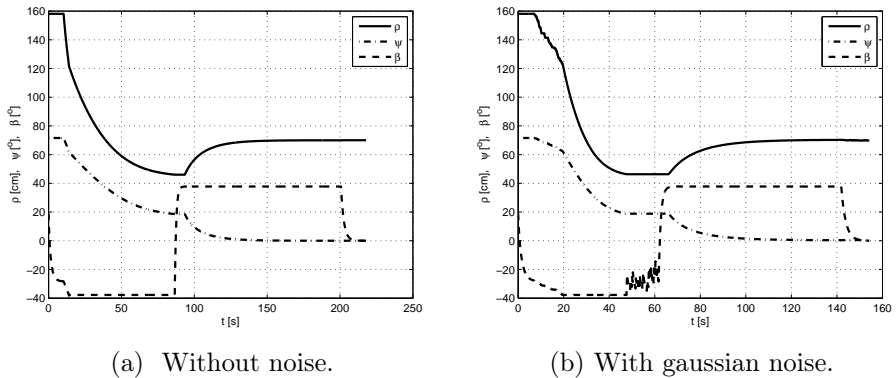
Figure 5.10: Evolution of state variables ρ, ψ and β along path $S^+T^{L+} * T_P^{R-}$ from region V$_c$.
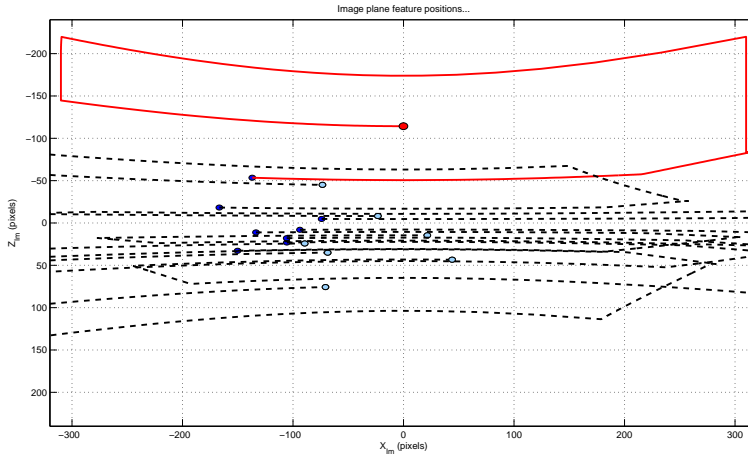
(a) Optimal path without noise.
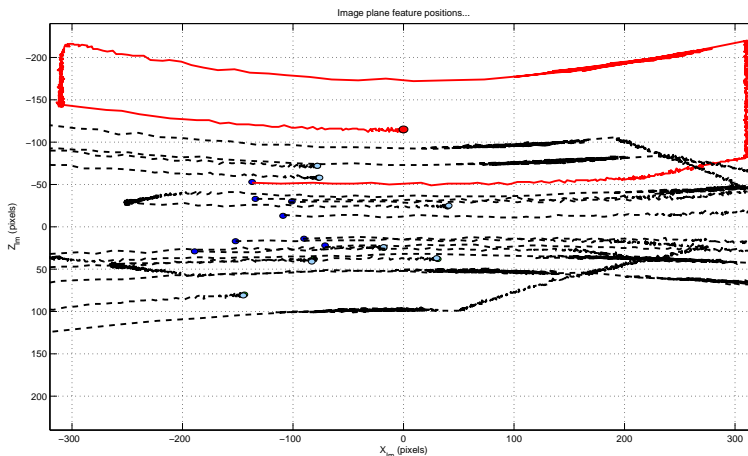
(b) Optimal path with gaussian noise.

Figure 5.11: Features trajectories for path $S^+T^{L+} * T_P^{R-}$ on image plane (solid line for the feature in O_w, dashed line the other ones). The trajectory of feature O_w is composed of a piece of conic through initial feature position, straight line through the principal point, a straight line coincident with the right image border, a conic from right to left border, a straight line coincident with the left image border and a final conic until desired position.
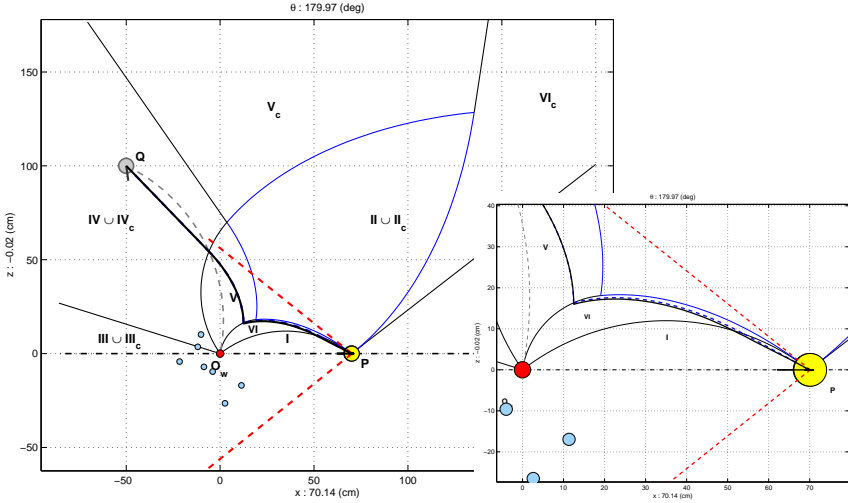
Figure 5.12: Optimal path from points Q in Region IV$_c$ ($S^+T^{L+}*T^{R-}S^-$ path) ($Q = [111.8, 116.56°, 18.9°]^T$ and $P = [70, 0°, 0°]^T$) (solid line the real robot trajectory, dashed line the ideal one. Notice that due mainly to localization problem caused by noise, sub-path $T^{R-}S^-$ is not followed exactly (see the small figure on the right). Anyway, the parking error is restrained).


(a) Without noise.

(b) With gaussian noise.
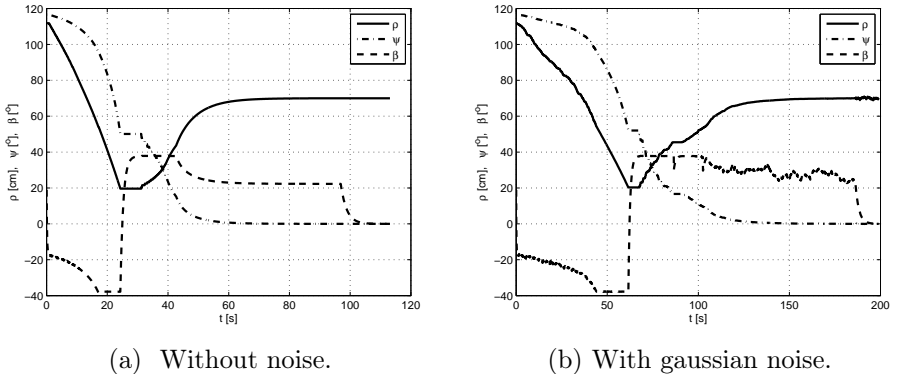
Figure 5.13: Evolution of state variables ρ, ψ and β along path $S^+T^{L+}*T_P^{R-}S^-$ from region IV$_c$.
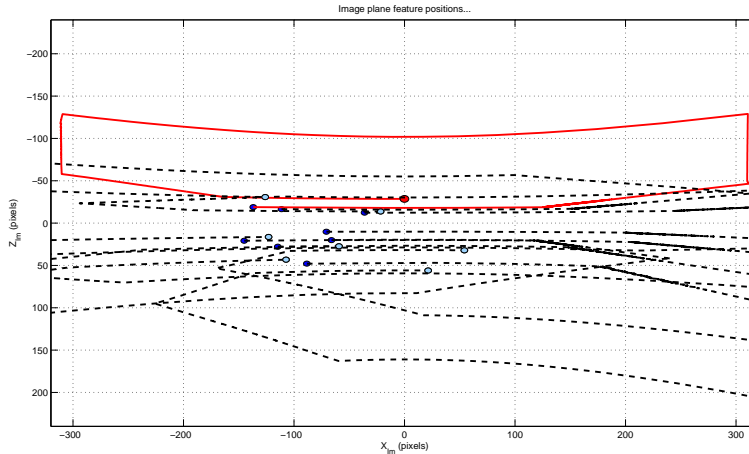
(a) Optimal path without noise.
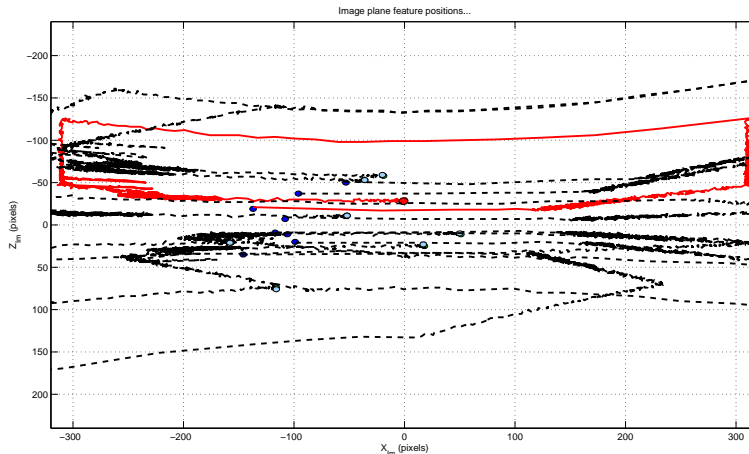
(b) Optimal path with gaussian noise.

Figure 5.14: Features trajectories for path $S^+T^{L+} * T_P^{R-}S^-$ on image plane (solid line for the feature in O_w, dashed line the other ones). The trajectory of feature O_w is composed of a piece of conic through initial feature position, straight line through the principal point, a straight line coincident with the right image border, a conic from right to left border, a straight line coincident with the left image border, a straight line through the principal point and a final conic until desired position.

Bibliography

Author's

[A1] P. Salaris, D. Fontanelli, L. Pallottino, and A. Bicchi, "Optimal paths for mobile robots with limited field-of-view camera," in *48th IEEE Conference on Decision and Control*, Dec 2009, pp. 8434–8439.

[A2] ——, "Shortest paths for a robot with nonholonomic and field-of-view constraints," *IEEE Transactions on Robotics*, vol. 26, no. 2, pp. 269–281, April 2010.

[A3] P. Salaris, L. Pallottino, and A. Bicchi, "Shortest paths with side sensors," in *Proc. IEEE Int. Conf. on Robotics and Automation*, May 2011, accepted.

[A4] P. Salaris, L. Pallottino, S. Hutchinson, and A. Bicchi, "From optimal planning to visual servoing with limited field-of-view," in *Proc. IEEE Int. Symp. Intelligent Robots and Systems*, Sept. 2011, submitted.

[A5] F. Belo, P. Salaris, and A. Bicchi, "3 known landmarks are enough for solving planar bearing slam and fully reconstruct unknown inputs," in *Proc. IEEE Int. Symp. Intelligent Robots and Systems*, Oct. 2010, pp. 2539–2545.

[A6] D. Fontanelli, P. Salaris, F. A. W. Belo, and A. Bicchi, *Visual Servoing via Advanced Numerical Methods*. Springer, 2010, vol. 401, ch. Unicycle–like Robots with Eye-In-Hand Monocular Cameras: from PBVS Towards IBVS, pp. 335 – 360.

[A7] D. Fontanelli, A. Danesi, F. A. W. Belo, P. Salaris, and A. Bicchi, "Visual servoing in the large," *International Journal of Robotics Research*, vol. 28, no. 6, pp. 802 – 814, June 2009.

[A8] P. Salaris, F. Belo, D. Fontanelli, and A. Bicchi, "Visual slam for servoing for appearance based topological maps," in *Proc. Ints. Symp. Experimental Robotics*, ser. Experimental Robotics, Springer-Verlag, Ed., vol. 39/2008, 2008, pp. 277–286.

[A9] P. Salaris, L. Pallottino, and A. Bicchi, "Optimal synthesis for nonholonomic vehicles with constrained side sensors," 2011, technical Report.

[A10] P. Salaris, F. A. W. Belo, D. Fontanelli, L. Greco, and A. Bicchi, "Optimal paths in a constrained image plane for purely image-based parking," *Proc. IEEE Int. Symp. Intelligent Robots and Systems*, pp. 1673–1680, Sept. 2008.

Miscellaneous

[11] L. E. Dubins, "On curves of minimal length with a constraint on average curvature, and with prescribed initial and terminal positions and tangents," *American Journal of Mathematics*, pp. 457–516, 1957.

[12] X. Bui, P. Souères, J.-D. Boissonnat, and J.-P. Laumond, "Short-est path synthesis for Dubins non–holonomic robots," in *IEEE International Conference on Robotics and Automation*, 1994, pp. 2–7.

[13] J. A. Reeds and L. A. Shepp, "Optimal paths for a car that goes both forwards and backwards," *Pacific Journal of Mathematics*, pp. 367–393, 1990.

[14] H. Sussmann and G. Tang, "Shortest paths for the reeds-shepp car: A worked out example of the use of geometric techniques in nonlinear optimal controlò," Department of Mathematics, Rutgers University, Tech. Rep., 1991.

[15] H. Souères and J. P. Laumond, "Shortest paths synthesis for a car-like robot," *IEEE Transaction on Automatic Control*, pp. 672–688, 1996.

[16] D. Balkcom and M. Mason, "Time-optimal trajectories for an omnidirectional vehicle," *The International Journal of Robotics Research*, vol. 25, no. 10, pp. 985–999, 2006.

[17] H. Wang, Y. Chan, and P. Souères, "A geometric algorithm to compute time-optimal trajectories for a bidirectional steered robot," *IEEE Transaction on Robotics*, pp. –, 2009.

[18] H. Chitsaz, S. M. LaValle, D. J. Balkcom, and M. Mason, "Minimum wheel-rotation for differential-drive mobile robots," *The International Journal of Robotics Research*, pp. 66–80, 2009.

[19] F. Chaumette and S. Hutchinson, "Visual servo control, Part I: Basic approaches," *IEEE Robotics and Automation Magazine*, vol. 13, no. 4, pp. 82–90, December 2006.

[20] ——, "Visual servo control, Part II: Advanced approaches," *IEEE Robotics and Automation Magazine*, vol. 14, no. 1, pp. 109–118, March 2007.

[21] A. C. Sanderson and L. E. Weiss, "Image–based visual servo control using relational graph error signals," in *Proc. IEEE Int. Conf. on Robotics and Automation*, 1980, pp. 1074–1077.

[22] Y. Fang, D. M. . Dawson, W. E. Dixon, and M. S. de Queiroz, "Homography-based visual servoing of wheeled mobile robots," in *IEEE Conf. on Decision and Control*, vol. 3, Las Vegas, Nevada, USA, December 2002, pp. 2866–2871.

[23] E. Malis and P. Rives, "Robustness of image-based visual servoing with respect to depth distribution errors," in *Proc. IEEE Int. Conf. on Robotics and Automation*, vol. 1, sept. 2003, pp. 1056 – 1061.

[24] E. Malis, F. Chaumette, and S. Boudet, "2 frac12;d visual servoing," *Robotics and Automation, IEEE Transactions on*, vol. 15, no. 2, pp. 238 –250, Apr. 1999.

[25] D. Lowe, "Distinctive image features from scale-invariant keypoints," in *Int. Jour. of Computer Vision*, vol. 20, 2003, pp. 91–110.

[26] S. Benhimane and E. Malis, "A new approach to vision–based robot control with omni–directional cameras," in *Proc. IEEE Int. Conf. on Robotics and Automation*, Orlando, Florida, USA, May 2006, pp. 526–531.

[27] Y. Mezouar and F. Chaumette, "Path planning for robust image–based control," *IEEE Transactions on Robotics and Automation*, vol. 18, no. 4, pp. 534–549, August 2002.

[28] G. L. Mariottini, G. Oriolo, and D. Prattichizzo, "Image-based visual servoing for nonholonomic mobile robots using epipolar geometry," *Robotics, IEEE Transactions on*, vol. 23, no. 1, pp. 87 –100, feb 2007.

[29] G. López-Nicolás, C. Sagüés, J. Guerrero, D. Kragic, and P. Jens-felt, "Switching visual control based on epipoles for mobile robots," *Robotics and Autonomous Systems*, vol. 56, no. 7, pp. 592 – 603, 2008.

[30] X. Zhang, Y. Fang, and X. Liu, "Visual servoing of nonholonomic mobile robots based on a new motion estimation technique," in *Decision and Control, 2009 held jointly with the 2009 28th Chinese Control Conference. CDC/CCC 2009. Proceedings of the 48th IEEE Conference on*, dec 2009, pp. 8428 –8433.

[31] P. Murrieri, D. Fontanelli, and A. Bicchi, "A hybrid-control approach to the parking problem of a wheeled vehicle using limited view-angle visual feedback," *Int. Jour. of Robotics Research*, vol. 23, no. 4–5, pp. 437–448, April–May 2004.

[32] N. Gans and S. Hutchinson, "Stable visual servoing through hybrid switched system control," *IEEE Transactions on Robotics*, vol. 23, no. 3, pp. 530–540, June 2007.

[33] ——, "A stable vision-based control scheme for nonholonomic vehicles to keep a landmark in the field of view," in *Proc. IEEE Int. Conf. on Robotics and Automation*, apr. 2007, pp. 2196 –2201.

[34] G. Chesi and Y. Hung, "Global path-planning for constrained and optimal visual servoing," *IEEE Transactions on Robotics*, vol. 23, no. 5, pp. 1050–1060, October 2007.

[35] K. Deguchi, "Optimal motion control for image-based visual servoing by decoupling translation and rotation," in *IEEE/RJS Intl. Conf. on Intelligent Robots and Systems*, Victoria, B.C., Canada, October 1998, pp. 705–711.

[36] Y. Mezouar, A. Remazeilles, P. Gros, and F. Chaumette, "Images interpolation for image-based control under large displacement,"

in *IEEE Intl. Conf. on Robotics and Automation*, Washington, DC, May 2002, pp. 3787–3794.

[37] N. Dias, C. Almeida, H. Ferreira, J. Almeida, A. Martins, A. Dias, and E. Silva, "Manoeuvre based mission control system for autonomos surface vehicle," *in Proceeedings of OCEANS '09*, May 2009.

[38] F. Langner, C. Knauer, W. Jans, and A. Ebert, "Side scan sonar image resolution and automatic object detection, classification and identification," *in Proceeedings of OCEANS '09*, May 2009.

[39] V. Tucker, "The deep fovea, sideways vision and spiral flight paths in raptors," *J Exp Biol*, vol. 203, no. 24, pp. 3745–3754, 2000.

[40] V. Tucker, A. Tucker, K. Akers, and J. Enderson, "Curved flight paths and sideways vision in peregrine falcons (Falco peregrinus)," *J Exp Biol*, vol. 203, no. 24, pp. 3755–3763, 2000.

[41] S. Bhattacharya, R. Murrieta-Cid, and S. Hutchinson, "Optimal paths for landmark-based navigation by differential-drive vehicles with field-of-view constraints," *IEEE Transactions on Robotics*, vol. 23, no. 1, pp. 47–59, February 2007.

[42] G. López-Nicolás, N. Gans, S. Bhattacharya, C. Sagüé, J. Guerrero, and S. Hutchinson, "Homography-based control scheme for mobile robots with nonholonomic and field-of-view constraints," *Systems, Man, and Cybernetics, Part B: Cybernetics, IEEE Transactions on*, vol. 40, no. 4, pp. 1115 –1127, Aug 2010.

[43] P. Lucibello and G. Oriolo, "Stabilization via iterative state steering with application to chained-form systems," in *Decision and Control, 1996., Proceedings of the 35th IEEE*, vol. 3, dec 1996, pp. 2614 –2619.

[44] S. Arimoto, J.-H. Bae, and K. Tahara, "Stability on a manifold: simultaneous realization of grasp and orientation control of an object by a pair of robot fingers," in *Proc. IEEE Int. Conf. on Robotics and Automation*, vol. 2, sept 2003, pp. 2336 – 2343.

[45] J. P. LaSalle, "An invariance principle in the theory of stability," *Eds. New York: Academic*, pp. 277–286, 1967.

[46] B. Siciliano and O. Khatib, Eds., *Springer Handbook of Robotics*. Springer, 2008.

[47] A. Bryson and Y. Ho, *Applied optimal control.* Wiley New York, 1975.

[48] R. Hartley and A. Zisserman, *Multiple View Geometry in Computer Vision.* Cambridge University Press, 2003.

[49] L. Cesari, *Optimization-theory and applications: problems with ordinary differential equations.* Springer-Verlag, New York, 1983.

[50] R. Bellman, *Dynamic Programming.* Princeton University Press, Princeton, N.J., 1957.

[51] X. Zhang, Y. Fang, and X. Liu, "Visual servoing of nonholonomic mobile robots based on a new motion estimation technique," in *Decision and Control, 2009 held jointly with the 2009 28th Chinese Control Conference. CDC/CCC 2009. Proceedings of the 48th IEEE Conference on*, dec 2009, pp. 8428 –8433.

[52] G. L. Mariottini, G. Oriolo, and D. Prattichizzo, "Image–based visual servoing for nonholonomic mobile robots using epipolar geometry," *IEEE Transactions on Robotics*, vol. 23, no. 1, pp. 87–100, February 2007.